phd 256 12/27/66

ok

IDO-14680

CHEMICAL AND PROCESS DEVELOPMENT BRANCH ANNUAL REPORT FISCAL YEAR 1966

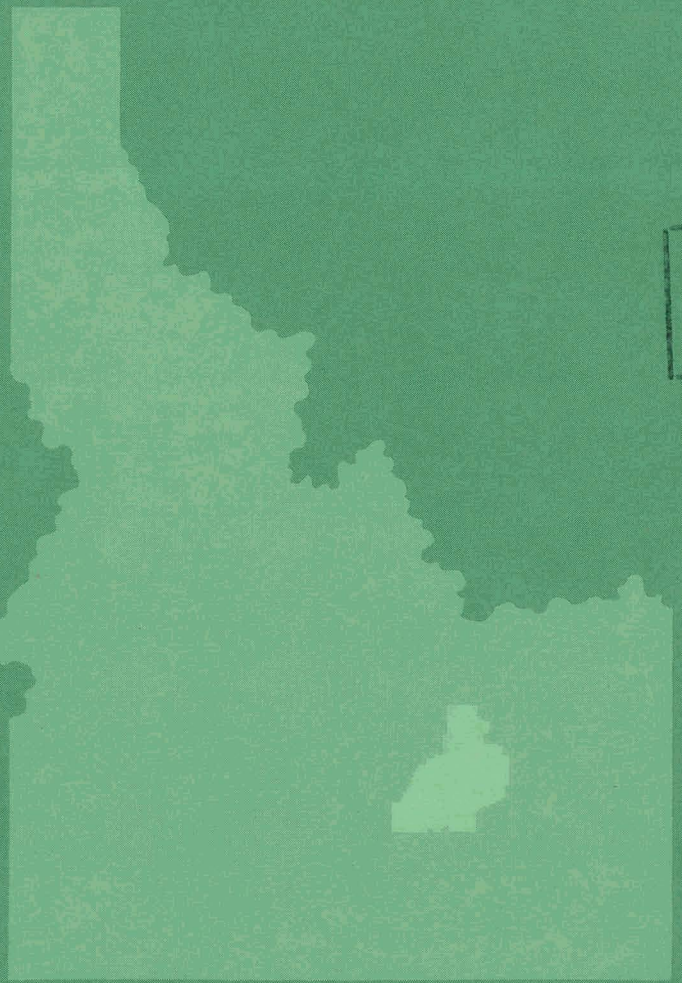

PHILLIPS PETROLEUM COMPANY

PHILLIPS 66

ATOMIC ENERGY DIVISION

NATIONAL REACTOR TESTING STATION

US ATOMIC ENERGY COMMISSION

DISCLAIMER

PRINTED IN USA. PRICE $4.00. AVAILABLE FROM THE CLEARINGHOUSE FOR FEDERAL SCIENTIFIC AND TECHNICAL INFORMATION, NATIONAL BUREAU OF STANDARDS, U. S. DEPARTMENT OF COMMERCE, SPRINGFIELD, VIRGINIA 22151

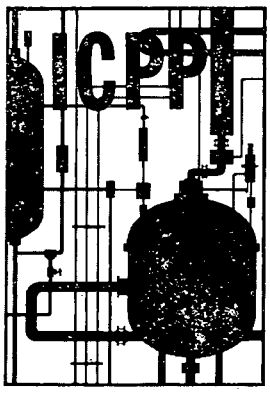

IDO-14680
AEC Research and Development Report
General, Miscellaneous, and Progress Reports
TID-4500
Issued: October 1966

CFSTI PRICES

HC $3.00 ; MN .65

CHEMICAL AND PROCESS DEVELOPMENT BRANCH ANNUAL REPORT

FISCAL YEAR 1966

D. R. deBoisblanc
ASSISTANT MANAGER
ATOMIC ENERGY DIVISION

J. A. Buckham
MANAGER, CHEMICAL
AND PROCESS DEVELOPMENT

J. R. Bower
EDITOR

B. R. Wheeler
PLANT PROCESS ASSISTANCE
SECTION

K. L. Rohde
CHEMISTRY SECTION

B. M. Legler
DEVELOPMENT ENGINEERING
SECTION

PHILLIPS
PETROLEUM
COMPANY

Atomic Energy Division
Contract AT(10-1)-205
Idaho Operations Office
U. S. ATOMIC ENERGY COMMISSION

SUMMARY

The ICPP processed aluminum- and zirconium-based fuels during the first part of the reporting period, and was well along in the second processing campaign in the Waste Calcining Facility at the close of the period. Uranium recovery from the aluminum fuel process was satisfactory, even though unusual surfactancy of the feed solutions caused some processing difficulties. The versatility of the new semi-continuous, boron-poisoned, hydrofluoric acid process for zirconium-based fuels was amply demonstrated by the successful processing of standard PWR-type fuels, zirconium fuels containing stainless steel pins, and aluminum cans filled with zirconium scrap. Approximately 1.1 kg of Np-237 were recovered during routine processing of aluminum and zirconium fuels.

In process-associated support studies, boron carbide in ATR fuel was shown to promote emulsion formation under extraction column conditions; boiling with gelatin appeared to alleviate the problem. Hydrogen formation during charging of zirconium fuel to a dissolver was found to be significant if the boric acid (6.3 g/l) solution in the dissolver (at 20°C) contained 0.003 M or greater hydrofluoric acid residue. The recovery of uranium from zirconium-fuel dissolver heels was found to be hampered by the presence of stainless steel in the residue. Sulfuric acid was effective in releasing the uranium which was not dissolved by the usual chromic acid reagent while stainless steel was present. Corrosion effects on the Monel dissolver are reported for the cleanout reagents.

Recovery of uranium from EBR-II scrap resulting from the pyrometallurgical process was shown to be practical at the ICPP by use of a nitric acid dissolution process. Recovery of uranium from a melted LOFT reactor core (uranium dioxide partly fused with Zircaloy-4) appears to be possible by use of alternate nitric acid and hydrofluoric acid dissolution steps in a Carpenter-20 vessel. Uranium dioxide-zirconium dioxide fuel clad in Zircaloy-4 was completely dissolved in a three-step aqueous process using varying concentrations of hydrofluoric acid for decladding and core dissolution, and chromic acid for uranium recovery. Calcium oxide in the core slows the dissolution process, but the rate of corrosion on the Monel dissolver may offer the greatest drawback to the process. A modified burn-leach process for graphite fuels has demonstrated the possibility, on a pilot-plant scale, of separating the metal oxide combustion products from the fluidized-bed alumina particles by carrying the ash overhead in the off-gas stream. Uranium was leached essentially quantitatively from the elutriated product by nitric acid treatment. Alternate processes for graphite fuels, a grind-leach process and a nitric acid-sulfuric acid oxidation process, were shown to be chemically feasible and to give essentially quantitative recovery of uranium.

In miscellaneous equipment performance studies, final refinement of the air pulser mathematical model has been accomplished. Further, a mathematical and experimental study on the effects of pulsation on heat transfer in a liquid-fluidized bed has been completed.

The ICPP Waste Calcining Facility (WCF) started operation on its second processing campaign during the last quarter of FY 1966, and at the end of the period was operating smoothly and had calcined about 142,000 gallons of waste on this campaign. The net feed rate to the calciner has averaged 67.5 gallons per hour for a 90-day period; this is 12 percent above design and was attained in spite of some feed system plugging problems. Pilot plant calcination of

zirconium-, ammonium-, and sodium-containing wastes has disclosed a number of important variables involved in handling the varied wastes which may be processed in the WCF. A pilot plant run with normal aluminum nitrate-type waste, made under the same conditions used in the first WCF run, gave a basis for comparison between the two calciner systems and, hence, a basis for predicting the operating performance of the WCF when processing the other types of waste. All appear to be processable either in proper combination or, under certain circumstances, with the use of additives. A theory of particle growth and size distribution in fluidized-bed processes is presented in terms of a mathematical model, and computer solutions compare favorably with observed experimental results.

Other calcination development studies reported include: (a) a determination of the ruthenium dioxide-oxygen-ruthenium tetroxide equilibrium and its relation to ruthenium in the calciner off-gas; (b) a finding that mercury contained in the calcine will migrate out of areas hotter than 400°C and will collect in a maximum concentration in the 125°C zone; and (c) a study of the leachability of fission products from WCF calcine. Heat transfer studies affecting the calcination process and the storage of the calcined product include findings that: (a) the rate of heat transfer to a fluidized bed can be increased by the use of finned tubes; (b) shrouds to promote convection around calcine storage bins inside a vault are not necessary since the reflection of radiant heat back to the bin negates any improvement in heat transfer by convection; and (c) a mathematical model formulated for predicting the temperature distribution around a heat source buried in soil was found to give reliable results when compared with an actual experimental study.

LOFT assistance studies have continued to be directed toward decontamination of possible reactor containment shell coatings. Several coatings have been found to have adequate resistance to the anticipated exposure conditions, but decontamination behavior was disappointing for all coatings. Effective decontamination from iodine within the first few days after the simulated nuclear accident can only be obtained by removing a layer of the surface from the material being decontaminated. The Contamination-Decontamination Experiment (CDE), an experimental unit for releasing fission products from melted, irradiated fuel specimens into a confined, controlled-atmosphere test chamber, has been constructed and operated successfully. The CDE is being used to study contamination and decontamination of protective coatings, to test various LOFT sampling devices, and to provide samples for development of analytical methods needed to assess the LOFT experiments from a radiochemical standpoint. A continuous sampler-monitor for the LOFT containment building atmosphere and possible absorptive reagents for use in the device are undergoing development; progress is reported but a final design is not yet established.

Fission gas retention properties of several fuel plates were studied. Fuel particles of either U_3O_8 or UAl_3 in aluminum matrices released fission gases on reaching a temperature of 575 to 600°C; the gas release was more rapid from UAl_3 particles than from U_3O_8.

CONTENTS

FIGURES

TABLES

CHEMICAL AND PROCESS DEVELOPMENT BRANCH
ANNUAL REPORT
FISCAL YEAR 1966

I. FUEL REPROCESSING

1. PERFORMANCE OF ICPP FUEL RECOVERY PROCESS

1.1 Aluminum Fuel Processing

(B. R. Wheeler, W. P. Palica; Plant Process Assistance Section)

1.11 Summary of Operations. High-enriched uranium-aluminum alloyed fuels containing 426 kg of uranium were processed in a short campaign during December 1965 and January 1966. The fuels processed and the amount of uranium in each are shown in Table I; the uranium recovery from the various extraction cycles is summarized in Table II. An acceptable overall uranium recovery of 99.74 percent was obtained. The overall decontamination of the uranium was excellent, and the product easily met the required specifications.

TABLE I

ALUMINUM ALLOYED FUELS
PROCESSED DURING FISCAL YEAR 1966

Fuel Type	Number of Elements Dissolved	Total Uranium Charged (kg)
Unirradiated	[a]	60.31
MTR	375	63.92
ETR	616	195.15
LITR	216	32.99
LPTR	14	2.07
OWR	28	5.06
GETR	140	41.71
SPERT	84	14.80
GTR	37	6.94
ASTR	34	3.68[b]
Total	> 1544	426.63

[a] Miscellaneous fuel elements, plates, and scrap from ATR, MTR, ETR, and SPERT.

[b] Uranium from 10 of the ASTR fuel elements is included in the uranium from the GTR fuel.

Dissolution of the aluminum alloyed fuel in the normal manner was followed by uranium extraction using the tributyl phosphate (TBP) flow sheet shown in Figure 1. This flow sheet differs from previous flow sheets [1, 2] primarily in four aspects: (a) an increase in first-cycle TBP concentration from 3.25 to 5 percent; (b) a change in concentration of the first-cycle feed constituents; (c) an increase in volume of first-cycle waste; and (d) a change in composition of the scrub solution. The first three changes were made because the feed and waste evaporators were inoperable due to tube corrosion encountered during the previous operating period with zirconium alloyed fuel [3]. The fourth change was made to improve the acid scrubbing efficiency and to simplify the scrub solution preparation; the aluminum nitrate concentration was reduced from 1.0 to 0.75M, and the ammonium hydroxide was omitted.

TABLE II

URANIUM RECOVERY FACTORS FOR ALUMINUM ALLOYED FUELS

Extraction Cycle	Recovery (percent)
First	99.76
Second	99.99
Third and Fourth	99.99
Overall	99.74

After all of the aluminum alloyed fuel was processed through the first extraction cycle, the intercycle product was processed through three additional extraction cycles using methyl isobutyl ketone (Hexone) and then bottled for shipment. Because the decontamination of the first-cycle uranium product was poorer than usual a fourth extraction cycle was employed, following the usual three cycles, to ensure the desired decontamination.

1.12 Process Performance. Although the overall decontamination of the uranium easily met the required specifications, the decontamination factors obtained in the first extraction cycle [4] varied from approximately the same as, to as low as one-tenth of, those obtained during the previous aluminum alloyed fuel campaign [2]. Two factors were probably responsible for the poor first-cycle decontamination. First, the higher feed radioactivity in this run (the fuel had been out of the reactor for a shorter length of time than for previous runs) caused a higher than normal fission product activity in the solvent. The higher activity in the solvent, in turn, produced a higher than normal product activity; a similar phenomena has been discussed previously [5]. Secondly, emulsion formation in the first-cycle extraction column caused a fission product carry-over into the stripping column, as discussed below, and contributed further to the high activity.

Product recovery was, likewise, not as good as that obtained in the previous reporting period [1] and was primarily the result of higher than normal losses in the first extraction cycle where only 99.76 percent of the uranium was extracted, compared to the usual 99.9 percent. Recovery in the succeeding cycles was comparable to the previous campaign [2].

The formation of stable emulsions in the extraction column appeared to be the cause of the high losses and the accompanying slightly erratic column behavior. Several dispersion-coalescence tests using various combinations of aqueous and organic feed materials proved that surface-active materials (highly hydrated forms of zirconium and silica) tended to form stable emulsions

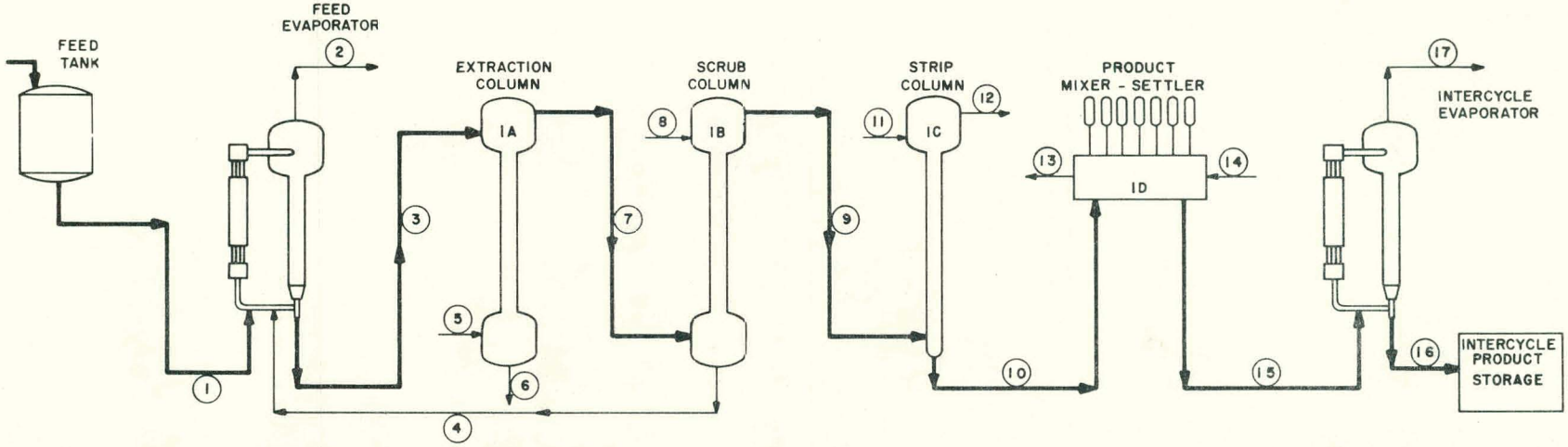

STREAM	1	2	3	4	5	6	7	8	9	10	11	12	13	14	15	16	17
DESCRIPTION	DISSOLVER PRODUCT	EVAPORATOR OVERHEAD	1AF	1BR	1AX	1AR	1AP	1BS	1BP	1CP	1CX	1CR	1DR	1DX	1DP	FIRST CYCLE PRODUCT (d)	EVAPORATOR OVERHEAD (d)
FLOW, l/batch																6.44	193
FLOW, l/hr	480 (c)		550	70	380	550	380	70	380	200	200	380	10	10	200		
TBP, %					5		5		5			5					
DILUENT					Amsco		Amsco		Amsco			Amsco	Amsco	Amsco			
SP. GR. AT 25°C	1.296		1.279	1.150	0.77	1.273	0.78	1.123	0.77	1.01	1.00	0.77	0.76	0.76	1.01	1.29	
$Al(NO_3)_3$ M	1.60 (c)		1.49	0.75		1.49		0.75									
HNO_3 M	1.30		1.24	0.84		1.12	0.16		0.005	0.02	0.01				0.02	0.62	
CrO_3 M	0.011		0.01	0.01		0.01		0.01									
$Hg(NO_3)_2$ M	0.007		0.007			0.007											
U(a) g/l	2.69		2.42	0.60		$5x10^{-4}$	3.50		3.39	6.44		$2x10^{-4}$			6.44	200	
U(b) g/l	3.34		3.00	0.71		$5x10^{-4}$	4.34		4.22	8.02		$2x10^{-4}$			8.02		
U(b) kg/hr	1.6		1.65	0.05			1.65		1.6	1.6					1.6	1.6	

(a) Irradiated ETR fuel (21 percent burnup).
(b) Unirradiated ETR fuel.
(c) Based on 500 kg of aluminum per day.
(d) Based on irradiated ETR fuel. For unirradiated ETR fuel this stream would be: flow 8.02 l/h; HNO_3 0.50M.

INC-B-9645

Fig. 1 First cycle extraction flow sheet for aluminum fuel.

during the extraction step. By adding geletin, and by increasing the feed acidity from about 1.3 to 2.4M, the coalescence properties of the plant feed and solvent were improved. Tolerable plant operation was obtained by this treatment.

Limited laboratory data indicated that the inoperability of the headend evaporator may have contributed to the large amount of surfactancy experienced in the extraction column during this run. During previous runs, the extraction column feed had been held at the boiling temperature in the evaporator for about three minutes and then cooled before introduction to the column. It is believed that this limited amount of heat treatment may condition the silica and zirconium sufficiently to affect their surfactancy properties under extraction column operating conditions. This hypothesis is partially substantiated by several dispersion-coalescence tests in which the coalescence time for a heat-treated sample was significantly lower than for a nontreated sample. Further laboratory investigations in this area are planned.

On several occasions during the run, a reduction in the capacity of the mixer-settler, used to scrub TBP and its degradation products from the aqueous first-cycle product, caused a small decrease in the processing rate. Partial blockages by an emulsion formed in the extraction column and carried through the scrub and strip columns to the mixer-settler were the direct cause of the reduction in capacity. However, even under ideal conditions, the mixer-settler has a marginal flow capacity.

The only significant processing problem during the run in the Hexone system involved the formation of iron-aluminum solids which caused a plug in the organic outlet of the extraction column in the third (second Hexone) cycle. The solids were formed in both the second and third cycles, but plugging of the line occurred only in the third cycle. Iron and aluminum are routinely added to the scrub streams for both of these cycles, as ferrous sulfamate to reduce plutonium to an inextractable species, and as aluminum nitrate to salt uranium into the organic phase. As a result of laboratory work [3], it is believed that the ferrous sulfamate was oxidized to form solids, either by air being introduced at the bottom of the columns in a liquid level probe or by some unidentified oxidizing agent in the feed streams. Further investigations are planned to establish the mechanism by which the iron-containing solids were formed.

The feed evaporator and product mixer-settler will be replaced before the next fuel processing campaign; it is believed that these modifications will prevent many of the problems experienced on this campaign.

1.2 Zirconium Fuel Processing

(B. R. Wheeler, G. F. Offutt; Plant Process Assistance)

1.21 Summary of Operations. The zirconium fuel processing campaign, completed at ICPP during FY 1966, proved the feasibility of using a high-capacity aqueous process (briefly described in Section 1.22) for zirconium alloyed fuels. Operation of this high-capacity process was made possible by employing a soluble neutron poison to guarantee nuclear safety in a non-geometrically-safe dissolver,

an approach pioneered during this campaign [6]. The start of this campaign was reported in the FY 1965 annual report [1]. Use of the soluble poison enabled more fuel to be charged per batch than would have otherwise been possible and resulted in an increase in the zirconium fuel capacity of the ICPP from 90 to approximately 800 kg of zirconium per day. The versatility of this new process is indicated by the processing on this campaign of PWR (Shippingport) zirconium fuels and others of similar composition, zirconium fuels containing stainless steel pins, and aluminum cans filled with zirconium scrap. The results of the campaign are summarized in the following paragraphs; full details are reported in a topical report, IDO-14675 [3].

The processing rate for the campaign was quite satisfactory. For at least a one-month period, the actual processing rate achieved through dissolution and the first extraction cycle was 765 kg zirconium per day; for the full campaign an average rate of 535 kg per day was achieved.

The average dissolution rate of irradiated fuel was somewhat lower than anticipated in the original design bases; this resulted in a lower zirconium concentration in the dissolver product, which averaged 0.90M instead of the 1.0M originally expected. An undesirable side effect from this less concentrated dissolver product was that an 11 percent greater volume of waste was generated on the run than was expected. The average volume of waste generated was 6.8 gallons per kg of zirconium. Minor equipment modifications are under consideration before the next processing campaign to permit operation of the dissolver with higher liquid levels and higher temperatures; it is believed that these modifications will lead to increased dissolution rates and decreased volumes of waste.

First cycle extraction of uranium, using an organic stream containing both 5- and 10-percent TBP, was very successful. Recovery efficiency averaged 99.5 percent. Performance of second, third, and fourth extraction cycles using Hexone as a solvent was also excellent; the recovery efficiency here averaged 99.98 percent. Decontamination of the uranium from fission products and plutonium was entirely satisfactory in both the TBP and Hexone extraction systems as shown in Table III. Two cycles of extraction are adequate; the third and fourth cycles were employed here only to determine the maximum plutonium decontamination possible in existing equipment.

TABLE III

AVERAGE LOG DECONTAMINATION FACTORS OBTAINED
DURING THE PROCESSING OF ZIRCONIUM ALLOYED FUEL

Extraction Cycle	Pu	Gross β	Gross γ	Zr-Nb-95
First	1.9	4.0	3.9	4.8
Second	3.6	3.0	2.4	2.2
Third	1.9	0.6	0.3	1.2
Fourth	0	0.4	No Analysis	0.5
Overall (for four cycles)	7.4	8.0	6.6	8.7

During the campaign, various corrosion coupons in the Monel dissolver were examined periodically to estimate the corrosion rate occurring in the dissolver. Based on these measurements, it is believed the corrosion rate of the dissolver was less than seven mils per month, an acceptable rate.

1.22 Process Description. Zirconium alloyed fuels are dissolved batchwise in hydrofluoric acid solutions containing dissolved boron for nuclear safety. Up to 600 kg of zirconium fuel are charged per batch; the fuel charge is held in a 13-inch-diameter slotted basket inside the 42-inch-diameter dissolver. After charging, dissolvent is fed continuously to the dissolver until most of the fuel has been dissolved.

Dissolver product overflows continuously from the dissolver and is transferred by a nitrogen gas lift to a feed-adjustment tank for continuous complexing. Complexing establishes proper conditions for low corrosion, long stability, and good uranium extraction. Complexed dissolver product overflows continuously from the feed adjustment vessel to tanks in the first-cycle extraction system. The first extraction cycle uses 5- to 10-percent TBP in Amsco as a solvent. To assure solution stability, the feed and waste streams in the first extraction cycle are never heated or evaporated.

Several flow sheets employing 5- or 10-percent TBP in Amsco as a solvent were used during the run. However, a 5-percent-TBP flow sheet, as shown in Figure 2, was used for about 80 percent of the processing campaign. Use of a 5-percent TBP, rather than a 10-percent TBP, flow sheet theoretically results in about 15 percent more waste. However, in order to achieve the theoretical benefits of the 10-percent flow sheet, it is necessary to generate a more concentrated dissolver product than was practical on this run with irradiated fuel. The low concentration resulted from a lower dissolution rate for irradiated fuel in the plant dissolver than was achieved with unirradiated fuel in development studies.

The second and third solvent extraction cycles used for the zirconium fuel were identical to those routinely used for other fuels at ICPP.

1.23 Processing Problems. Various problems occurred during the startup portion of the campaign; these problems were not entirely unexpected, since thorough pilot plant proving of this process was bypassed to save both time and money. The early problems encountered included corrosion of an evaporator with titanium tubes, corrosion of a flowmeter having a vitreous enamel liner, and corrosion of a transfer jet.

Fuel element bridging in the dissolver basket became an increasingly troublesome problem as the run progressed, perhaps because the basket walls were gradually roughened, making it easier for elements to bridge. Fuel bridges prevented fresh fuel from falling into the dissolvent, thus terminating dissolution until the bridge was collapsed. At first these bridges were broken mechanically; later a temporary method of introducing dissolvent into the top of the dissolver was improvised which was very effective. Based on this experience, permanent modifications are being considered to make it possible to introduce dissolvent either to the top or to the bottom of the dissolver, or to split the dissolvent between the two locations as desired. With such a modification, it is believed fuel bridging will cease to be a major problem.

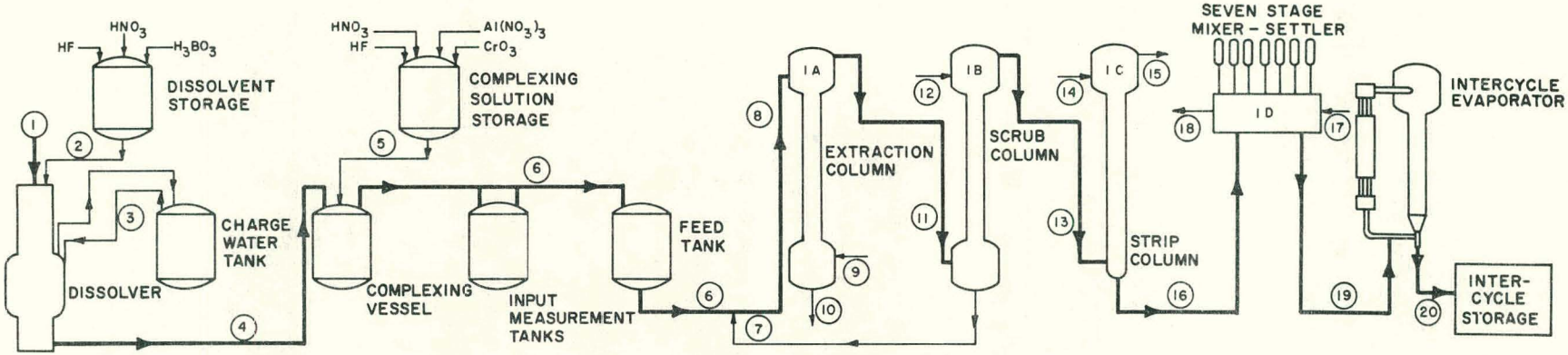

STREAM	1	2	3	4	5	6	7	8	9	10	11	12	13	14	15	16	17 and 18	19	20
DESCRIPTION	FUEL CHARGE	DISSOLVENT	CHARGE WATER	DISSOLVER PRODUCT	COMPLEXING SOLUTION	COMPLEXED DISSOLVER PRODUCT	1BR	1AF	1AX	1AR	1AP	1BS	1BP	1CX	1CR	1CP	1DX 1DR	1DP	FIRST CYCLE PRODUCT
Flow, l/batch		7115	1400	7310(c)	3700	11600(e)													
Flow, l/hr		532		532(d)		600(f)	60	660	415	660	415	60	415	200	415	200	10	200	2.7
Zr M				0.90		0.57		0.52		0.52									
F, M		6.60		6.42		4.05		3.68		3.68									
Al, M					1.96	0.62	0.75	0.63		0.63		0.75							
H, M (a)		6.63		2.83	1.41	2.23	0.55	2.07		2.02	0.08		0.001	0.005	0.0	0.007		0.007	0.4
NO_3^-, M		0.03		0.03	7.29	2.31	2.80	2.35		2.29	0.09	2.25	0.01	0.005	0.0	0.02		0.02	2.1
Sn, g/l				1.27		0.80		0.73		0.73									
Cr, g/l					2.50	0.80		0.73		0.73									
B, g/l		4.1	5.0	4.1		2.6		2.4		2.4									
U, g/l (no burnup)				1.41		0.89	0.20	0.83		4×10^{-3}	1.32		1.29		1×10^{-4}	2.67		2.67	200
Sp gr at 25°C		1.05		1.18		1.20	1.15	1.20	0.78	1.20	0.79	1.14	0.79	1.00	0.79	1.00	0.76	1.00	1.29
U, kg/batch (no B.U.) 10^{-3} (b)																			
Zr, kg/batch	600																		
Sn, kg/batch	9.3																		
TBP, %								5		5		5		5					
Diluent								Amsco		Amsco		Amsco		Amsco		Amsco			

(a) Neglecting any contribution from H_3BO_3.
(b) Based on PWR Core 1, Seed 1 with no burnup.
(c) Includes 195 liters of charge water heel.
(d) Actual flowrate after dissolver fills.
(e) Includes 590 liters of jet dilution. The process is continuous from this point forward.
(f) Average rate for a 24 hour period. Dissolution time per cycle is 13.4 hours. It is assumed that down time between dissolution cycles is 5.9 hours.

Fig. 2 Dissolution and first cycle extraction flow sheet for zirconium fuel.

Toward the end of the run, a minor hydrogen explosion occurred in the dissolver while it was being charged with fuel. There was no equipment damage, no spread of radioactive material, and no personnel injury. Subsequent investigation showed that the charge water, which is used to cushion the fall of the fuel elements into the dissolver, had picked up some hydrogen fluoride from residual dissolvent that remains in the dissolver after each dissolution cycle. The acid in the charge water reacted with metal in the dissolver and released a small but significant volume of hydrogen. Changes in the fuel charging procedure were made to improve the venting and purging of the dissolver. Thereafter, no further hydrogen problem was encountered.

Final cleanout of the dissolver was complicated by the presence of an accumulation of stainless steel pins which had been present in some of the fuel. The stainless steel residue was dissolved in 6M sulfuric acid, but in the course of this work it was found that the presence of stainless steel interfered with the dissolution of uranium residues by the usual chromic acid reagent. A discussion of this problem is given in Sections I-2.3 and I-2.4, dealing with laboratory support studies for the plant process.

1.3 Dissolution of SNAPTRAN 2/10A-3 Core in the ICPP Hot Pilot Plant
(A. P. Roeh, Development Engineering Section)

A temporary system for dissolving the fuel debris recovered from the SNAPTRAN 2/10A-3 test [a] was designed and installed in the ICPP Hot Pilot Plant. Though the core material could have been dissolved in the ICPP zirconium fuel system, a new hydrofluoric acid dissolution system was installed so an accurate determination could be made of the Cs-137 present in the fuel debris by analysis of the dissolver solution. The ICPP zirconium process dissolver would have been unsuitable because the SNAPTRAN solution would pick up Cs-137 from the walls of the contaminated dissolver. The Cs-137 measured was used to calculate the total fissions during the nuclear excursion and thus to arrive at an estimate of the total energy release. Installation of the new system in the Hot Pilot Plant also presented the opportunity to generate a substantial quantity of "cold" zirconium fluoride solutions for waste calcination development studies.

1.31 Dissolution System. The primary elements of the SNAPTRAN dissolution system, shown in Figure 3, were a dissolver system, an off-gas treatment system, a complexing tank, and a product receiver tank. The dissolver system, hydrogen fluoride addition system, and off-gas treatment system were located on the upper level (process makeup area) of the Hot Pilot Plant, while the complexing tank and the product receiver were located in adjacent cells, but at lower floor levels, to utilize gravity transfer through the system. Processing was done batchwise. Prior to the start of dissolution, the dissolver system was filled with a hydrofluoric acid solution. Fuel pieces were then charged and dissolved until a predetermined metal concentration in the solution was reached. This batch was then drained into the complexing tank, where the corrosive dissolver solution was "complexed" with aluminum nitrate, nitric acid, and chromic acid to produce a stable, noncorrosive solution compatible with the stainless steel extraction systems at the ICPP. After being complexed and sampled for accountability and

---

[a] SNAPTRAN fuel is 10 percent uranium and 90 percent zirconium hydride.

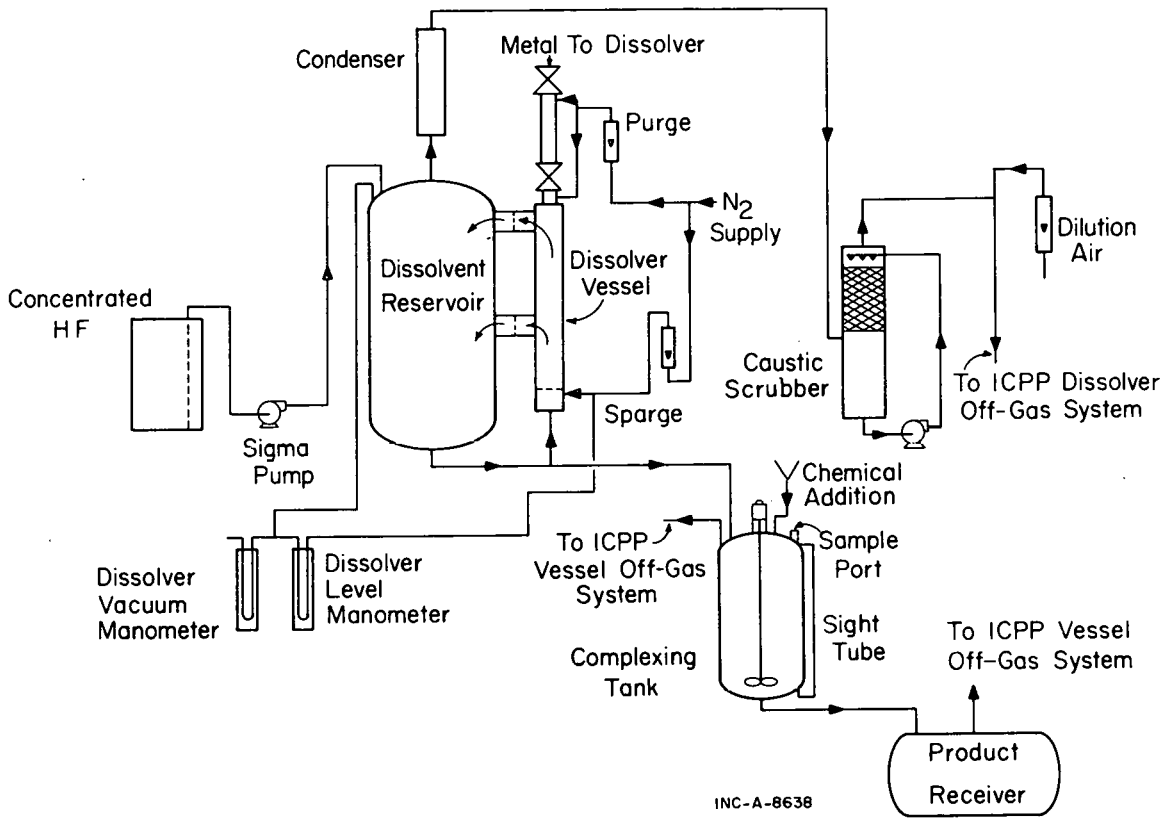

Fig. 3 SNAPTRAN (zirconium) fuel dissolution system.

Cs-137, the dissolver solution was drained into the product receiver for transfer into the main plant, where the uranium was recovered by solvent extraction.

The recirculating dissolver system consisted of a 350-gallon Monel vessel and a five-inch-diameter dissolution chamber connected so that dissolvent could be continuously circulated from the vessel through the chamber and back to the vessel. This configuration provided a critically safe chamber for the fuel and yet permitted the dissolver solutions to be made up in large batches. Perforated Monel plates were located in the recirculation path to retain the dissolving fuel in the critically safe dissolution chamber. A nitrogen sparge introduced at the bottom of the dissolution chamber, gases evolved during the reaction, and thermal gradients from the heat of reaction combined to maintain the recirculation flow between the dissolution chamber and the dissolvent reservoir. Fuel and zirconium metal were charged to the top of the dissolution chamber through a three-inch-diameter Monel pipe containing two block valves.

A condenser in the dissolver off-gas line removed most of the water and hydrogen fluoride from the off-gas. A caustic scrubber removed any remaining traces of hydrogen fluoride. Dilution air was added near the dissolver to reduce the hydrogen concentration below the lower explosive limit before the off-gas was introduced into the plant off-gas system.

Complexing was done in a 220-gallon stainless steel tank equipped with an agitator. Chemicals were added to the complexing tank through an inlet line connected to an addition funnel in the PM area. The product receiver served

also as a product transfer tank. The lines connecting the product receiver to the complexing tank were fitted with unions so the lines could be taken apart whenever the tank was to be removed from the cell. When filled, the tank was lifted out of the cell by an overhead crane and loaded onto a truck for transport to the ICPP processing area or the pilot plant calciner feed storage area, as desired.

1.32 Summary of Operations. Dissolution of scrap zirconium to produce simulated zirconium waste solutions for waste calcination development studies was completed before the SNAPTRAN fuel was processed. The cold scrap was processed first to prevent the possibility of contaminating the nonradioactive solutions if the dissolution system could not have been thoroughly decontaminated after processing the SNAPTRAN fuel. A total of 1,587 kilograms of scrap zirconium was dissolved to produce approximately 14,500 liters of complexed zirconium fluoride solution with an average concentration of 1.2M zirconium.

The process flow sheet for dissolving the SNAPTRAN 2/10A-3 fuel and complexing the dissolver solution is shown in Figure 4. The SNAPTRAN fuel is a 10 percent uranium (93 percent enriched) and 90 percent zirconium hydride material (1.8 weight percent H_2). Uranium solubility in hydrogen fluoride-zirconium solutions limits the metal dissolved to a maximum uranium content of approximately 2.2 percent. Therefore, additional zirconium metal was dissolved with the fuel so the weight of uranium would be less than 2.2 percent of the total weight of fuel plus zirconium metal. Despite the addition of the extra zirconium metal, considerable amounts of uranium-containing precipitates (predominately $UF_4 \cdot 3/4\ H_2O$) were formed. These were believed to have been caused by a high operating temperature ($\approx$ 90°C) in the dissolver and local uranium concentrations in the 5-inch-diameter section exceeding 2.2 percent of the dissolved metal. The precipitates adhered to the interior surfaces of the vessel during the hydrogen fluoride dissolution and were subsequently removed with heel cleanouts using 0.1M chromic acid at room temperature.

A total of 42.07 kilograms of core debris from the SNAPTRAN 2/10A-3 test was dissolved in the SNAPTRAN dissolution system. This material was dissolved in five dissolver batches and three heel cleanout batches. A total of 3.975 kilograms of uranium and 1.048×10^{17} atoms of Cs-137 were dissolved from this material.

1.4 Neptunium Recovery at the ICPP

(B. R. Wheeler, W. P. Palica; Plant Process Assistance Section)

About 1.1 kg of neptunium-237 were recovered at ICPP this year during routine processing of aluminum and zirconium alloyed fuel elements. Previous recovery had been limited to process demonstration quantities [1] with the bulk of the neptunium going into the liquid waste storage system. Currently, the neptunium at ICPP is stored as an intercycle nitric acid solution slightly contaminated with plutonium and fission products. The plutonium will be partitioned from the neptunium-bearing solution in existing small-scale extraction equipment; however, final purification of the neptunium must await the installation of an ion exchange and packaging facility [1]. Detailed design and construction of this facility are anticipated during the next year or two.

1.41 Process Description. The method employed at ICPP for recovering neptunium has been described in detail in the FY 1965 annual report [1]. Briefly, the process is as follows: The valence of neptunium in the dissolver product

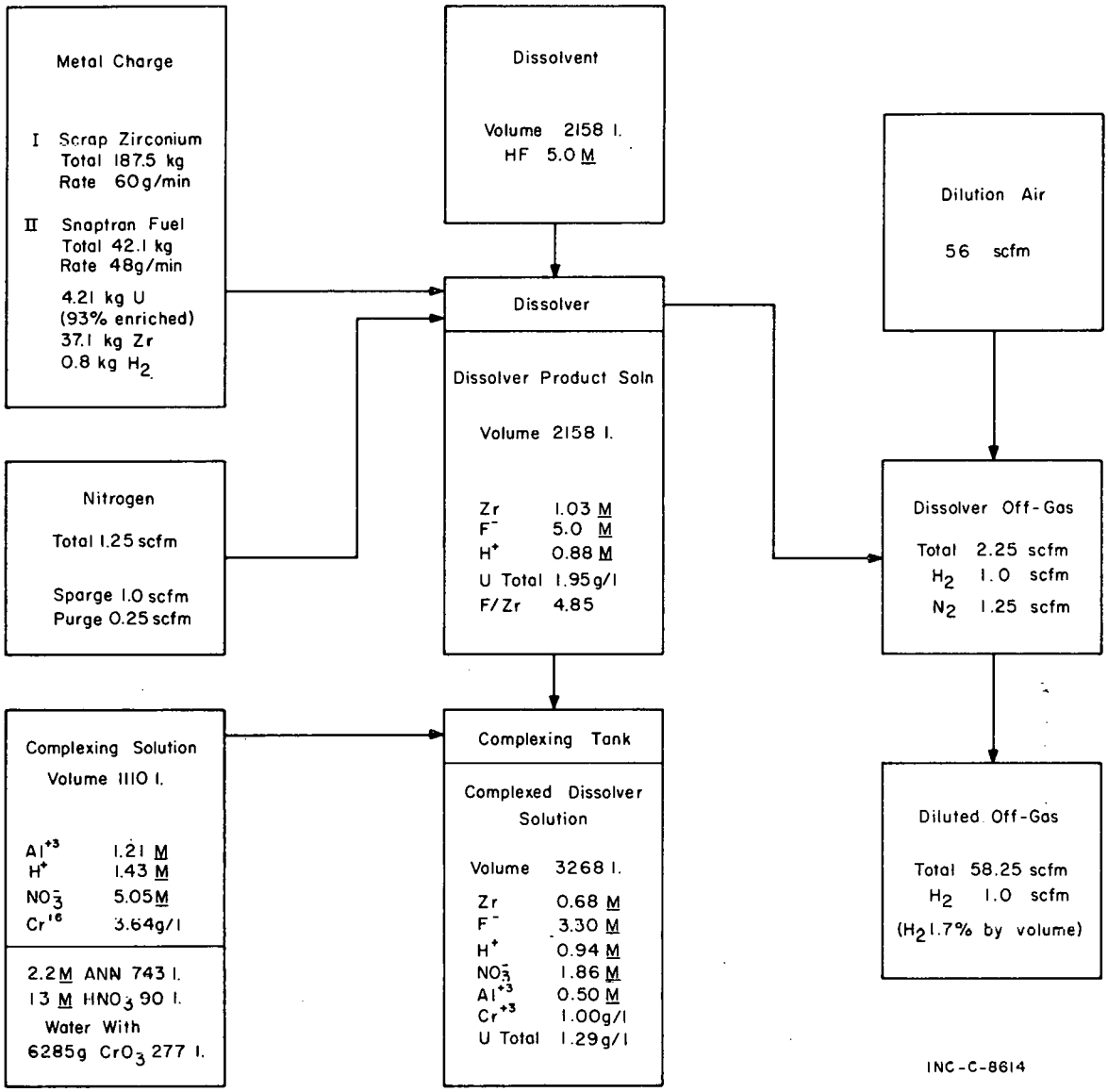

Fig. 4 SNAPTRAN fuel dissolution flow sheet.

is shifted to an extractable (VI) state with chromic acid. The neptunium and some plutonium are then extracted along with uranium in the first solvent extraction cycle using a TBP flow sheet. In the second cycle, neptunium and plutonium are reduced with ferrous sulfamate and are partitioned from uranium using an acid-deficient Hexone flow sheet. The neptunium and plutonium appear in the second cycle raffinate; this raffinate is concentrated and then processed through another solvent extraction cycle using the TBP flow sheet shown in Figure 5. The intercycle product from this cycle (the material currently in storage at ICPP) will be processed further through a TBP extraction system to partition the plutonium from the neptunium, and the neptunium will undergo final decontamination by an ion exchange process.

1.42 Process Performance. The feasibility of using five-percent TBP to recover neptunium from the second cycle raffinate, instead of the previously

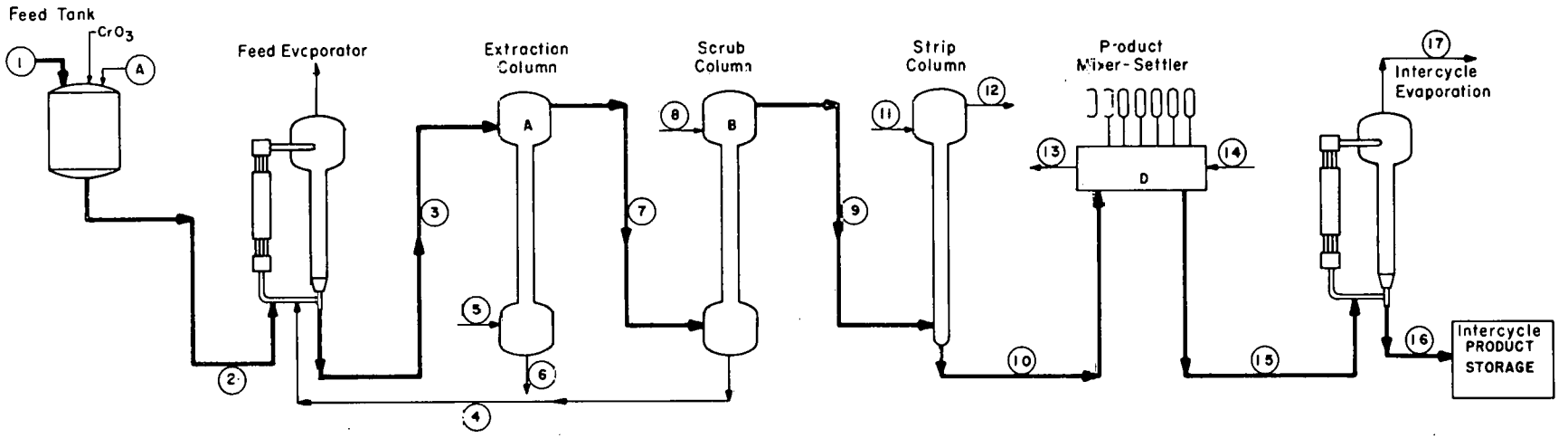

STREAM	(a)	A	2	3	4	5	6	7	8	9	10	11	12	13	14	15	16	17
DESCRIPTION	SECOND CYCLE RAFFINATE	ADDITIVE	RAW FEED	AF	BR	AX	AR	AP	BS	BP	CP	CX	CR	DR	DX	DP	PRODUCT	EVAPORATOR OVERHEAD
FLOW, l/batch																		
FLOW, l/hr			475	500	25	500	500	500	25	500	200	200	500	10	10	200	2.5	197.5
TBP, %						5		5		5			5					
DILUENT						Amsco		Amsco		Amsco			Amsco	Amsco	Amsco			
SP. GR. AT 25°C	1.274		1.281		1.159	0.78	1.280	0.78		0.78			0.78	0.76	0.76	1.001	1.02	
$Al(NO_3)_3$ M	1.75		1.57	1.54	1.00		1.54		1.00									
HNO_3 M		13	1.05	1.00			1.00				0.01	0.01				0.01	0.8	
NH_4OH M	0.23																	
NH_4NO_3 M	0.21		0.40	0.38			0.38											
CrO_3 M			0.01	0.01	0.01		0.01		0.01									
Np g/l	0.03		0.027	0.026			1.3×10^{-2}	0.024		0.024	0.06		2.4×10^{-1}			0.06	4.8	
U g/l	5.8×10^{-3}		5.3×10^{-2}	5.0×10^{-3}			2.0×10^{-4}	4.8×10^{-6}		4.8×10^{-3}	0.01		4.8×10^{-5}			0.01	0.8	

(a) Estimated Composition Of Raffinate From The Second Extraction Cycle

INC-8-8644

Fig. 5 Neptunium concentration cycle flow sheet.

considered 10-percent TBP [1], was established during the plant operation. Use of the five-percent TBP was tested as a matter of convenience only. This TBP concentration was being used during the fuel reprocessing operations, and any change in concentration for the initial neptunium recovery would have required two adjustments of the organic composition.

Chromic acid was added routinely to the dissolver product (with the complexer solution) for zirconium alloyed fuels as indicated in the first extraction cycle flow sheet, Figure 2 (Section I-1.2), to oxidize the uranium; chromic acid was added to the dissolver product in the aluminum alloyed fuels flow sheet, as indicated in Figure 1 (Section I-1.1), specifically to improve neptunium recovery. Early during the zirconium-alloyed-fuel processing campaign, high neptunium losses were experienced until chromic acid was also added to the IBS stream. After that, chromic acid was specified in the IBS stream for aluminum fuels also, and neptunium losses were decreased to 5 to 15 percent in the first extraction cycle of the fuel-processing flow sheets. Neptunium losses from the second cycle were nil, and less than one percent loss was experienced in the neptunium concentration cycle.

2. LABORATORY SUPPORT STUDIES FOR CURRENT ICPP FUEL RECOVERY PROCESSES

2.1 Effect of Boron Carbide Upon the Extraction Cycle During Reprocessing of ATR Fuel

(B. E. Paige; Chemistry Section)

It is very likely the fuel from the Advanced Test Reactor (ATR) will have a composition which is different from the fuels from the Material Testing Reactor (MTR) and the Engineering Test Reactor (ETR) which have been processed previously at the Idaho Chemical Processing Plant (ICPP). The dissolution rate of proposed ATR fuels has been studied and reported previously [7]. The additional work reported here was performed to determine the effect of the boron carbide (B_4C), which may be present in the dissolver product from ATR fuel, upon the first extraction cycle.

Coalescence tests performed in this work indicate that the boron carbide solids could cause difficulty in the operability of the extraction column in the first cycle. The coalescence characteristics of this type of solution were improved by either the addition of 100 ppm of gelatin or the removal of the solids. Solutions from the scrubbing, stripping, and product and solvent cleanup steps did not form stable emulsions and should cause no processing difficulty.

2.11 Fuel Description and Experimental Technique. The ATR fuel core may be either UAl_3, U_3O_8, or UO_2 in Type X-8001 aluminum and may contain about 0.19 percent boron carbide added as solids having a size of less than 325 mesh (44μ). The intended cladding material is Type 6061-0 aluminum. Coupons prepared for irradiation tests [8] were used for the current experiments and contained about 0.06 percent boron carbide, the same as the overall composition of the fuel.

Two coupons, one containing UAl_3 and one containing UO_2, were dissolved in 6.6M nitric acid containing 0.05M mercuric nitrate to give solutions about

1.3M in aluminum. A tenfold excess of boron carbide, sieved to less than 325 mesh was added to half of each dissolver product solution, and the solution was heated at reflux for one hour. These solutions were each extracted, scrubbed, and stripped in single stages under flow sheet conditions. The extraction was performed with 3.25-percent tributyl phosphate (TBP) in kerosene, using an aqueous-to-organic ratio of 1.31/1. The organic product from the extraction step was scrubbed with 0.75M aluminum nitrate containing 0.01M chromic acid, using an aqueous-to-organic ratio of 0.16/1. The organic product was then stripped with 0.05M nitric acid, using an aqueous-to-organic ratio of 0.53/1. Portions of the products and raffinates from each of these steps were tested with an emulsion stability indicator [9], a device which measures the dispersion and coalescence times and thereby indicates the tendencies of solutions to form stable emulsions.

2.12 Experimental Results. The dispersion-coalescence tests indicated possible difficulty in the operability of the plant extraction column. When aqueous dissolver product containing a normal amount of boron carbide was dispersed with the TBP-kerosene, the main body of the emulsion coalesced in about 150 to 180 seconds (an acceptable time), but a spider web type film was left behind, indicating that some difficulty may be encountered in the operation of the extration column. The amount of the spider web and its stability decreased with repeated dispersions. In experiments with solutions containing a tenfold excess of boron carbide, coalescence times were slightly longer, and solids were observed to collect at the organic-aqueous interface during the extraction step. This showed that the boron carbide in the fuel could indeed have an effect upon the column operability. Dispersion-coalescence tests were very satisfactory for the scrubbing, stripping, and kerosene washing steps, indicating that no difficulty should be encountered in the rest of the first cycle.

When 100 ppm of gelatin was added to the dissolver product solutions and these were boiled for about five minutes, the dispersions with TBP-kerosene coalesced more rapidly, and no solids appeared at the aqueous-organic interface. This technique has been used to alleviate emulsion problems with fuels containing silicon and apparently is also effective with boron carbide. Upon the addition of the gelatin, the fine boron carbide particles appeared to agglomerate, but the solids redispersed readily upon agitation. Removal of the boron carbide from solutions which had not been treated with gelatin by filtration also improved the coalescence of the dissolver product solution during extraction with TBP-kerosene.

2.2 Dissolution Rates for Zircaloy-2 and Aluminum in Dilute Hydrofluoric Acid Containing Boric Acid

(B. E. Paige; Chemistry Section)

During the processing of zirconium fuel at the ICPP, significant quantities of hydrogen have occasionally accumulated in the dissolver during the charging of the fuel. Zircaloy-2 clad fuel and zirconium scrap in aluminum cans are dropped into the dissolver, which is partially filled with water to cushion the impact of the fuel on the dissolver vessel. The cushioning water, which contains sufficient boric acid to provide 6.3 grams of boron per liter as a neutron poison, may also contain small amounts of residual hydrofluoric acid from the dissolver since the water is recycled between the dissolver and a holding vessel for a number of chargings. Dissolution rates at 95°C for Zircaloy-2 in 0.5 to 1.0M hydrofluoric acid have been reported previously [10]. In the current work,

initial dissolution rates for Zircaloy-2 and aluminum (at 20.6°C and hydrofluoric acid concentrations of 0.1, 0.01, and 0.001M in the boric acid solutions) were determined to be sufficient to generate the quantities of hydrogen observed in the dissolver.

The dissolution rates obtained are presented in Figure 6. The rates for Zircaloy-2 and aluminum, Type 6061-T6, are similar at about 0.02M hydrofluoric acid, but the slope of the dissolution curve for Zircaloy-2 is greater; therefore, the dissolution rate for the Zircaloy-2 increases more rapidly than the rate for aluminum at higher concentrations of hydrofluoric acid. The rates at 0.001M hydrofluoric acid are possibly low because of the decrease in the concentration of the hydrofluoric acid during the dissolution. The coupling of the two metals during dissolution does not increase the dissolution rate of either metal in boric acid solutions containing 0.01M hydrofluoric acid.

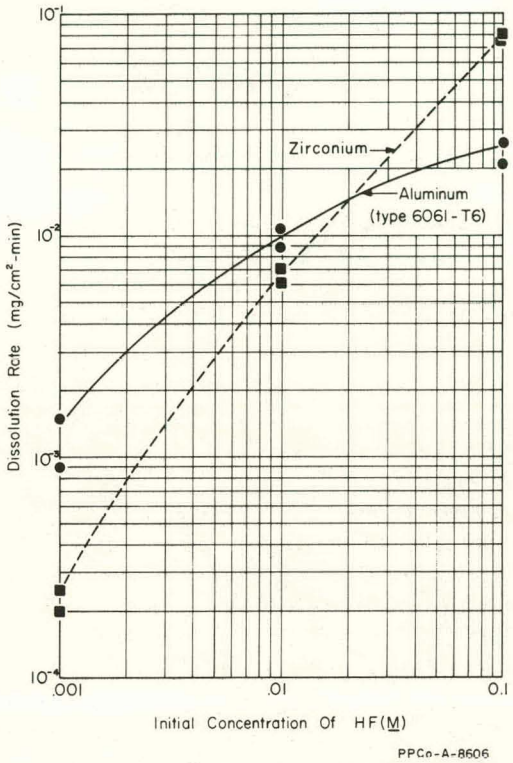

Fig. 6 Dissolution rates for Zircaloy-2 and aluminum in boric acid and dilute hydrofluoric acid at 20°C.

Based on the observed rates, 0.01M hydrofluoric acid in a 20°C boric acid solution containing 6.3 grams of boron per liter will produce about three liters of hydrogen per hour per square meter of Zircaloy-2 surface. The addition of the aluminum cans to the fuel charge is not the primary cause of the production of the quantities of hydrogen measured in the dissolver, because neither the aluminum nor the aluminum-zirconium couple has rates significantly higher than the rate for zirconium, and the surface area of the cans is relatively low compared to the surface area of the fuel. Based on estimated surface area and fuel charge for zirconium fuel, quantities of hydrogen equivalent to that found in the dissolver can be produced in a nonventilated system at concentrations as low as 0.003M hydrofluoric acid which can conceivably be present in the cushioning water because of repeated use of the same water.

The accumulation of hydrogen in the dissolver during charging of the fuel is now avoided by adequately ventilating the vessel.

2.3 Cleanout of Zirconium-Fuel Dissolver Heel with Chromic and Sulfuric Acids (R. G. Butzman; Chemistry Section)

Following the 1965 zirconium alloy fuel processing campaign, the dissolver vessel contained a visible accumulation of Type 304 stainless steel pins (known to have been in some of the fuel charged) and a significant amount of uranium (indicated by material accountability balances) presumably deposited as uranium tetrafluoride. A combination of cleanout treatments, chiefly 0.05M CrO_3

solution, varying concentrations of hydrofluoric acid, and water rinses were used individually and alternately in attempts to recover this uranium. When the uranium in the last several 0.05M CrO_3 washes leveled off at a low concentration, use of this solution was discontinued and several batches of 6M H_2SO_4 were put through the dissolver to dissolve out the stainless steel. Unexpectedly, a substantial portion of the total uranium recovered during the cleanout procedure (about 60 percent) was found in the sulfuric acid solutions. A laboratory demonstration was set up to explore why the final few 0.05M CrO_3 washes (the reagent normally used for UF_4 heel cleanouts accompanying zirconium fuel processing) had dissolved only negligible amounts of uranium when about eight kilograms of it were still in the dissolver.

Simulation of the plant dissolver heel-out was performed in a Monel laboratory-scale dissolver with a Monel fuel basket present. The dissolver was charged with Type 304 stainless steel strips and zirconium-uranium alloy pieces. Every effort was made in the laboratory to simulate the known conditions of the plant dissolver. Examination of the laboratory dissolver contents, following a prolonged hydrofluoric acid digestion period, revealed a moderately heavy coating of dark green crystals on all immersed surfaces and particularly on the stainless steel pieces (Figure 7). Exposure to two batches of 0.05M CrO_3 solution resulted in only partial removal of the green crystalline deposit and the coating of the remaining deposit with a brown residue. The third and final heel-out step, 6.0M H_2SO_4, dissolved everything -- brown residue, fluoride salts, and stainless steel. The recovered uranium was distributed as follows:

1st chromic acid batch	22%
2nd chromic acid batch	46%
sulfuric acid batch	32%.

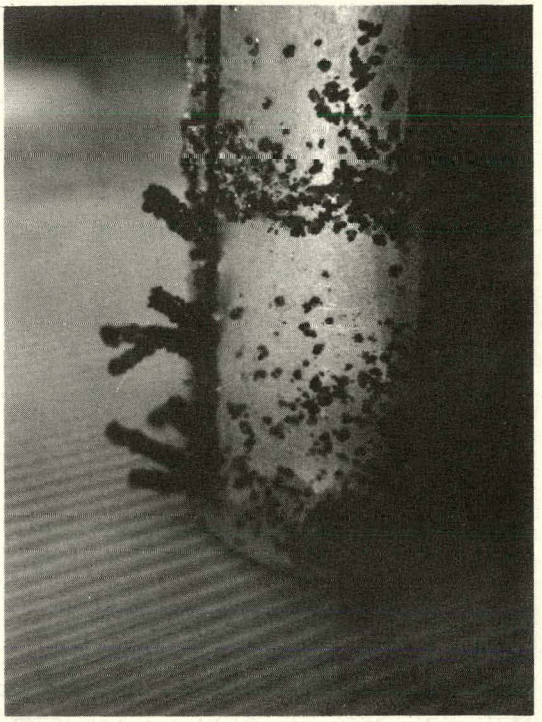

Fig. 7 Dissolver basket showing fluoride crystal deposit on stainless steel and Monel.

The laboratory scale demonstration showed that the presence of the stainless steel was responsible for the peculiar cleanout behavior experienced. The reaction between hydrofluoric acid and stainless steel was sufficient to supersaturate the fluoride dissolvent with iron, chromium, and nickel fluorides, which are of limited solubility. These fluorides crystallized out on the immersed surfaces, forming a matrix for the inclusion of uranium tetrafluoride. Upon reaction with chromic acid solution, these mixed fluorides produced a residue which coated the remainder of the crystalline deposit and inhibited further reaction between chromic acid and the uranium tetrafluoride. (Spectrographic analysis of the brown residue revealed it to be about 35 percent iron; X-ray diffraction identified the chief crystalline component as beta iron (III) oxide-hydroxide. It

dissolved very readily in 6.0M H_2SO_4 at 90°C.) The distribution of recovered uranium in the laboratory demonstration differed noticeably from the plant results; however, this is probably due to the fact that in the plant dissolver the mixed fluoride crystal deposit was built up over many days, as opposed to only 45 hours in the laboratory dissolver.

2.4 Corrosion of Monel Dissolver During Cleanout with Chromic and Sulfuric Acids

(D. W. Rhodes, T. L. Hoffman, C. A. Zimmerman; Chemistry Section)

Processing of spent zirconium-containing reactor fuels is accomplished at ICPP by dissolution of the fuel in fluoride-containing solutions in a Monel-400 vessel (Section I-1.2). Cleanout of the dissolver during and upon completion of the recent processing operation was accomplished by use of solutions of hydrofluoric acid (7 to 20M), chromic acid (0.05 and 0.1M), and sulfuric acid (6M) (see Section I-2.3).

Laboratory investigation of the corrosive effects of these reagents indicates that sulfuric acid is the most corrosive (8 mils per month) of the cleanout solutions tested and should be used with caution in cleaning the Monel-400 plant dissolver. The hydrofluoric acid and chromic acid cleanout solutions are not excessively corrosive and can be used as desired in cleaning operations in this vessel; however, when possible, chromic acid use should be avoided immediately following use of 20M hydrofluoric acid.

Actual plant specimen corrosion data obtained in one cleanout operation at the end of a campaign indicated a corrosion loss of 0.64 mil of metal from the Monel-400 dissolver (a corrosion rate equivalent to 1.9 mils per month).

2.41 Laboratory Test Program. Laboratory experiments were conducted to determine the corrosion rates for Monel-400 in each of the individual acids and the corrosion rates resulting from alternate exposure to the different acids. Each test, conducted under the conditions outlined in Table IV, involved four 24-hour periods of exposure to acid reagents; fresh acid was used for each of the 24-hour periods. The acid was sparged for at least one-half hour by bubbling water-pumped nitrogen through the solution prior to introducing the test specimen into the solution. The nitrogen flow was then reduced, but was maintained throughout the test periods. The welded Monel-400 specimens were flushed thoroughly with tap water and then rinsed in boiling acetone before being weighed at the beginning of the test and after each portion of the test.

The laboratory data presented in Table IV indicate that Monel-400 does not corrode excessively in any of the individual acids except 6M sulfuric acid; that reagent produced an average corrosion rate of 8.0 mils per month over four consecutive 24-hour periods at 114°C. In the alternating systems, the corrosion of Monel-400 is appreciably increased in chromic acid following 20M hydrofluoric acid. The corrosion of Monel-400 in chromic acid (0.05 and 0.1M) shows a tendency to increase upon a second exposure to chromic acid in a system of alternating 7M hydrofluoric acid and chromic acid.

2.42 In-Plant Test. Two Monel-400 test cylinders were placed in the plant Monel-400 dissolver just before the final cleanout operation started and were withdrawn following the operation. Table V lists the chemical solutions used for cleanout as well as the plant dissolver service temperature. The observed

TABLE IV

CORROSION OF WELDED MONEL-400 IN ACID MEDIA
(Mils per Month)

Test	Period	7M HF (65°C)	20M HF (65°C)	0.05M CrO_3 (65°C)	0.1M CrO_3 (65°C)	6M H_2SO_4 (114°C)
			Individual Acids			
1-5	1	0.06	0.02	0.01	0.06	8.94
	2	0.01	0.03	0.01	0.02	7.61
	3	0.03	0.07	0.02	0.01	7.45
	4	0.07	0.07	Weight Gain	0.00	7.80
Test	Period	7M HF (65°C)	20M HF (65°C)	0.05M CrO_3 (65°C)	0.1M CrO_3 (65°C)	6M H_2SO_4 (114°C)
			Alternating Acid Systems			
6	1	0.05	----	----	----	----
	2	----	----	0.02	----	----
	3	0.04	----	----	----	----
	4	----	----	0.14	----	----
7	1	0.04	----	----	----	----
	2	----	----	----	0.06	----
	3	0.03	----	----	----	----
	4	----	----	----	0.11	----
8	1	0.06	----	----	----	----
	2	----	----	----	----	7.31
	3	0.05	----	----	----	----
	4	----	----	----	----	6.57
9	1	0.06	----	----	----	----
	2	----	----	----	Weight Gain	----
	3	----	0.04	----	----	----
	4	----	----	----	0.28	----
10	1	0.11	----	----	----	----
	2	----	----	----	----	5.31
	3	----	0.05	----	----	----
	4	----	----	----	----	6.58
11	1	0.09	----	----	----	----
	2	----	----	----	0.09	----
	3	----	----	----	----	14.85
	4	0.07	----	----	----	----

TABLE IV (Contd.)

CORROSION OF WELDED MONEL-400 IN ACID MEDIA
(Mils per Month)

Test	Period	7M HF (65°C)	20M HF (65°C)	0.05M CrO_3 (65°C)	0.1M CrO_3 (65°C)	6M H_2SO_4 (114°C)
			Alternating Acid Systems			
12	1	0.12	----	----	----	----
	2	----	----	----	0.14	----
	3	----	0.09	----	----	----
	4	----	----	0.25	----	----
13	1	----	0.14	----	----	----
	2	----	----	0.34	----	----
	3	----	----	----	----	7.70
	4	----	----	0.10	----	----
14	1	----	0.10	----	----	----
	2	----	----	----	0.29	----
	3	----	----	----	----	8.36
	4	----	----	----	0.09	----

TABLE V

REAGENTS USED TO CLEAN OUT MONEL-400 DISSOLVER

Order of Addition to Dissolver	Solution	Concentration	Temperature (°C)	Service (hours)
1	Hydrofluoric Acid	20.0 M	75	4.5
2	Hydrofluoric Acid	14.0 M	75	12.5
3	Chromic Acid (CrO_3)	0.1 M	60 to 70	11.5
4	Hydrofluoric Acid	7.0 M	60 to 70	14.0
5	Chromic Acid (CrO_3)	0.05 M	60 to 70	36.5
6	Sulfuric Acid[a]	6.0 M	92	164.5
			Total Hours	243.5

[a] The sulfuric acid treatment was necessary to remove a heel of stainless steel spine which had been incorporated in the zirconium fuel elements.

average corrosion rate on the test cylinders was 0.64 mil in 243.5 hours, which is equivalent to 1.9 mils/month. Microscopic examination of these cylinders indicated that very mild denickelization occurred; the original machining marks were still present on most of the surface area.

3. SUPPORT STUDIES FOR SCHEDULED ICPP PROCESSING OPERATIONS

3.1 Recovery of Uranium from EBR-II Scrap

(D. W. Rhodes, M. W. Wilding, M. E. Jacobson; Chemistry Section)

A significant amount of uranium is present in "scrap" from the melt refining crucible (skull oxide) and the injection casting molds (Vycor glass) from the pyrometallurgical process at the EBR-II Fuel Cycle Facility. Laboratory tests undertaken to study the feasibility of recovery operations indicate that about 99 percent of this uranium can be recovered from the scrap materials by dissolving or leaching with a solution of nitric acid. It is anticipated that these materials will be processed at the Idaho Chemical Processing Plant in the near future.

3.11 Dissolution of Skull Oxide Material. The skull oxide is a black granular material containing 75 to 85 percent uranium and 2.8 to 5.8 percent fission oxides. This material is shipped in 6061-T-1 aluminum cans with a weight ratio of aluminum can to skull oxide in the range 1.3 to 1.6. In laboratory experiments, the uranium in the skull oxide was approximately 99 percent dissolved in 8 hours using a dissolvent containing 7.5M HNO_3, and 0.007M $Hg(NO_3)_2$ at 105°C. Aluminum metal was used to represent the dissolved aluminum can. The composition of the dissolver product resulting from the nitric acid dissolution is shown in Table VI, and the time dependence of the dissolution of uranium in the nitric acid system is shown in Table VII.

TABLE VI

COMPOSITION OF DISSOLVER PRODUCT[a]

U (g/l)	H (M)	NO_3 (M)	Al (g/l)	Hg	Dissolved (percent)
18.06	2.65	6.04	31.7	Not Determined	98.8

[a] Dissolvent: 7.5M HNO_3-0.007M $Hg(NO_3)_2$
Scrap Concentration: 24 g skull oxide/liter.

Approximately 99 percent of the uranium and 85 to 90 percent of the skull oxide dissolved in 8 hours. The undissolved skull oxide remaining from the nitric acid dissolution was in a finely divided form, estimated microscopically to be 10 to 100 microns diameter, with the greatest percentage in the range 10 to 50 microns. This material was nearly all dissolved (97 percent) in 4.0M HNO_3-0.7M HF in five hours at 105°C.

3.12 Dissolution of Injection Casting Mold (Vycor glass). The Vycor glass tubing, which is used as a mold for forming the uranium fuel pins in the EBR-II Fuel Cycle Facility, is removed from the fuel pins by crushing the glass; however, small amounts of uranium adhere to the glass. This uranium was leached in laboratory experiments using a four-step procedure, as follows, to determine what treatment was necessary to recover the uranium.

(1) The glass was leached in 6M HNO_3 at room temperature for 5.5 hours, the solution decanted, and the glass rinsed with about 25 ml of distilled water.

(2) The glass was leached in boiling 6M HNO_3 for five hours, the solution decanted, and the glass rinsed with about 25 ml of distilled water.

(3) The glass was leached in boiling 6M HNO_3-0.1M HF for five hours, the solution decanted, the glass rinsed with about 25 ml of distilled water.

(4) To obtain a material balance for the uranium, the remaining material was dissolved in warm 20M HF (about 40°C) and the dissolver rinsed with about 25 ml of distilled water.

TABLE VII

EFFECT OF TIME ON URANIUM DISSOLUTION FROM SKULL OXIDE[a]

Time (hours)	Uranium Dissolved (percent)
0.5	95.6
1.0	96.7
2.0	97.2
3.5	98.6
8.0	98.8
24.0	99.4

[a] Dissolvent: 7.5M HNO_3-0.007M $Hg(NO_3)_2$

Temperature: 105°C.

The results obtained on a small sample of glass, using the four preceding steps in the order listed, are given in Table VIII. Inasmuch as 99 percent of the uranium was recovered by the first treatment (Step 1), this will probably be the only treatment used in the actual processing of the glass scrap. Plutonium and thorium recoveries are of no concern because of the small quantities involved.

TABLE VIII

QUANTITY (OR ACTIVITY) OF CONSTITUENTS RECOVERED BY LEACHING

Type Number	Volume (ml)	U Recovered		Pu Recovered		Th Recovered[a]	
		g/l	Percent	Disintegrations/min-ml	Percent	Mg/ml	Percent
1	47.0	3.4×10^{-2}	99.15	2740	90.0	0.06	8.8
2	53.0	5.0×10^{-5}	0.15	90	2.9	0.03	4.4
3	61.5	5.0×10^{-5}	0.15	107	3.5	0.03	4.4
4	46.0	1.91×10^{-4}	0.55	109	3.6	0.56	82.4

[a] A coating of ThO_2 is used on the glass prior to forming the fuel pin.

3.13 Extraction and Stripping of Uranium. A dispersion-coalescence test was performed on the nitric acid-uranium dissolver product from the skull oxide dissolution. Complete coalescence occurred in 1.5 minutes, a satisfactory coalescence performance; however, there was a slight "holdup" of organic material in the aqueous phase beneath the plates. Three extraction stages were run using five-percent TBP and an adjusted dissolver product that contained 1.6M Al^{+3}, about 1.3M H^+, and about 21 g/l uranium; the ratio of organic to

aqueous was 1:1. Uranium distribution coefficients for the extraction and stripping systems are shown in Table IX.

TABLE IX

RESULTS OF MULTISTAGE URANIUM EXTRACTION AND STRIPPING OF SKULL DISSOLVER PRODUCT

Extraction[a]

Products	g/l	Raffinates	g/l	E o/A
IAP_1	9.12	IAR_1	0.218	42
IAP_{11}	0.443	IAR_{11}	0.0034	130
IAP_{111}	0.006	IAR_{111}	0.0003	19

Stripping[b]

Products	g/l	Raffinates	g/l	E a/o
ICP_1	41.1	ICR_1	2.01	20
ICP_{11}	1.48	ICR_{11}	0.03	49

[a] Extractant: 5 percent TBP

[b] Strip Solution: 0.02M HNP_3.

The distribution coefficients for uranium extraction from the dissolver product indicate that adequate uranium recovery is possible. Small quantities of residual oxides that carried over from the dissolver to the extraction column did not impair the efficiency of the laboratory extraction-stripping process.

3.2 Dissolution and Recovery of Fuel from the LOFT Reactor (R. G. Butzman; Chemistry Section)

Following a LOFT experiment the fuel from the reactor core will be processed to recover the uranium and to provide representative samples of dissolved fuel. The concentration of selected fission products in these samples will be determined to complete the fission product material balance and to describe fission product behavior during the experiment. Dissolution of the fuel rods of uranium dioxide clad in Zircaloy-4 which are not affected by the experimental conditions can be accomplished simply; however, where melting of the cladding and the uranium dioxide has occurred, and physical mixing and possibly compound formation may have taken place, quantitative dissolution will be more difficult. To represent this latter situation, the melted fuel residue from the Contamination-Decontamination Experiments (CDE) (Section III-1.2) is being dissolved. This work

will provide developmental experience for the reprocessing of the LOFT cores and will furnish analytical samples for the study of fission product behavior in the CDE.

In preliminary studies with unirradiated Zircaloy-clad uranium dioxide (which had been melted) it was learned that various mixtures of nitric and hydrofluoric acids, at times with chromic acid present, were fairly effective in dissolving the fuel. However, these mixtures were incompatible with any known metallic construction material, suggesting that their use in the Chemical Processing Plant was highly improbable. As a substitute for the mixed acids, alternate pure 8M HNO_3 and 10M HF were used in dissolving the melted fuel pin from Run 1 in CDE (with water rinses after each acid to minimize mixing of the acids). A Carpenter-20 vessel was used for the dissolution. The dissolver product solutions and rinses were combined by adding the hydrofluoric acid to the nitric acid solution; this order of mixing avoids the formation of a permanent precipitate. Dissolution appeared to be complete using alternate application of nitric and hydrofluoric acids. The resulting dissolver product was sparged with nitrogen and sampled three times each at the top and bottom of the 12 liter volume; good analytical agreement between samples indicated that a homogeneous dissolver product had been obtained.

3.3 Dissolution Studies of Zirconium Dioxide-Uranium Dioxide Fuels (R. G. Butzman; Chemistry Section)

In 1964, a preliminary flow sheet was developed for the aqueous reprocessing of sintered wafers of enriched uranium dioxide-zirconium dioxide clad in Zircaloy-4[11]. This type of fuel constitutes the first seed of the second core of the Pressurized Water Reactor (PWR) at Shippingport, Pennsylvania. Recently, some additional work was performed in the laboratory to investigate in more detail several important aspects of the dissolution portion of the flow sheet. For this supplemental study, a laboratory dissolver was designed and fabricated entirely of Monel to represent the existing plant dissolver. (The laboratory-scale vessel had approximately 1/1000 the working volume of the plant vessel.) The proposed batch dissolution flow sheet consists of the following 3 steps:

(1) Decladding with 5.0M HF, 0.1M KF solution

(2) Dissolution of the ZrO_2 and conversion of the UO_2 to insoluble UF_4 in 20M HF, 0.05M KF

(3) Dissolution of the UF_4 with 0.1M CrO_3 solution.

All three dissolution steps were performed in an atmosphere of nitrogen. Addition of aluminum nitrate to the dissolver product solution yields a feed suitable for solvent extraction.

The primary goals in this study were: (a) to establish whether the proposed flow sheet can accomplish complete dissolution in the laboratory-scale dissolver under simulated plant dissolver conditions; (b) to see if centrifugation appears necessary for recovering suspended solid UF_4 from the withdrawn ZrO_2 dissolvent; (c) to make preliminary observations of the corrosion of Monel associated with the flow sheet; (d) to determine if some favorable revisions could be made in the flow sheet with respect to reagent quantities in the second and third dissolution steps.

Several runs in the laboratory-scale dissolver demonstrated that complete dissolution of the ceramic fuel could be achieved. The combined uranium loss to the waste streams amounted to less than 0.2 percent of the total uranium in the system. The uranium that escaped via the waste streams did so in solution; there was no evidence of any solid UF_4 being physically carried out of the dissolver. Preliminary corrosion measurements made on the components of the dissolver suggested that this flow sheet may result in a higher than desirable rate of attack on Monel. Alternating exposure to hydrofluoric and chromic acids is more corrosive than either reagent individually. (See Section I-2.4 on corrosion of Monel during cleanout operations.) Analyses have shown that the ZrO_2 dissolvent (20M HF) preferentially dissolves nickel. The chromic acid attacks both components of the alloy so there is little chance for passivation of the Monel to occur. The initially proposed flow sheet [11] was modified somewhat during this series of experiments. Complete dissolution was achieved in the same digestion periods using one-fourth of the original flow sheet quantity of ZrO_2 dissolvent, and one-half of the original flow sheet quantity of UF_4 dissolvent.

A single experimental run was made with this flow sheet on an irradiated fuel sample representative of PWR Core 2, Seed 1. Unexplainably, the uranium loss to the waste streams, although not unacceptably high, was several times greater than with the unirradiated fuel.

In attempting to predict the versatility of the flow sheet, some limited investigative work was done with UO_2-ZrO_2 wafers that contain about five-percent CaO. (Later seeds of PWR Core 2 are expected to contain UO_2-ZrO_2-CaO wafers.) In a comparative test, using identical flow sheets, it was shown that the wafers with CaO dissolve about one-tenth as rapidly as the UO_2-ZrO_2 fuel.

4. GRAPHITE FUEL REPROCESSING

A large amount of spent graphite fuel will be generated by the nuclear rocket test programs and the Peach Bottom and Colorado High Temperature Gas Cooled (HTGR) power reactors. No existing processing facility is capable of reprocessing graphite fuels; nor has a process for graphite fuels been fully developed. Development studies at ORNL and BNL indicate that a fluidized-bed burn-leach process is best suited for both the HTGR and nuclear rocket fuels. Development of this process is being continued at the ICPP on a pilot plant scale.

The burn-leach process as proposed by ORNL consists of burning the graphite fuel in a fluidized bed of inert alumina particles followed by leaching the uranium from the ash-alumina mixture and recycling the alumina to the fluidized-bed burner. Present pilot plant development effort at ICPP is centered around effecting a dry physical separation of the metal oxide combustion products (ash) from the inert alumina particles. Dry separation of the ash from the alumina will eliminate much of the solids handling and liquid-solids separation operations otherwise required in the burn-leach process.

In addition to the pilot plant development program, a moderate laboratory development program is being conducted to evaluate other processes proposed for graphite fuels.

4.1 Pilot Plant Studies on the Fluidized-Bed Burn-Leach Process

(L. T. Lakey, A. P. Roeh, W. B. Kerr; Development Engineering Section)

A four-inch-diameter fluidized-bed graphite burner and ash collection system was installed in the ICPP Hot Chemistry Laboratory to test the principle of in-bed separation of the metal oxide combustion products from the alumina by elutriation of these metal oxide particles from the burner in the off-gas stream. Results of initial tests, in which approximately 77 kilograms of Rover fuel have been burned, show that the dry separation is practical.

4.11 Equipment Description. A flow sheet of the four-inch-diameter fluidized-bed burner and associated equipment is shown in Figure 8. The burner and solids collection pot (Figures 9 and 10) are located in an enclosed hood in the Hot Chemistry Laboratory at the ICPP. Two glove boxes fastened end-to-end provide an enclosed space for breaking the fuel elements into small pieces suitable for charging and for weighing the individual charges. Instruments for controlling the burning operation are mounted near the burner.

(1) Burner. The burner is a jacketed vessel made from an externally finned 4-inch pipe surrounded by a sheet-metal shroud or jacket. Fuel is burned in a fluidized bed inside the pipe, and cooling or heating is provided in the jacket area.

The main body of the graphite burner is a 4-1/2-ft-long section of four-inch Schedule-40 pipe fitted with flanges at each end. A mating flange and cap at the bottom, with a 1/8-inch-thick sintered stainless steel disc placed between the flanges, provides a plenum and combination gas-distributor and bed-support plate for introducing the fluidizing gas. A blind flange closes the top of the burner. The fuel is supported within the fluidized bed by a grating having 1/4-inch-square openings. This grating is suspended approximately six inches above the bed support plate by three 1/4-inch rods fastened to the top flange. Two baffles, each composed of six 1/8-inch-thick plates placed at an angle of 45 degrees to the horizontal, are suspended on the three rods near the top of the burner to reduce the amount of material ejected from the burner by the fluidizing action of the bed.

Three main lines penetrate the burner body for charging fuel, draining bed material, and removing off-gas. A 1-1/2-inch charge line enters the burner 42 inches above the support plate. Two ball valves in this line permit the fuel and bed material to be added without releasing hot gases. Off-gas and elutriated solids leave the burner through a 1/2-inch line located 2-1/2 inches below the top of the burner and go directly to the solids collection pot. A 1/2-inch bed sampling and drain line is located about four inches above the support plate.

Several other entries are made into the burner. A jet grinder, a 1/4-inch-OD stainless steel tube with a 0.043-inch-diameter hole at the inner end, extends approximately 1/4 inch into the bed between the bed support plate and the fuel support grid. Pressure taps, 1/4-inch pipes welded into the burner wall, enter at 2, 33, and 37 inches above the support plate. Four 1/4-inch-diameter stainless steel sheathed thermocouples extend to the center of the bed at the 2-, 8-, 18-, and 32-inch levels above the support plate.

The jacket around the burner permits the temperature within the burner to be controlled. The fluidized bed is preheated to the graphite ignition temperature of about 600°C by heating the burner body with four 2.5-kW resistance heaters mounted between the fins on the exterior surface. During the burning operation,

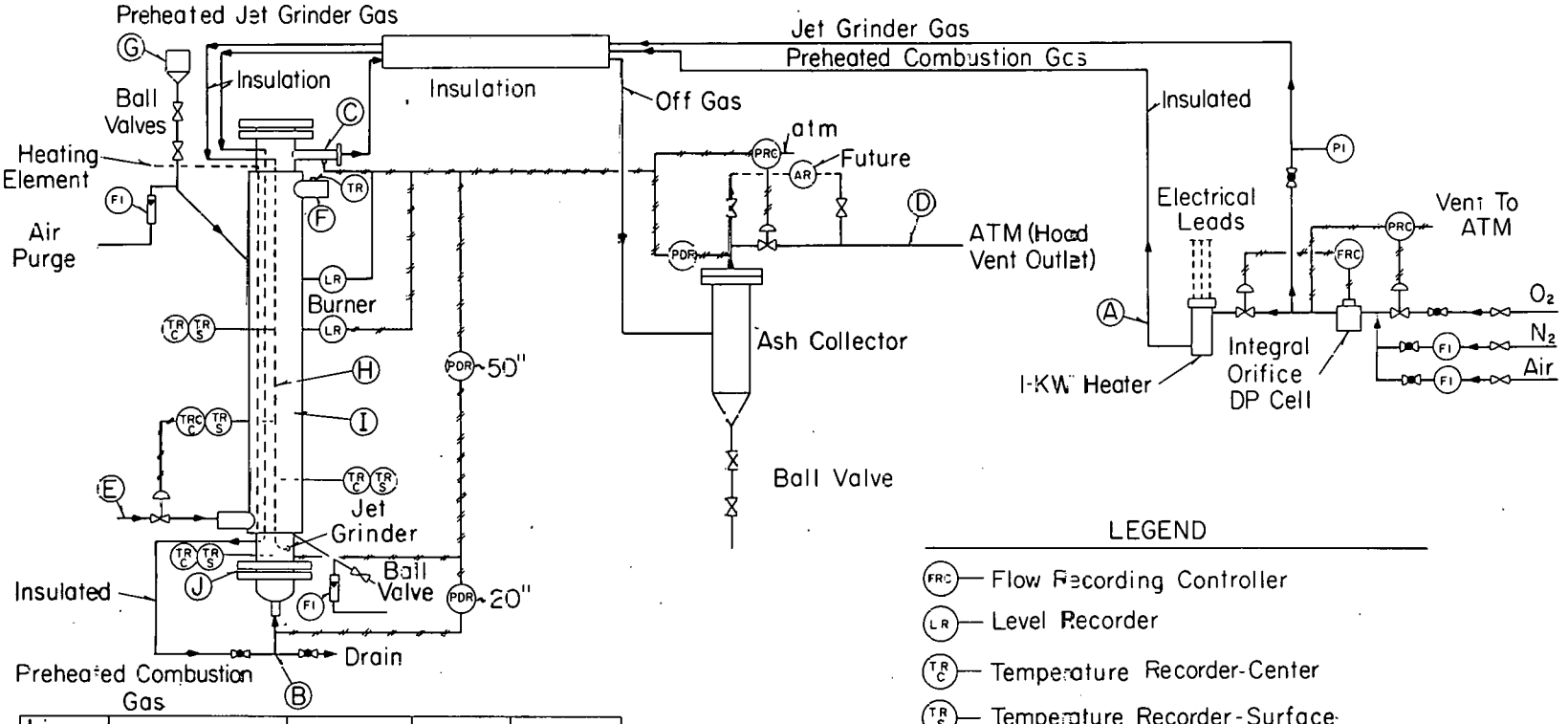

Line or Item No	Description	Volume	Temp	Pressure
A	Combustion Gas	1.54 scfm	25°C	~ 6.5 psia
B	Combustion Gas		700°C	~ 6.5 psia
C	Burner Off-Gas	5.28 acfm	750°C	14.7 psia
D	Burner Off-Gas		500°C	12.3 psia
E	Cooling Air	Nat. Circul	25°C	atm
F	Cooling Air		300-400°C	~ atm
G	Feed	as Reqd.		
H	Fluid Bed Top	5.28 acfm	<=750°C	14.7 psia
I	Burner Wall		650-700°C	
J	Support Plate Sintered S.S.T.	4.57 acfm	700°C	20" H_2O ΔP

Fig. 8 Schematic flow sheet of graphite burner system.

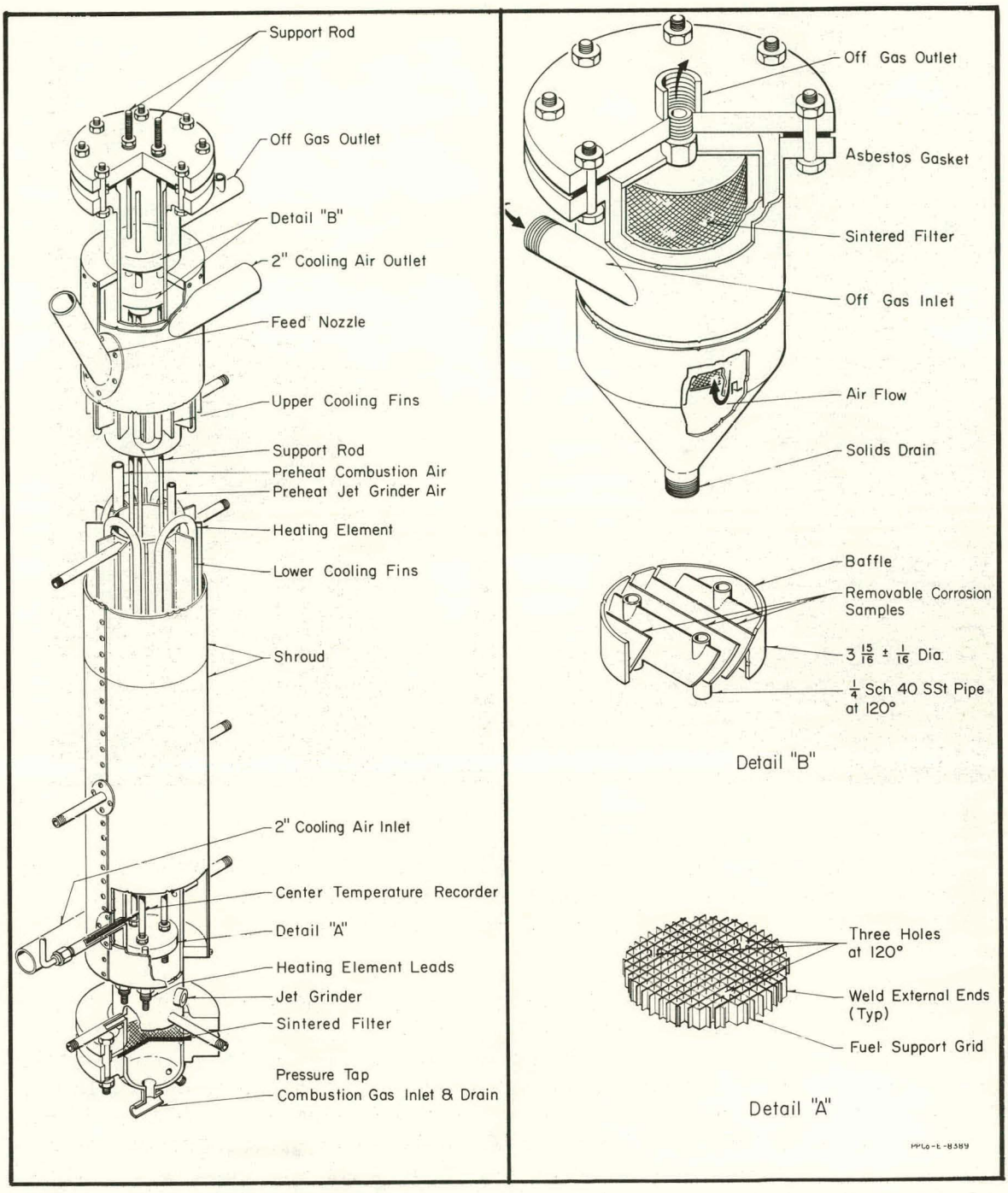

Fig. 9 Graphite burner and solids collection pot.

part of the heat of combustion is removed in the hot gas leaving the burner. The remainder is transferred by the fluidized bed from the burning fuel to the wall of the burner, where it is removed by a stream of air passing over the exterior fins located in the annular space between the burner and shroud. The cooling air is supplied by a blower mounted outside the burner hood. This air passes through a control valve to the shroud at the bottom of the burner, and from the top of the shroud directly to the hood exhaust duct.

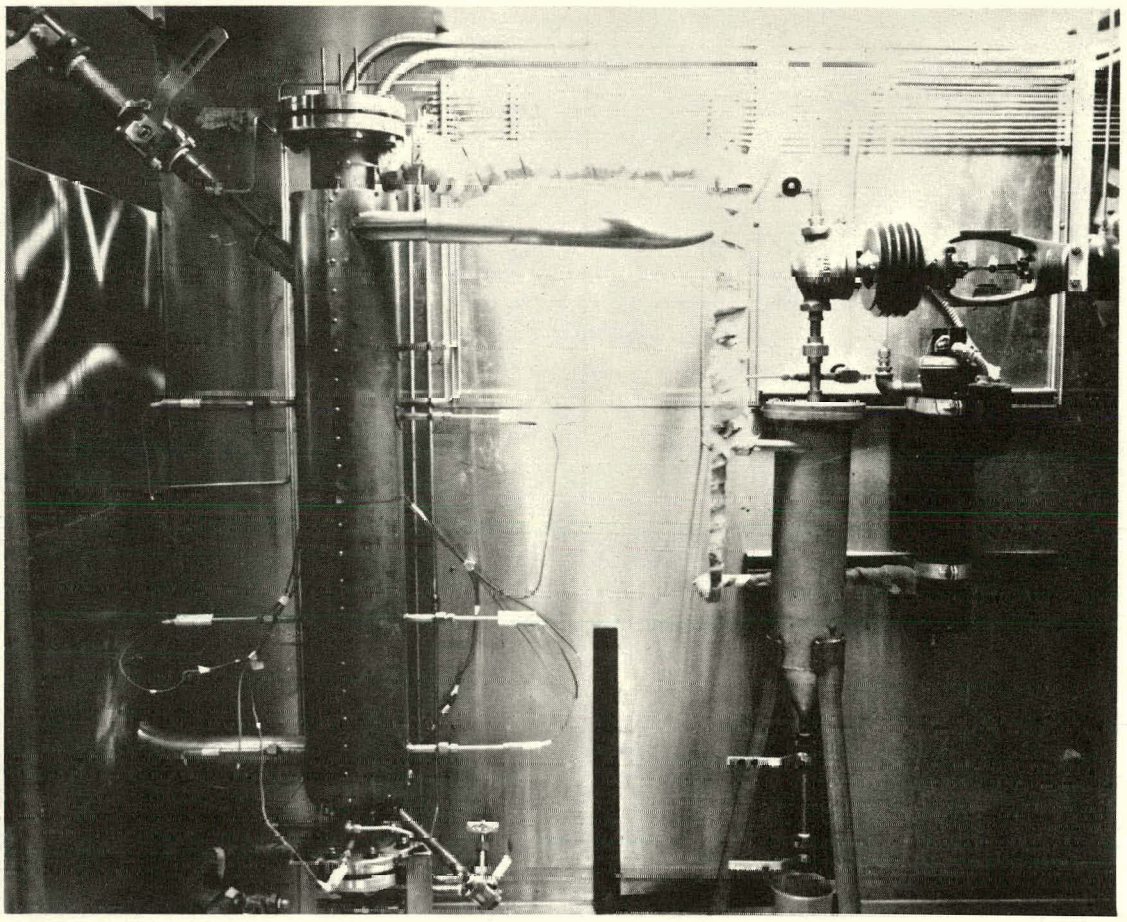

Fig. 10 Burner installation.

To provide proper combustion at the bottom of the bed, both the fluidizing gas and jet-grinder gas streams pass through tubing welded to the exterior of the burner, between the fins, to pick up heat in addition to that provided by the fluidizing gas preheater.

The burner body is fabricated of Type 310 stainless steel (20 Ni, 23 Cr, 2 Mn, 55 Fe). Different materials were used for other parts of the burner to evaluate their use as a burner construction material if Type 310 stainless steel proves unsatisfactory. These include Type 330 stainless steel (35 Ni, 15 Cr, 50 Fe, 0.1C) for one baffle; Type 304 stainless steel (8 Ni, 18 Cr, 74 Fe), Carpenter Alloy No. 20 (29 Ni, 20 Cr, 2 Mo, 3 Cu, 46 Fe), and Nichrome (60 Ni, 15 Cr, 25 Fe) for the suspension rods to support the baffles and fuel support grid; Type 347 stainless steel (9 Ni, 15 Cr, 1 Cb/Ta, 73 Fe) for thermocouple sheaths; and Type 316 sintered stainless steel (10 Ni, 16 Cr, 2 Mo, 72 Fe) for the bed support plate.

(2) Solids Collection (Filter) Pot. The off-gas leaving the burner goes directly, via a 1/2-inch pipe, to the solids collection (filter) pot shown in Figures 9 and 10. This unit is similar to a cyclone separator with an internal filter installed on the discharge line to retain the solids within the pot. The filter has a 3-inch by 1-inch oval cross section and an 18-inch length; sintered stainless steel is the filter media. According to the manufacturer's literature, the filter is capable

of removing 98 percent of the particles having 0.7-micron diameter and 100 percent of the particles 1.8-micron and larger in diameter. The pressure drop across the clean filter, also calculated from the manufacturer's literature, should be about five inches of water when fluidizing at a superficial velocity of 1 fps in the burner.

The pressure within the burner is controlled by a valve located downstream from the filter. As the pressure drop across the filter increases due to an accumulation of solids, the control valve opens to maintain a constant total pressure drop.

(3) Combustion and Fluidizing Gas Supply. The combustion and fluidizing gas supply system is shown as part of the flow sheet in Figure 8. This system permits measurement and control of the combustion and fluidizing gas supplied to the burner, whether partially supplied through the jet grinder or through the support plate. Metering equipment permits the use of oxygen, air, or nitrogen, or any mixture of the three, as required for the process.

When the jet grinder is in use, the gas will be supplied at a pressure high enough to produce flow at sonic velocity through the jet. At other times, the pressure at the jet will be slightly above the burner pressure to prevent bed material from entering and plugging the jet.

(4) Instruments. The instruments used in this system are indicated on the flow sheet in Figure 8. Instruments are provided to indicate, record, or record and control temperatures, pressures, pressure differences and flows as required to control and evaluate the process. The bed level is not indicated until the bed is 33 inches above the support plate. At this time, the increase in pressure due to the bed covering this pressure tap will provide a reading on the bed level instrument.

4.12 Test Results. Two runs were made in this system with Rover fuel elements containing natural uranium. The results of these runs (Table X) show that the elutriated product is cleanly separated from the alumina (60 grit Norton RR alundum) in the bed at superficial fluidizing velocities ranging from 1.0 to 1.5 feet per second. The overhead product contained less than 0.3 percent alumina.

From these tests, information was also obtained on the manner in which burning occurs in the fluidized bed. Visual inspection of fuel removed from the burner showed that burning occurs primarily on the surface of the fuel pieces in the vicinity of the fuel support grid (a fuel inventory of 2 to 4 kg was maintained in the burner). Fuel pieces located near the top of the fluidized bed showed little evidence of burning, whereas fuel pieces taken from the lower part of the bed were largely consumed. The partially burned fuel pieces showed that most of the burning takes place on the downward-facing side or end, and very little burning takes place on the upward side or end until the lower portion is consumed.

As the fuel burns, small particles are released, and a significant portion of these particles are graphite. The large pieces of fuel in the burner apparently cause poor mixing in the fluidized bed, with the result that the particles released from the surface of the burning fuel tend to accumulate in the upper portion of the burner. The fluidizing gas has a much higher velocity in the portion of the burner containing the solid fuel pieces because the void space is reduced by the solid fuel pieces. Particles released from the burning fuel are thus carried to the top of the bed in this higher velocity gas stream.

TABLE X

OPERATING CONDITIONS AND SUMMARIZED RESULTS FOR RUNS 1 AND 2 IN THE FOUR-INCH-DIAMETER FLUIDIZED-BED BURNER

								Overhead Product				Bed		
Run	Duration (hours)	Superficial Fluidizing Velocity (ft/sec)	Temperature (°C)	Pressure (psia)	Combustion Gas (percent)	Inert Bed Material	Rover Fuel Feed Rate (g/hr)	U_3O_8 (wt%)	Carbon (wt%)	Alumina (wt%)	Uranium Recovered by 70% HNO_3 (percent)	U_3O_8 (wt%)	Carbon (wt%)	Uranium Recovered by 70% HNO_3 (percent)
1A	~ 13[a]	1.3 to 1.5	600 to 930	14.7	Not Measured	60 Grit Norton RR Alundum	[a]	21.1	63.0	Trace	97.7	1.8[b]	2.3[b]	90.7[b]
1B	8½	1.0	600 to 720	14.7	46	60 Grit Norton RR Alundum	1100	24.0	57.6	Trace	98.5	1.7[c]	0.8[c]	95.8[c]
2	51	1.0	700 to 750[d]	14.7	46	60 Grit Norton RR Alundum	1100	38.9	56.0	0.27	99.6	4.4[b] 20.6[e]	4.1[b] 4.2[e]	95.0[b] 94.3[e]

[a] Run 1A was made to check out equipment; duration of run and fuel feed rate were not recorded.

[b] Samples taken from the bottom of the bed during the run.

[c] Samples of the mixed bed taken after residual fuel burnout.

[d] One temperature excursion to 955°C of less than 15 minutes duration occurred during a malfunction of the combustion gas supply system.

[e] Samples of the mixed bed -- the residual fuel was not burned out.

Uranium recovery from the elutriated product by dissolution in nitric acid was very good, averaging 99.6 percent for Run 2 which was of 51 hours duration. Uranium recovery from the bed material averaged 96.2 percent. The uranium in the bed that was not recovered by nitric acid amounted to only 0.7 percent of the total uranium fed to the burner during the second run. This uranium (not recovered by nitric acid) had stabilized at three to five weight percent of the bed material, so continued operation of the burner should not result in continual buildup in the bed. It is not known whether the uranium not recovered by nitric acid is associated with the niobium or with the alumina.

In conclusion, the overhead product take-off concept appears to be practical, but two problems will require further investigation before in-bed separation of the product ash from the inert alumina can be considered a satisfactory process approach. First, the overhead product contained a large amount of unburned graphite (greater than 50 weight percent). This unburned graphite was about one-third of the total carbon in the fuel bed to the burner. Second, a significant amount of uranium oxide particles (18 percent of the total uranium fed to the burner during the second run) did not elutriate from the burner. Approximately 80 percent of these particles were the same size as the uranium oxide particles that had elutriated from the burner during the run. Thus these particles would probably have elutriated from the burner if fluidizing had been continued after the fuel burning was completed.

Additional runs are planned to test methods of eliminating or reducing the unburned graphite in the overhead product and separating all the metal oxide combustion products from the alumina.

4.2 Alternate Processes for Reprocessing Graphite Fuels

(D. W. Rhodes, L. A. Decker, R. R. Hammer; Chemistry Section)

Three processes: (a) grind-leach, (b) electrolytic decomposition, and (c) mixed nitric-sulfuric acid oxidation, have been proposed as alternates to the

burn-leach process for separating uranium from graphite fuels. Of the three alternatives, the grind-leach and the nitric-sulfuric acid oxidation processes are chemically feasible and give essentially quantitative recovery of uranium. With additional development, either of these should represent a workable process for the fuel. Recent studies at ICPP on these alternate processes are reported in detail in IN-1018 [12]. The principal findings are summarized in the following paragraphs.

There are three unique problems which any successful process for treating graphite fuels must overcome: (a) separation of the uranium from a large amount of material which is relatively inert, (b) penetration of the coating of the uranium particles, and (c) recovery of the uranium which may be united as a solid solution with other metals, eg, niobium which is used in channel liners of niobium carbide in some graphite fuels. Each of the three alternate methods for reprocessing graphite fuels requires an efficient solids-liquid separation step in the process.

4.21 Grind-Leach Process. The protective coatings on the uranium carbide particles prevent contact between the nitric acid dissolvent and the uranium unless they are first ruptured. In laboratory experiments, greater than 99 percent of the uranium was leached in four hours with 70 percent nitric acid at the boiling point from fuel which had been ground to a small enough size to rupture the coating and expose the uranium.

4.22 Electrolytic Decomposition. Concentrated (70 percent) nitric acid will disintegrate pieces of graphite fuel when a potential is applied to an anode in contact with the piece. Disintegration occurs within a few minutes at 80°C at a potential of about 8 volts and a current density of about 0.5 amp/cm^2, with one side of the anode in contact with the fuel piece. This treatment does not appear to penetrate the coatings of all of the particles, and only about 11 percent of the uranium is dissolved during disintegration of the fuel. Addition of potassium dichromate (0.4M) increased the amount of uranium dissolved to 39 percent.

4.23 Mixed Nitric-Sulfuric Acid Oxidation. Disintegration of graphite fuel pieces and dissolution of the uranium carbide occurs in contact with a solution composed of 75 volume percent concentrated (98 percent) sulfuric acid and 25 volume percent concentrated (70 percent) nitric acid at elevated temperatures. Recovery of greater than 99 percent of the uranium present in a fuel specimen was obtained after reacting for 10 hours at 120°C. Solvent extraction of the adjusted solution with 10-percent TBP in Amsco resulted in losses of less than 0.1 percent for three stages each of extraction and stripping.

5. MISCELLANEOUS THEORETICAL EQUIPMENT PERFORMANCE STUDIES

5.1 Air Pulser Development

(S. J. Horn; Development Engineering Section)

All pulse columns at the ICPP have been equipped with air pulsers, and final phases of the experimental activity on air pulsers have been directed toward improving the accuracy of the mathematical model [13, 14] used to describe their

operation. From this final work, it has become obvious that the effort required to signficantly improve the accuracy of the analog simulations any further exceeds the value of the improvement in applying the results to pulser control and plant operation.

When the mathematical model was used in simulating operation of the small F-cell pulse columns (1.31 inches to 3.00 inches ID) it was found to be less accurate than when used in simulating operation of the large G-cell pulse columns (8 to 10 inches ID). The inaccuracy was found to be in the expression of frictional pressure drop through the pulse column sieve plates. The accuracy of the analog simulations was improved by using a varying orifice discharge coefficient in the computations [1].

An attempt was made to elucidate the nature of sieve plate friction in a pulse column. A small laboratory pulse column was erected (Figure 11) approximating the smallest plant pulse column at the ICPP. This pulse column had an inside diameter of 1.502 inches and an air pulser leg with an inside diameter of one-half inch. This pulse column was equipped with a differential pressure transducer for pressure drop measurements and a flow transducer for flow velocity measurements and pulse amplitude computations [15].

At maximum velocity, the liquid acceleration is zero, and a measured pressure differential across a portion of a pulse column would then be exclusively due to friction. In the absence of other major factors, this pressure differential is due to flow through the sieve plates.

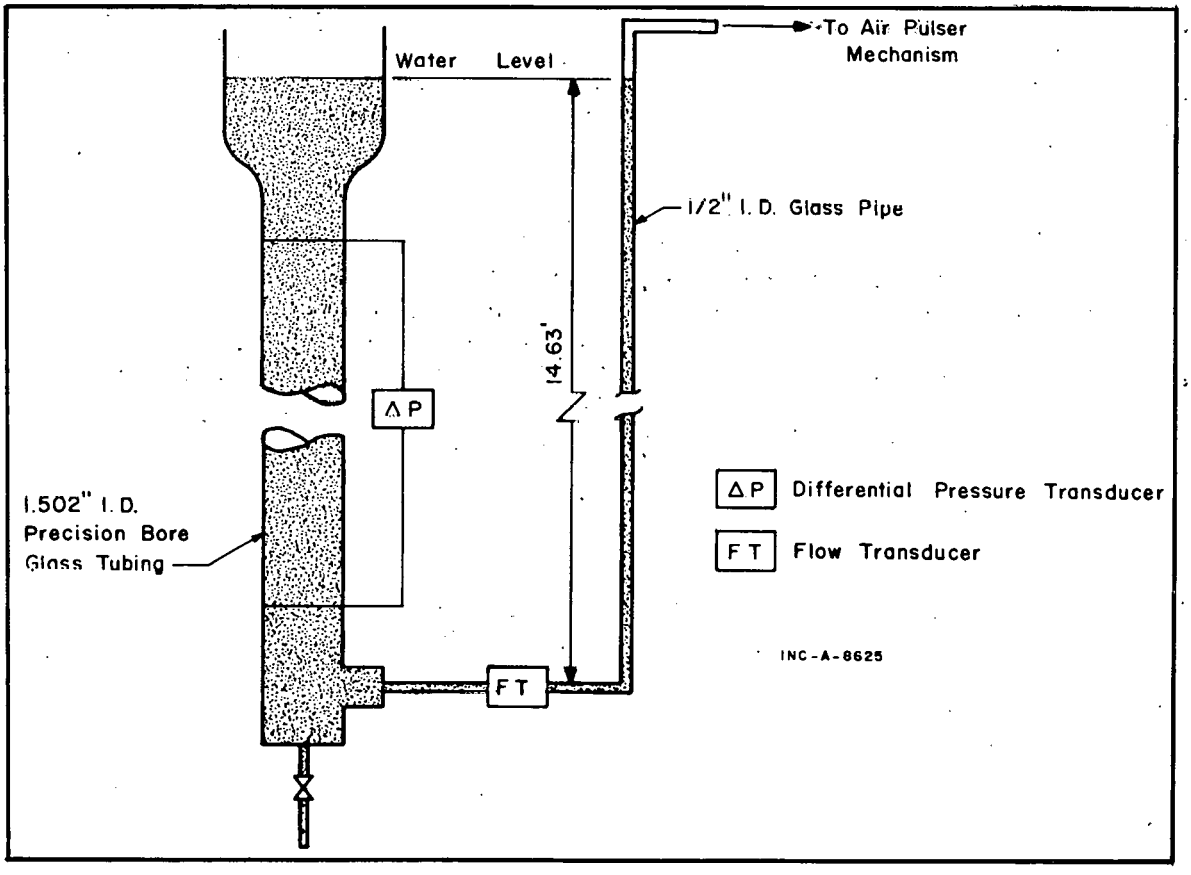

Fig. 11 Test pulse column setup.

Of the numerous factors which could influence the pressure drop through the sieve plates in a pulse column, only two were studied. These were the effect of clearance between the sieve plates and the inner wall of the pulse column, and "end effects". Sieve plates with diameters of 1.446 and 1.499 inches were used in the 1.502-inch column in studying wall clearance effects. Plate cartridges of 40 and 80 plates were used in studying end effects.

As expected, the pressure loss per plate was greater for the larger sieve plates. Surprisingly, comparison of experimentally measured pulse amplitudes with those obtained by analog simulation showed that the use of a constant orifice coefficient in the analog simulation gave better agreement with the experimental data than did a variable orifice coefficient, in contrast to the F-cell pulse columns where the opposite was found to be the case. Further, orifice coefficients calculated from experimental velocity, and pressure drop data from the experimental column, were found to be a function of the plate Reynolds number to the one-half power (Figure 12) rather than the one-eighth power[16].

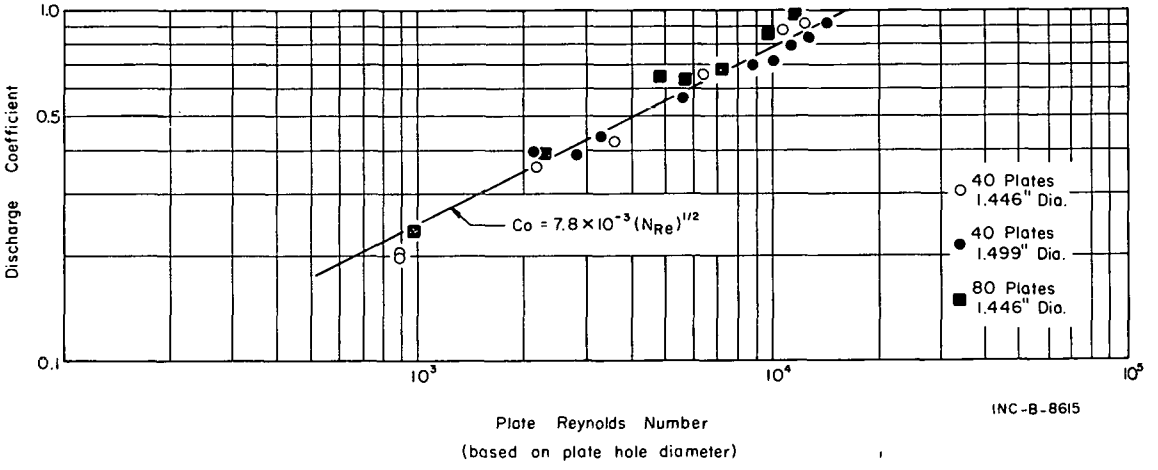

Fig. 12 Orifice discharge coefficients for sieve plates under pulsed conditions.

It is apparent that the fricitional resistance to flow through a pulse column, and particularly through a series of sieve plates, will require considerable study before a more generalized mathematical model can be evolved. The existing mathematical model is adequate for exploring most pulse column designs and can be used to provide operating data for nominal flow sheet conditions. However, since normal departures from nominal flow sheet conditions will result in changes in the pulse amplitude for constant pulser operating variables, attempting to cover all contingencies by analog simulation is an impractical approach, even if an accurate, completely general mathematical model were available.

A much more productive program of air pulser study would be to develop a system to measure the amplitude of the pulse in the pulse leg (or in the pulse column). Such a system would then provide a signal which could be used as the input to a closed-loop control system, which would hold the pulse amplitude at the desired value regardless of changes in the processing conditions.

5.2 Effects of Pulsation on Heat Transfer in a Liquid-Fluidized Bed

(E. S. Grimmett, G. W. Hogg; Development Engineering Section)

Heat transfer between a wall and a pulsated liquid-fluidized bed has been studied in the course of developing a continuous tray-column crystallizer for purifying and concentrating radioactive liquors [17] by successively forming and melting crystals in the presence of velocity pulsations at alternate cooling and heating trays. These studies indicate that heat transfer rates from a liquid flowing normal to a cylinder can be increased as much as two and one-half times when the cylinder is surrounded by a bed of fluidized particles, and an additional four times when the fluidized system is pulsed. The heat transfer rates were determined to be a strong function of pulse frequency and displacement amplitude, and the greatest improvement was realized at the highest pulse stroke -- which is defined as the product of the pulse frequency and the displacement amplitude.

5.21 Background. While the effect on heat transfer of velocity pulsations in various systems has been receiving increasing attention in recent years [18, 19], no prior work on heat transfer between a wall and a pulsated liquid-fluidized bed is evident in the literature. The results of heat transfer experiments for a number of different oscillating systems, and a few systems containing solid particles, do indicate that various degrees of success have been attained in improving heat transfer rates. In one experiment, heat transfer coefficients were improved by more than twentyfold for water in natural convection with a vibrating surface [20]. In another experiment, in which air flowed with velocity pulsations at low pulse frequencies and amplitudes in a pipe, the heat transfer coefficient decreased relative to steady conditions [20]. The effect of liquid-fluidized glass beads on heat transfer to a wall was studied by Caldas at various superficial fluidizing velocities and particle sizes [21]; the characteristic dense-phase and lean-phase fluidization and maximum heat transfer coefficients were particularly investigated. Grimmett and Brown have described the physical and operational features of a rapidly pulsed two-inch-diameter liquid-solids contactor column [22].

Detailed results of the current study were presented at the symposium on "Fundamental and Applied Fluidization" held at the 58th National Meeting of the AIChE in Dallas, Texas, February 6-9, 1966, and are published in the Chemical Engineering Progress Symposium Series covering that meeting [23]. A summary of the principal findings is presented here.

5.22 Mathematical Theory. Conventional methods of dimensional analysis indicate the following relationship between the independent dimensionless moduli:

$$\left(\frac{hD_t}{k}\right) = \phi\left[\left(\frac{D_t V \rho}{\mu}\right)^a, \left(\frac{C_p \mu}{k}\right)^b, \left(\frac{D_t}{D_p}\right)^c, \left(\pi\right)^d, \left(\frac{D_t f}{V}\right)^e, \left(\frac{D_t}{A}\right)^f\right].$$

The oscillating nature of the system suggests that the root-mean-square velocity of the pulsating system be used to determine the heat transfer characteristics of the system. This velocity is used in place of V, A, and f in the above relationship and results in a new relationship,

$$\left(\frac{hD_t}{k}\right) = \phi\left[\left(\frac{D_t V_{rms} \rho}{\mu}\right)^a, \left(\frac{C_p \mu}{k}\right)^b, \left(\frac{D_t}{D_p}\right)^c, \left(E\right)^d\right].$$

Nomenclature used in these relationships includes the following:

A = pulse amplitude, L

C_p = heat capacity of liquid, H/mT

D_p = particle diameter, L

D_t = tube diameter, L

E = void fraction, dimensionless

f = pulse frequency, cycles/t

h = heat transfer coefficient, H/t L^2 T

H = energy, m L^2/t^2

k = thermal conductivity of liquid, H/t L T

L = length, L

m = mass, m

p = period of oscillation, t

r = radius of eccentricity, L

t = time, t

T = temperature, T

V = fluid velocity, L/t

V_c = constant or superficial fluid velocity, L/t

V_{rms} = root-mean-square velocity, L/t

w = angular velocity, radians/t

μ = density of liquid, m/L^3

ρ = fluid viscosity, m/Lt.

5.23 Experimental Pulsed Column. Figure 13 is a flow diagram representing the experimental equipment used to verify the previous considerations. As the figure indicates, the heat exchanger is located in the pulsed column in such a manner that the shell side of the column is directly subjected to the hydraulic pulse.

Hot water, at controlled temperatures and flow rates, is pumped through the tube side of the heat exchanger. Cold water flows through the four-inch-diameter shell side of the heat exchanger, entering the bottom of the four-inch-bore column at regulated flow rates. The column and associated tubing are insulated to minimize heat losses to the surroundings.

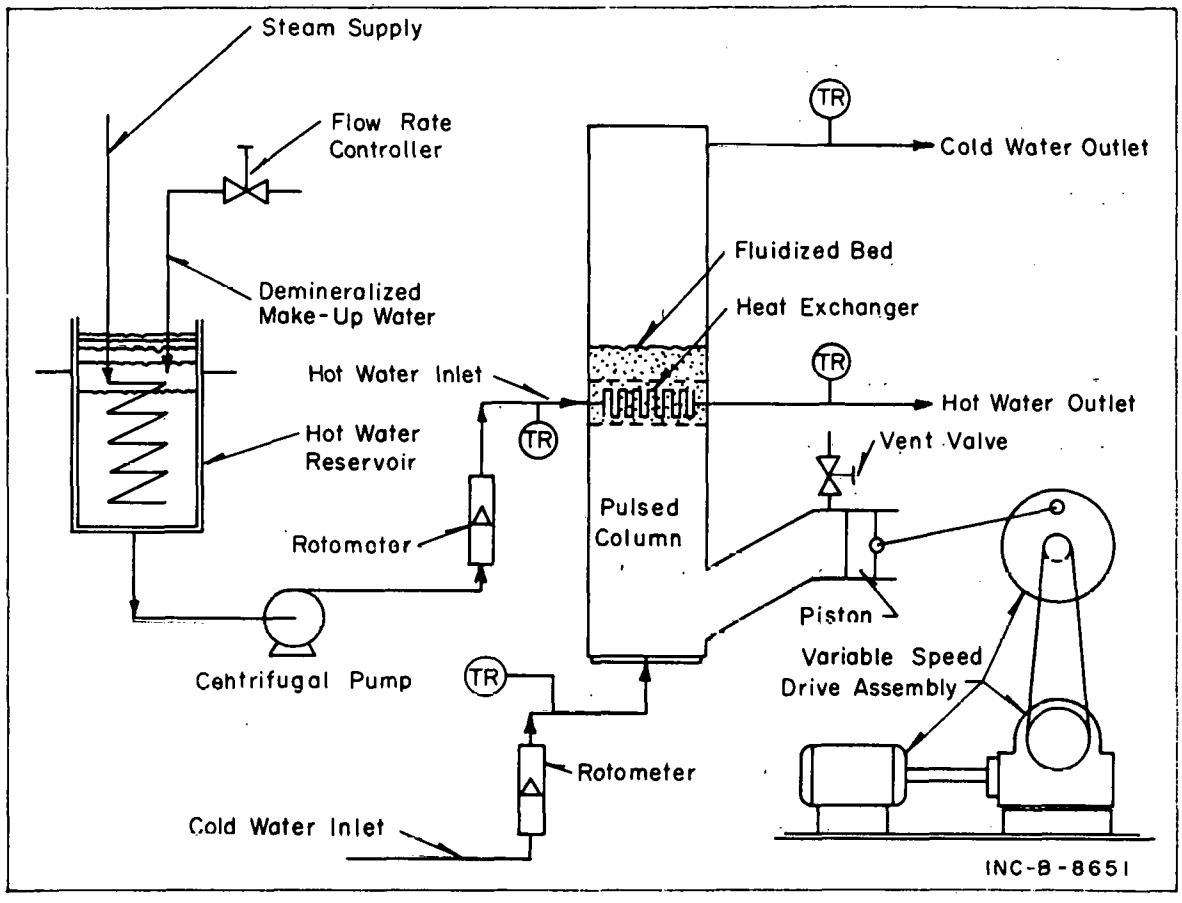

Fig. 13 Pulsed fluidized-bed experimental apparatus.

A pulse is imposed on the shell-side flow by a four-inch-diameter piston operating in a side branch of the column. The piston stroke and frequency are adjustable.

The heat exchangers used in the column are of two different types. One exchanger contains a single tube with several successive "hairpin" bends, as illustrated in Figure 14. The other exchanger contains three in-line tubes connected in parallel, as illustrated in Figure 15. Both exchangers are constructed of 1/4-inch-diameter copper tubing coils. These coils are positioned inside the 4-inch-diameter stainless steel pipe shell with rubber bushings to prevent leakage through the tube projection holes and to minimize heat transfer from the tubing to the heat exchanger wall. A 70-mesh (Tyler) wire screen is sandwiched between two perforated plates and permanently welded to the bottom of the exchanger to act as a grid to support the fluidized bed.

5.24 Heat Transfer to a Single Cylinder Submerged in a Pulsed Fluidized Bed. The experimental data obtained at various conditions in the one-coil heat exchanger were correlated in terms of dimensionless moduli as shown in Figure 16. The data, involving particle sizes ranging from 16 to 150 mesh, pulse frequencies ranging up to 750 cpm, displacement amplitudes ranging from 0 to 1/4 inch, and superficial fluidizing velocities ranging from 0.75 to 3.5 feet per minute, were correlated to within ± 30 percent. The most probable mathematical least-square representation of the data when using the root mean-square velocity is given by the equation:

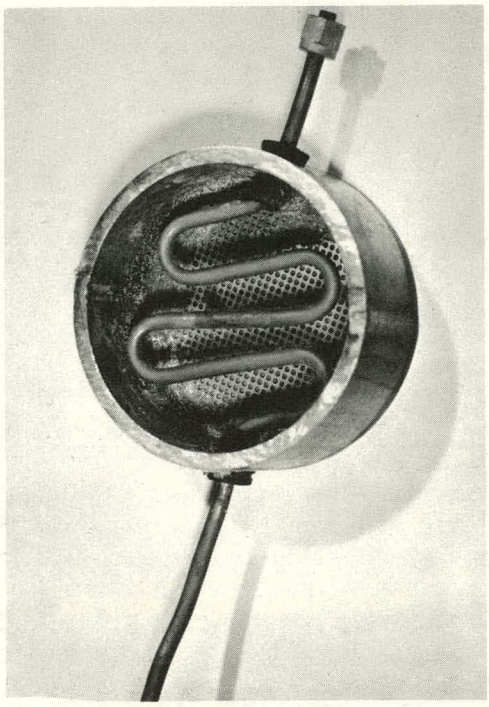

Fig. 14 Single-coil exchanger.

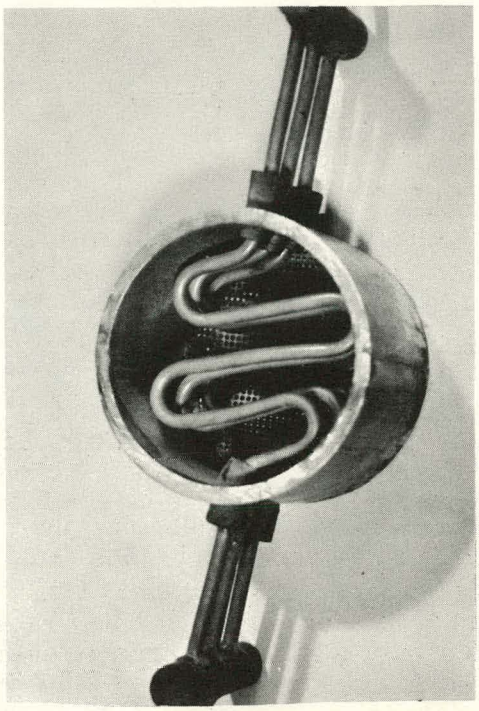

Fig. 15 Three-coil exchanger.

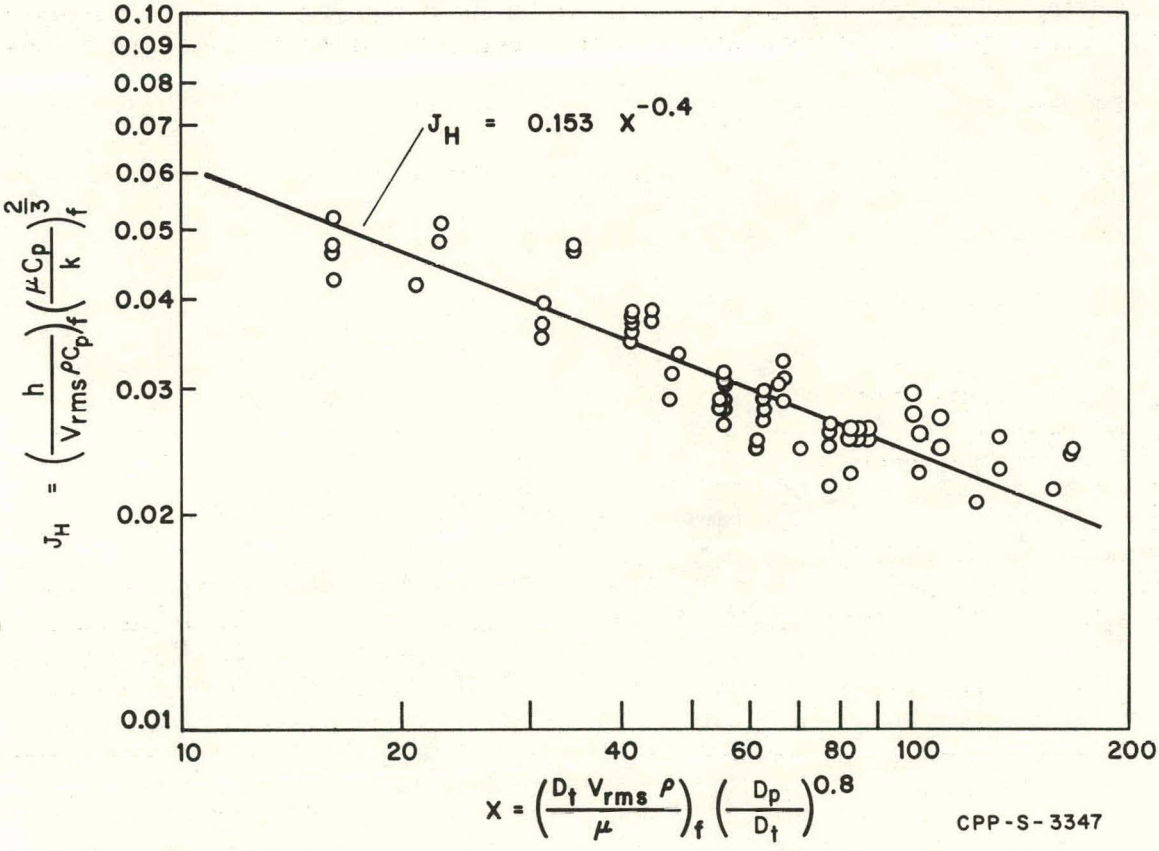

Fig. 16 Correlated data for heating water flowing with velocity pulsations normal to a single cylinder in a liquid-fluidized bed.

$$\frac{hD_t}{k} = 0.153 \left(\frac{D_t V_{rms} \rho}{\mu} \right)_f^{0.60} \left(\frac{D_t}{D_p} \right)^{0.32} \left(\frac{C_p \mu}{k} \right)_f^{0.33} .$$

The subscript f indicates that the physical properties of the fluid were evaluated at the film temperature, t_f, where

$$t_f = (t_{wall} + t_{bulk})/2 .$$

5.25 Efficiency of In-Line Tubes in the Pulsed Fluidized-Bed System. In-line-tube heat exchanger data were obtained at superficial fluidizing velocities ranging from 0.75 to 3.5 feet per minute using the three-coil heat exchanger. The data for 48- to 65-mesh sand particles at 300 cpm pulse frequency and 1/8-inch displacement amplitude indicate a rapidly increasing average shell-side film coefficient with increasing fluidizing velocity, as shown by Curve A of Figure 17. For steady flow in the absence of the fluidized particles, the data indicated only slight increases in average heat transfer coefficient with increasing fluidizing velocity as shown by Curve B of Figure 17. The effect of pulse frequency upon the average shell-side heat transfer coefficient for the three parallel-connected in-line tubes is indicated in Figure 18. Frequencies were varied up to 600 cpm at a constant 1/8-inch displacement amplitude and 1.75 feet per minute fluidizing velocity, using 48- to 65-mesh fluidized sand particles in the three-coil heat exchanger bed. As the pulse frequency was increased the average heat trans-

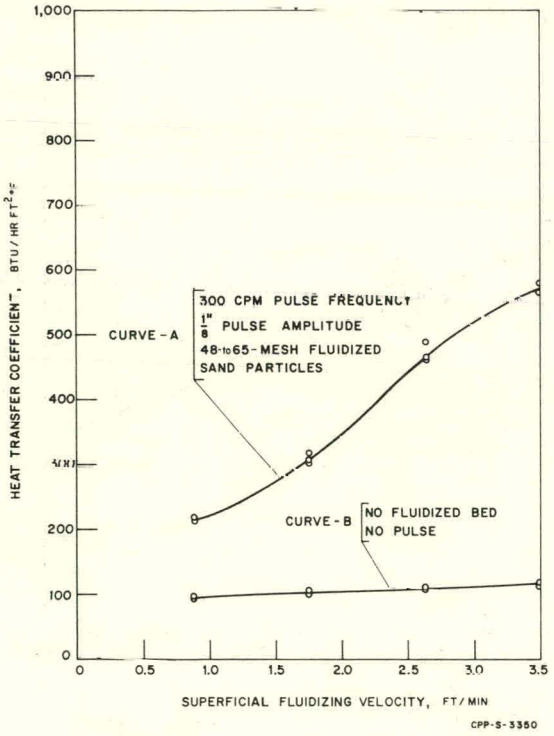

Fig. 17 Effect of pulse and fluidized bed on heat-transfer coefficient in the three-coil heat exchanger.

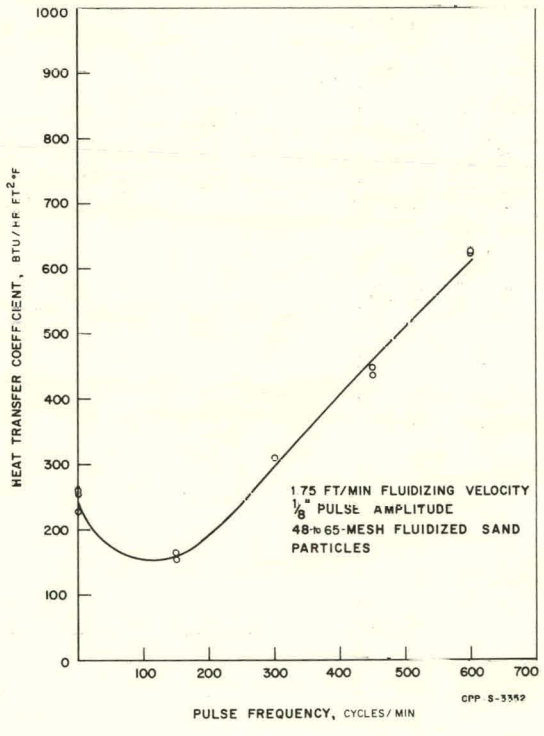

Fig. 18 Effect of pulse frequency on heat-transfer coefficient for a fluidized bed and the three-coil heat exchanger.

fer coefficient decreased to a minimum at approximately 120 cpm pulse frequency, then increased at a uniform rate over the entire frequency range investigated. The decrease in heat transfer coefficient is attributed to a typical initial contraction of the fluidized bed. The ratio of the heat transfer coefficient for three in-line rows of tubes to that of one row was found to vary from approximately 0.4 at 150-cpm pulse frequency to approximately 0.8 at 600-cpm pulse frequency when operating at a constant superficial fluidizing velocity of 1.75 feet per minute.

II. WASTE MANAGEMENT

1. THE IDAHO WASTE CALCINING FACILITY

1.1 Preparation for the Second WCF Processing Campaign
(G. E. Lohse; Plant Process Assistance Section)

The first processing campaign in the Idaho Waste Calcining Facility (WCF) was completed in October 1964 when the original solids storage facility was filled [1]. The WCF was down at that time for an extended period while a storage facility for an additional 30,000 cubic feet of solids was constructed. This new storage facility consists of seven storage bins, 12 feet in diameter and 42 feet high, in a concrete vault[1]. Construction of this facility was completed in February 1966, and operation of the WCF was resumed in March 1966.

The time available because of the forced shutdown for construction of solids storage facilities was utilized to thoroughly decontaminate and inspect the facility, to make a number of desirable improvements, and to prepare the WCF for its second prolonged processing campaign. Ruthenium was washed from the silica gel adsorbers, and the silica gel was dried in preparation for reuse. Details of specific preventative inspection and maintenance items and specific equipment repairs and modifications are presented in the paragraphs which follow.

1.11 Inspection and Repair.

(1) Calciner. Internal portions of the calciner vessel showed no evidence of wear or corrosion. The NaK tubes and support were intact and no scoring of the tubes was visible. The caps on the distributor plate remained firmly in place and abrasion appeared negligible. Metallurgical examination of the baffle in the calciner vapor space indicated no carbide precipitation or sigma phase, and the oxide film on the surface of the Type 347 stainless steel plate was estimated to be less than one micron thick.

No repairs to the calciner were necessary.

(2) Feed System. The air nozzle caps of the pneumatic atomizing nozzles, which had been made of Type 440C martensitic steel, showed considerable corrosion cracking and some surface attack. However, the "austenitic" liquid nozzles were not attacked. The air caps were replaced with precipitation-hardened austenitic steel Type 17-4 PH, Condition H-900.

Borescopic inspection of the vitreous enamel liners of the electro-magnetic flowmeters was inconclusive. There appeared to be some deterioration of the liners in the vicinity of the platinum electrodes, and the measured electrical resistance to ground indicated a considerable drop from that of new meters. Therefore, new meters were installed in all three lines. The vitreous enamel linings in the electrode areas of these new meters were photographed (with the aid of a borescope using a fiber optic lighting system) to provide a permanent record of the initial condition of the linings.

(3) Scrubbing System. Nine valves were removed from the scrubbing system for replacement of the bellows-seals and for rebuilding of the valve plugs and seats. Two of these valves had failed during or following the first campaign, and

the others were found to be damaged or defective on subsequent inspection. Several had unacceptably high in-line leakage caused by corrosion of the Stellite facings on the plugs and seats. Three of the bellows developed leaks due to improper construction materials or to poor assembly techniques. Defects in other bellows (Type 304L stainless steel) were probably due to localized sensitization, as intergranular attack and stress corrosion were not prominent in the structure. The bellows-seals of all of the valves were replaced with corrosion tested materials, and the seats and plugs of those valves containing stellite facings were repaired by "puddle-welding" low-carbon stainless steel to the parts and then machining.

The quench pumps performed satisfactorily during the campaign and, for the most part, during decontamination also. During maintenance testing following decontamination, both pumps failed and were removed for inspection. The retaining nuts on both impellers loosened and dropped from the shafts into the tank. The pumps were modified to allow locking of the impeller retaining nuts, and new bearings were installed. The shaft on one of the pumps was replaced. Measurements of the impeller and pump housing indicated essentially no wear of these parts during nearly 8000 hours of operation.

Several Type 304 stainless steel nuts, installed on the quench pump flanges submerged in the scrubbing solution tank, loosened because of severe intergranular corrosion. The accompanying Type 304L stainless steel bolts were not attacked. Failure of the nuts was attributed to excessively high carbon content (0.15 percent). Replacement nuts were made from Type 304L stainless steel.

(4) Adsorber Manifold Cell. Although complete decontamination of the ruthenium adsorbers was not attempted, radiation levels in the adsorber manifold cell were low enough to permit visual inspection of valves, piping, and expansion joints. No failures were detected.

(5) High Efficiency Filters. During the last two months of the campaign, relatively inexpensive filters containing magnesia asbestos spacers in lieu of stainless steel spacers were tested. Failure of the magnesia material due to attack by nitric acid vapor, however, precludes its use in future campaigns. Spacers fabricated from silica-type materials were satisfactory in laboratory tests, and filters with this type of spacers are being tested in the current campaign. Considerable savings will result if these filters prove satisfactory.

(6) Off-Gas Blowers. Inspection indicated that the alignment of the main off-gas blowers was still "true", except for a slight shift in the radial alignment between one of the drivers and the blower. This minor misalignment was corrected.

(7) Equipment Vent Blower. During the initial campaign a motor bearing on the equipment vent blower failed, and this unit was taken out of service until the motor bearing was replaced. New bearings for both motor and blower were installed, and alignment and vibration measurements indicated that the blower was in good condition at the start of the current campaign.

(8) Thermocouple Lead Wire. The thermoplastic lead-wire insulation for thermocouples in the calciner cell was found to be severely cracked due to high-temperature deterioration. Lead wire with asbestos insulation was installed for all of the thermocouples in this cell.

1.12 Equipment Modifications. Observations during the first campaign indicated that several process and equipment deficiencies could be eliminated by minor equipment modifications. The following modifications were made.

(1) An evaporator system which used existing equipment at the ICPP was designed and installed in a tank previously used for adsorber regeneration. The evaporator will concentrate the feed solutions which have been diluted by steam jetting, thus increasing process throughput.

(2) The equipment vent condenser was modified to allow downward gas flow through the condenser, thereby increasing the capacity of the condenser and permitting higher sparge air flow rates.

(3) The solids transport line was relocated and straightened to eliminate a severe pocket and to reduce the pressure drop in this system.

(4) A leak detection pot for collecting leakage from the bellows-seals of valves was installed in the off-gas cell. Provisions for returning leakage to the scrubbing solution tank were included.

(5) The bonnets for certain valves, previously fabricated from carbon steel or cast iron, were replaced with similar designs fabricated from stainless steel.

(6) The scrubbing solution recycle strainers were removed from the facility. A strainer installed in the calciner feed tank performs the necessary function.

(7) Improved stations were provided for sampling the off-gas at intermediate points throughout the system. These are similar in design to the final off-gas monitoring station and are suitable for sampling radioactive streams.

(8) Three-way plug valves in the decontamination system were replaced with two-way valves and removable connections to prevent cross contamination of steam and decontaminating solution headers due to valve leakage.

(9) A new level probe was installed in a NaK expansion tank. Continuous level measurements are possible with this probe.

(10) Supports for the NaK expansion tanks were modified to allow expansion of the main NaK header between the tanks.

(11) An additional vent line was installed from the remote sample cabinet to provide adequate vacuum at the blister opening.

(12) A surge tank was installed in the fluidizing air line to dampen pulsations which had affected metering.

1.2 Operating Experience to Date on the Second WCF Processing Campaign (G. E. Lohse; Plant Process Assistance Section)

The WCF was started up in mid-March with nonradioactive simulated waste solution to test equipment performance and to establish equilibrium conditions before radioactive waste was introduced. Some difficulties were encountered, primarily due to carryover of sand particles from the starting bed to the scrubbing system. A brief shutdown was required to flush out the scrubbing and feed system. During this interim, plugged lines in the NaK oxide removal system were replaced, and new bellows seals were installed in the three feed control valves. By April 1, equilibrium conditions were established throughout the process, and waste from storage tank WM-183 was started to the calciner. Operation has been virtually uninterrupted since that time, and about 142,000 gallons of waste have been converted to solids which are stored in the new storage bins. The net feed rate to the calciner has averaged about 67.5 gallons per hour (12 percent above design) for a 90-day period, even though feed control problems have been encountered.

Wastes from three tanks have been used as calciner feed. About 86,000 gallons from WM-183 tank had been processed when serious feed flow control problems occurred. At this time the waste in tank WM-183 had been reduced to a heel of less than ten percent of the tank volume, and some pickup of solids or sludge may have occurred. Operation was switched to tank WM-182 which, like WM-183, was essentially a normal aluminum nitrate waste.

After about 26,000 gallons of this waste were calcined without undue difficulty, a changeover to feed supply from tank WM-180 was made. Tank WM-180 waste contains a high concentration of ammonium nitrate, and it was desired to see whether this material would calcine satisfactorily, either by itself or in a blend with normal aluminum nitrate waste, before using up the normal waste in WM-182. About 19,000 gallons of WM-180 waste have been processed thus far, and operation is satisfactory.

The cause of the feed control problems with WM-183 waste is uncertain. Laboratory tests indicate that a sticky precipitate formed if the feed solution was held at boiling temperature for 16 hours. However, such a formation in the WCF has not been confirmed. Some feed control problems have also been encountered with WM-182 and WM-180 waste solutions. With the former, the restrictions generally occurred between the feed tank and the throttling valve. With WM-180 waste, the restrictions generally were at the feed nozzles, though occasional line plugging was also observed. Restrictions have been removed by flushing through the lines or nozzles with water or nitric acid.

The environmental release rate for strontium-90 averaged 0.4 millicuries per day during operation with WM-183 and WM-182 wastes. This rate is less than 0.02 percent of that value which would produce ground level concentrations, under adverse weather conditions, equal to those given in the Radioactivity Concentration Guide (RCG) for occupational exposure. During operation with WM-180 waste, the release rate dropped to about 0.23 millicuries per day. For ruthenium-106, the release rate averaged near 1,500 millicuries per day during the first part of the operation with WM-183 waste. This rate is 2.9 percent of that which could result in ground-level RCG concentrations. The off-gas temperature was then lowered by 5°C, thus increasing the relative humidity of the off-gas. The ruthenium release rate during the remaining operation with WM-183 waste, and during operation with WM-182 waste, averaged 760 millicuries per day. During operation with WM-180 waste, the ruthenium release rate has averaged

about 290 millicuries per day. This lower release rate was expected due to the lower concentration of ruthenium in WM-180 waste.

Overall operation of the WCF is quite satisfactory during this second campaign as the reporting period ends. Operation is expected to continue throughout most of the next fiscal year, until scheduling plans for ICPP fuel processing operations require shutdown of the WCF.

2. ADVANCED WASTE CALCINATION DEVELOPMENT STUDIES

2.1 Pilot Plant Calcination of Zirconium-, Ammonium-, and Sodium-Containing Wastes

(J. C. Petrie; Development Engineering Section)

Recent pilot plant calcination studies have been directed toward developing methods for calcining the following types of radioactive wastes in the WCF[1]:

(1) Zirconium fluoride-aluminum nitrate waste resulting from zirconium-uranium alloy fuel processing

(2) Ammonium nitrate-aluminum nitrate waste resulting from aluminum fuel processing by a Redox-type process

(3) Second- and third-cycle aqueous raffinates which contain high concentrations of sodium ion.

In addition to calcination of solutions simulating the above wastes, a pilot plant calciner run was made under very nearly the same conditions used during the original WCF campaign (WCF Run H-1[1]). Comparisons between results of the pilot plant and plant runs give a basis for predicting operating performance of the WCF during calcination of the other types of wastes scheduled for processing. All appear to be processable in proper combination or with the use of additives under certain operating conditions.

The following paragraphs summarize the results of pilot plant calcination of feeds simulating the various types of wastes.

2.11 Calciner Process Comparison. A pilot plant run has been made to provide data that would be directly comparable to data from WCF operation. This comparison will be helpful in using pilot plant data for predicting operation at the WCF. Operating conditions used in the pilot plant simulated as nearly as possible operating conditions used during WCF Run H-1 to calcine more than a half-million gallons of radioactive acidic aluminum nitrate wastes [1].

Comparison of data from WCF Run H-1 and from the similar pilot plant calciner run has shown that:

(1) Relatively more fines are elutriated from the WCF calciner than from the pilot plant calciner

(2) The composition of the recirculated off-gas scrubbing solution in both calciner systems was nearly the same, although the equipment is different

(3) Control of the product particle size can be effected by a lower nozzle air-to-liquid flow ratio at the WCF than in the pilot plant.

The basic calcination process is shown in Figure 19. The principal process units consist of the fluidized bed calciner, a primary cyclone for separating solids, and an off-gas scrubbing system. Further processing of the off-gas from the WCF involves equipment to lower the radioactivity before the off-gas is released to the atmosphere. Off-gas from the pilot plant calciner is vented directly to the atmosphere because no radioactivity is involved; therefore, no comparison of final decontamination efficiency was involved.

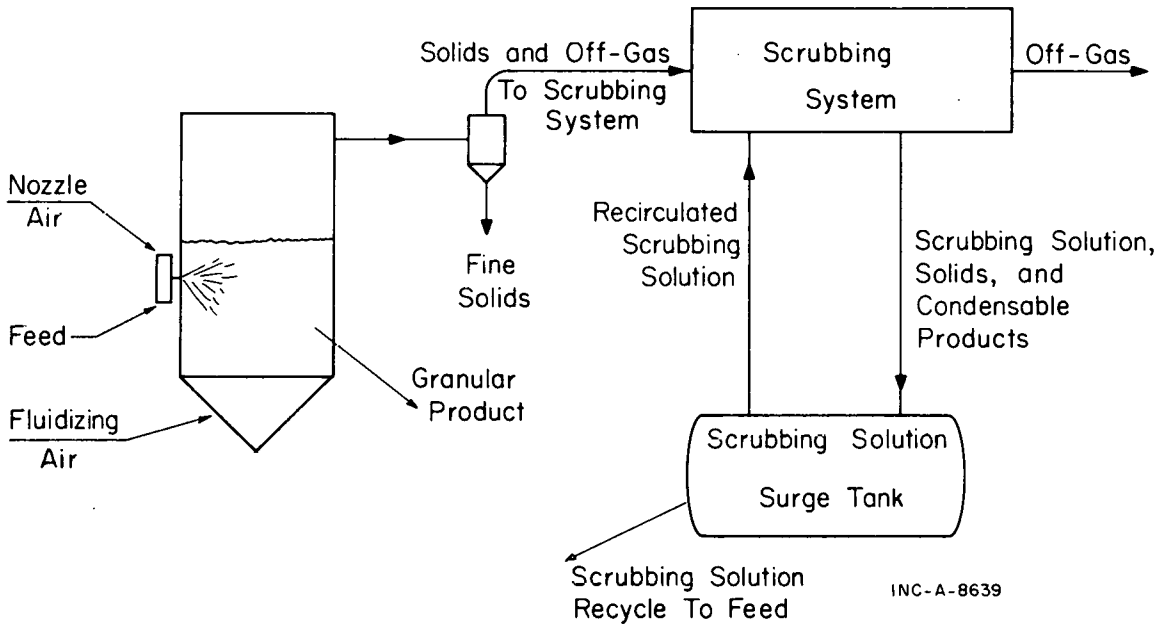

Fig. 19 Generalized calciner process flow sheet.

About 40 percent of the total solids production was elutriated from the WCF calciner vessel during Run H-1, with an estimated 25 percent being collected by the primary cyclone and 15 percent being collected by the off-gas scrubbing equipment. By comparison, 16 percent was elutriated from the pilot plant calciner, with 11 percent being collected by the primary cyclone and 5 percent being collected by the scrubbing system. The higher relative elutriation rate from the WCF calciner may be explained by the difference in total vapor space velocity in the respective calciner vessels. Although both beds are fluidized at a velocity of 1.0 ft/sec, the true vapor space velocity in the WCF calciner vessel is about 2.25 ft/sec, compared to 1.54 ft/sec in the pilot plant calciner vessel. This difference is caused by the difference in feed rate per unit cross-sectional area of the calciner vessel. The feed rate at the WCF is about 6.45 gal/hr-ft^2 [24]; at the pilot plant the feed rate is 3.36 gal/hr-ft^2. In addition to relatively more decomposition products, more nozzle atomizing air is required to give the same air-to-liquid volumetric flow ratio in the WCF.

Equilibrium composition of the recirculated off-gas scrubbing solutions from both calciner systems should be similar if (a) temperatures of the off-gas released from the scrubbing systems are the same, (b) no liquids or solids are lost due to equipment deficiencies, and (c) condensable or collectable components enter the scrubbing system at the same proportional concentration. These assumptions are borne out by comparing the composition of the off-gas scrubbing solutions from WCF Run H-1 and the pilot plant run (see Table XI). The outlet gas temperature from both off-gas scrubbing systems was about 130°F.

TABLE XI

COMPOSITION OF OFF-GAS SCRUBBING SOLUTION FROM FLUIDIZED-BED CALCINER SYSTEMS

	Composition			
	H^+ (N^a)	Al (g/l)	NO_3 (M)	Undissolved Solids (g/l)
WCF Calciner	4 to 5	26	4.2	0.5
Pilot Plant Calciner	5.5	4	5.5	0.5

The major difference in compositions is in the aluminum concentration; this is probably caused by the difference in the amount of solids carried into the scrubbing system from the cyclone.

The mean particle size of the bed product was controlled near 0.6 mm during WCF Run H-1 by a nozzle air-to-liquid flow ratio (NAR) of about 580. Under comparable operating conditions in the pilot plant calciner, the particle size was not stable, but was increasing at the rate of 0.6×10^{-3} mm/hr with the NAR at 650, the maximum available. The pilot plant run was terminated before the mean particle size reached equilibrium.

There were some indications that a further increase in the NAR would have controlled the particle size. Increasing the NAR from 500 to 650 reduced the growth rate from 1.8×10^{-3} to 0.6×10^{-3} mm/hr, and the smaller sized (48 and 65 Tyler mesh equivalent) particles appeared in the bed product.

The difference in NAR's required for particle size control in the respective calciner systems may occur because larger nozzles are used to atomize the calciner feed at the WCF, or because product from the WCF has a longer residence time at the calciner temperature, thus having more opportunity for attrition. Other factors, not now apparent, may also be important to particle size control.

2.12 Zirconium Fluoride-Aluminum Nitrate Waste. Pilot plant calcination of simulated zirconium fluoride-aluminum nitrate wastes has shown that:

(1) Calcium must be added to the feed to provide a Ca/F mole ratio of 0.5 to retain corrosive fluorides in the calcined solids

(2) A 400°C bed temperature yields a suitable product with a minimum of fines elutriated from the calciner vessel

(3) Compared to aluminum nitrate waste, a higher fluidizing velocity is required to provide good heat transfer to the more dense product from zirconium fluoride-aluminum nitrate waste.

The effect of the Ca/F mole ratio in the calciner feed on the amount of fluorides volatilized during calcination at 400°C is shown in Figure 20. Fluoride volatilization decreases with an increasing Ca/F mole ratio. At the stoichiometric mole ratio of 0.50, the fluoride volatilization was less than one percent. Fluorides not volatilized at the lower Ca/F mole ratios were converted to calcium fluoride and aluminum tri-fluoride.

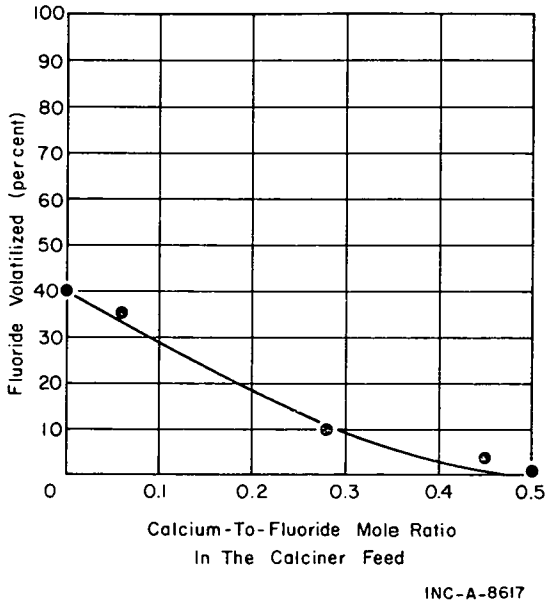

Fig. 20 Effect of calcium-to-fluoride mole ratio on fluoride volatilization rates.

Table XII shows the effect of bed temperature on the calcination of zirconium fluoride-aluminum nitrate waste that was blended before calcination with recirculated off-gas scrubbing solution and a concentrated calcium nitrate-water slurry. This feed make-up procedure follows the procedure that would most likely be used at the WCF.

Of the three temperatures tested, the 400°C bed temperature appears most favorable. The smallest amount of fines was elutriated from the calciner vessel at that bed temperature. Operating the WCF at 500°C would require a reduction in feed rate since less heat could be transferred to the bed [a]. Thus, unit processing costs would increase. Operation at 300°C bed temperature gave a very soft product (attrition index of 0) which resulted in a high fines elutriation rate from the calciner vessel.

Nonradioactive ruthenium was added to the calciner feed to determine ruthenium volatilization rates during calcination of zirconium fluoride-aluminum nitrate waste. The results, shown in Figure 21, along with the ruthenium volatilization rates from acidic aluminum nitrate wastes [25], indicate that a higher fraction of the ruthenium will be volatilized during zirconium fluoride-aluminum nitrate waste calcination than during acidic aluminum nitrate waste calcination. However, the actual radioactive ruthenium release rate from a calciner system will depend, among other things, on the age of the waste being processed.

Corrosion of the calciner equipment and special coupons located within the process was related directly to the amount of fluoride released during calcination.

[a] The NaK heating system already operates near its upper safe temperature, so that the thermal driving force for heat transfer would be lowered if the bed temperature were increased.

TABLE XII

EFFECT OF BED TEMPERATURE ON CALCINATION OF ZIRCONIUM FLUORIDE-ALUMINUM NITRATE WASTE

Process Variable	Bed Temperature 300°C	400°C	500°C
Solids Carry-Over Rate (g/hr)	(350)[a]	180	231 (277)[a]
Product Rate (g/hr)	(1030)[a]	1200	1149 (1003)[a]
Product Properties:			
Bulk Density (g/cc)	1.5	1.5	1.4
Porosity	0.3	0.3	---
Crystalline Components	CaF_2	CaF_2	(CaF_2 and tetragonal ZrO_2)
Attrition Resistance Index[b]	0	60	60

[a] Values shown in parentheses were obtained at 1.25 ft/sec fluidizing velocity, the others at a 1.0 ft/sec fluidizing velocity.

[b] Attrition resistance index is defined as the weight percent of a closely sized screen fraction remaining unchanged in size after undergoing attrition by a jet grinder for a given length of time.

Process equipment and corrosion coupons showed little or no evidence of corrosion at the low fluoride volatilization rates corresponding to a Ca/F mole ratio of 0.5, but were severely corroded when large amounts of fluorides were volatilized.

The fluidizing velocity was increased as the run progressed and the bed material became more dense to maintain good heat transfer rates during calcination of zirconium fluoride-aluminum nitrate solutions. The relatively high density zirconia solids require more air for fluidization than the lower density alumina solids.

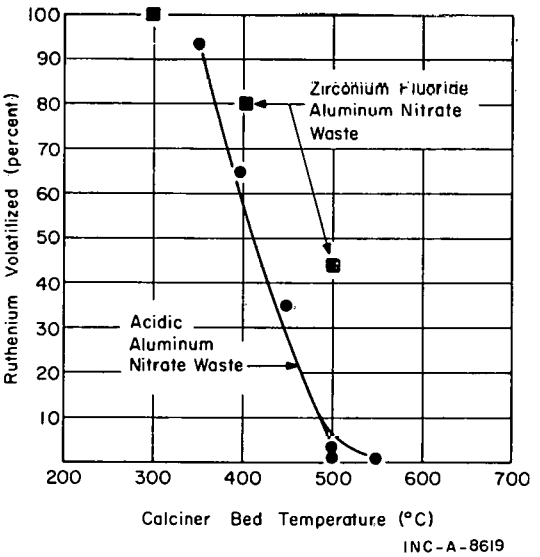

Fig. 21 Ruthenium volatilization during pilot plant waste calcination.

2.13 Ammonium Nitrate-Aluminum Nitrate Wastes. During WCF Run H-1[1], acid deficient ammonium nitrate-aluminum nitrate was used as calciner feed for three days. A very high carryover rate of solids to the off-gas scrubbing system prompted the discontinuation of processing this type of feed, and acidic

aluminum nitrate waste was calcined for the remainder of the run. Subsequent analysis of the undissolved solids in the off-gas scrubbing solution detected an amidonitrate-mercury complex, similar to Millon's base.

Pilot plant calcination of a solution simulating the ammonium nitrate-aluminum nitrate waste in tank WM-180 has shown that:

(1) A high fines generation rate is inherent with this type of calciner feed

(2) Acidifying the feed reduces the fines generation rate

(3) The amidonitrate-mercury complex has not been positively identified in samples of the off-gas scrubbing solution in the pilot plant calciner system.

A high fines rate is inherent with the acid-deficient ammonium nitrate-aluminum nitrate waste. Adding acid to the feed, either by recycle of the off-gas scrubbing solution or blending with acidic nitrate wastes, will reduce the fines elutriation rate. Recycling off-gas scrubbing solution to the feed during one of the pilot plant runs increased the acidity of the feed from neutral to 1.0N acid and reduced the fines elutriation rate from 25 to 17 percent of the theoretical solids production rate.

The amidonitrate-mercury complex is believed to form either in the calciner off-gas upstream of the scrubbing system or in the off-gas scrubbing solution. Ammonium nitrate decomposes at the calcination temperature by any or all of the following reactions:

(a) $4NH_4NO_3 \longrightarrow 2NO_2 + 3N_2 + 8H_2O$

(b) $2NH_4NO_3 \longrightarrow 2NO + N_2 + 4H_2O$

(c) $2NH_4NO_3 \longrightarrow NO_2 + NH_3 + 4H_2O$.

Ammonia, formed by reaction (c), is completely trapped by the scrubbing system. Analysis of samples of calciner off-gas upstream from the scrubbing system showed the presence of NH_3, while NH_3 was not detected in samples of the calciner off-gas taken downstream from the scrubbing system.

Millon's base can be formed by a reaction between mercuric oxide and ammonia by the following reaction:

$$2HgO + NH_3 \longrightarrow \left[-Hg - NH - Hg-\right]^{+2} + 2\ OH^- .$$

Another possible source of NH_3 is the dissociation of ammonium nitrate in the off-gas scrubbing solution. Ammonium nitrate may have been transported to the scrubbing system in partially calcined, spray-dried fines.

The effect of the amidonitrate-mercury complex should be negligible to the process except in one important area -- the complex is insoluble in the nitric acid off-gas scrubbing solution.

2.14 Second- and Third-Cycle Waste. Pilot plant calcination of simulated second- and third-cycle waste has shown that:

(1) Unless the calciner feed is adjusted, sodium nitrate causes agglomerates or cakes in the fluidized bed

(2) Adding sugar to the waste and operating at 500°C makes the process operable

(3) A decided heat benefit is gained by combustion of the sugar

(4) A normal amount of solids was elutriated from the calciner vessel.

The composition of the solution calcined in the pilot plant (see Table XIII) approximates that of the second- and third-cycle wastes stored in the ICPP underground tanks. Decontamination solutions (tartrate, citric acid, soap, etc) are also contained in the tanks, but the exact concentration of these compounds cannot be determined by available techniques.

TABLE XIII

COMPOSITION OF PILOT PLANT CALCINER FEED SIMULATING SECOND- AND THIRD-CYCLE WASTES

Component	Concentration
H^+	0.91 N[a]
Al	0.68 M
Na	2.4 M
NO_3	5.5 M
NH_4	0.05 M
PO_4	0.03 M
SO_4	0.08 M
Hg	0.19 M
Sugar[a]	2 lbs/gal

[a] Sugar is not in the waste solution as stored, but is added as an aid to the calcination process.

A bed temperature of 500°C and a sugar concentration of 4.3 grams sugar/gram sodium are necessary to maintain satisfactory calciner operation. A lower bed temperature (450°C) or a lower sugar concentration (3.2 grams sugar/gram sodium) resulted in bed caking.

The presence of sugar in the feed caused complete mercury precipitation and partial aluminum precipitation. The precipitate was very finely divided and did not settle out in the process equipment. There was no perceptible effect on the process because of the precipitate in the feed solution.

A heat benefit is realized by sugar combustion within the calciner vessel. Table XIV gives the average heat required by the pilot plant calciner process for calcination of different feeds. As shown by the comparison given in Table XIV, less external heat is required to calcine simulated second- and third-cycle waste, containing 2 lbs of sugar/gallon, at 500°C than is required to calcine simulated acidic aluminum nitrate waste at 400°C.

Fines generation rates determined during the pilot plant run were about 10 percent of the theoretical solids production rate. A similar generation rate was observed during calcination of acidic aluminum nitrate waste.

TABLE XIV

COMPARISON OF HEAT REQUIREMENTS FOR VARIOUS FEED SOLUTIONS IN THE TWELVE-INCH-DIAMETER CALCINER

Feed[a]	Temperature	Sugar Content in the Feed	Heat Required (Btu/hr)
Simulated Second- and Third-Cycle Waste	500°C	2 lbs/gal	67,100
Simulated Acidic Aluminum Nitrate Waste	400°C	0	69,600
Raw Water	500°C	0	92,500

[a] Nominal feed rate at 10 l/hr.

2.15 Blend of Zirconium Fluoride-Aluminum Nitrate and Second- and Third-Cycle Wastes. Calcination of a simulated one-to-one volumetric blend of zirconium fluoride-aluminum nitrate waste with second- and third-cycle waste has shown that:

(1) The blend can be calcined at 500°C with 4.3 grams sugar/gram sodium added to the feed

(2) The blend cannot be calcined at 400°C because of cake formation on hot surfaces within the bed

(3) Cryolite (Na_3AlF_6) is formed in the calcined solids and minimal fluorides are volatilized

(4) A high fines generation rate is experienced during 500°C calcination of the sugar-spiked blend.

The sugar concentration and bed temperature were selected to correspond to conditions used to calcine simulated second- and third-cycle waste (500°C bed temperature and 4.3 grams sugar/gram sodium). Other conditions might be used, but they have not been investigated in pilot plant tests.

The blend cannot be calcined at 400°C without sugar. Such a pilot plant run was involuntarily terminated by heater failure. Material from the calciner feed migrated to the hot heater surface and formed very hard, dense cakes. The cakes severely limited heat transfer, which in turn burned out the electrical heaters.

Sodium, aluminum, and the fluorides combined at 500°C in the presence of sugar to form cryolite (Na_3AlF_6), identified by X-ray analysis. As a result, essentially no fluorides were volatilized, and corrosion of the off-gas scrubbing equipment was minimal.

A very high fines rate, approaching 50 percent of the theoretical solids production rate, was experienced during calcination of this blend.

2.2 Particle Growth and Size Distribution in Fluidized-Bed Processes -- A Mathematical Model with Computer Solutions

(E. S. Grimmett; Development Engineering Section)

A study of the factors which influence the particle population and size distribution in a fluidized-bed process has recently been completed at the ICPP. The full report has been published as IDO-14650 [26]; a brief summary of the findings is presented here.

Most fluidized-bed processes involve particles which may grow or disintegrate, enter or leave the system, take up or reject heat, transfer heat from one part of the bed to another, provide surface area for catalytically induced reactions, or react with the fluidizing medium. The fluidized-bed calcination process which converts aqueous nuclear reactor wastes into granular solids is an excellent study example because it embodies most of the phenomena associated with a typical fluidized-bed process.

A mathematical model has been developed which predicts the steady state or transient particle size distribution in a fluidized bed. Although the various rate processes have been derived on the basis of the fluidized-bed calcination process, the basic differential equation should be applicable to a variety of systems, with the proper modifications. This present study shows how the significant operating variables affect the system of particles in a fluidized bed. The individual rate processes are postulated and simplified as required, and employed in the derivation of a general partial differential equation which describes the particle size distribution as a function of particle size and time. Particle size distributions predicted by the mathematical model are then compared with experimental data.

2.21 Basic Rate Equations. The mass of particles within any particle size interval can be determined as a function of time by considering the mass of material entering and leaving the interval as a result of various rate processes. The equivalent solids feed rate, the total bed weight, the seed rate, the particle size distribution of seeds, the fluidizing velocity, and the properties of the fluidizing gas are specified functions.

Consider the particles lying within the interval L and $L + \Delta L$ as shown in Figure 22. An unsteady state material balance around the particle size interval yields the following equation:

$$\left\{\begin{array}{l}\text{Input by growth}\\ \text{Feed deposition}\\ \text{Seed addition}\\ \text{Input by attrition}\end{array}\right\} - \left\{\begin{array}{l}\text{Output by growth}\\ \text{Particle elutriation}\\ \text{Output by attrition}\\ \text{Product removal}\end{array}\right\} = \text{Accumulation.}$$

The mechanisms of particle growth and attrition actually move mass across the particle size boundaries, while the other rate processes remove mass from or deposit mass into the interval directly. Descriptions of the individual rate processes and detailed derivations of the expressions for these processes are given in the topical report IDO-14650 [26].

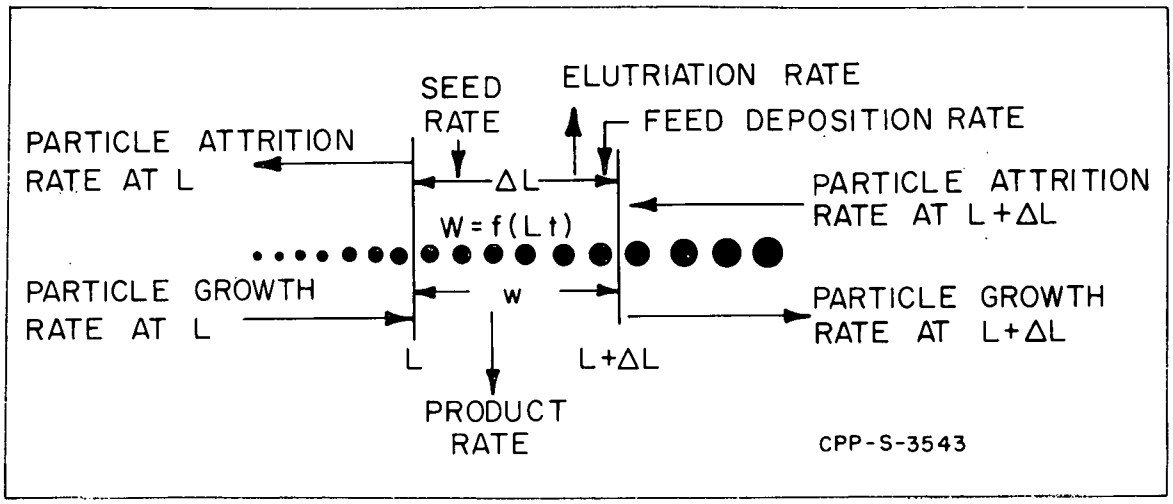

Fig. 22 Pictorial illustration of mass transfer processes around any particle size interval.

2.22 General Partial Differential Equation. The general partial differential equation describing the particle size distribution as a function of particle size and time was obtained by substitution of the expressions for the various rate processes into the unsteady state material balance equation. Use of the Theorem of the Mean of differential calculus and the Mean Value Theorem of integral calculus, and application of the limit as the independent variables ΔL and Δt simultaneously go to zero, yields the partial differential equation describing the particle size distribution as a function of particle size and time.

$$\left[\frac{PS(t)\ \partial W(L,t)}{\partial L}\right] + \left[\frac{6C_g PF(t)}{\rho_s} \cdot \frac{\partial W(L,t)}{\partial L}\right]$$

$$+ \left[g_i(L)\ \frac{\partial^2 W(L,t)}{\partial L^2} + \frac{\partial g_i(L)}{\partial L} \cdot \frac{\partial W(L,t)}{\partial L}\right]$$

$$- \left[\frac{R_a(L)\ \partial^2 W(L,t)}{\partial L^2} + \frac{\partial R_a(L)}{\partial L} \cdot \frac{\partial W(L,t)}{\partial L}\right]$$

$$- \left[\frac{P_r(t)}{W} \cdot \frac{\partial W(L,t)}{\partial L}\right] - \left[\frac{AK_e}{W} \cdot \frac{\partial W(L,t)}{\partial L}\right] = \frac{\partial^2 W(L,t)}{\partial L\ \partial t} \quad .$$

Reference 26 should be consulted for nomenclature.

Since an analytical solution of Equation (1) was not possible, an approximation method was used to obtain the desired solution. The finite difference method used was a modified Runge-Kutta method for solving differential equations. This procedure resolved the partial differential Equation (1) into a number of ordinary differential equations which had to be solved at each time step. A digital computer program was written to obtain the solution.

2.23 Testing of the Mathematical Model. To test the validity of the model, the results of experimental fluidized-bed calcination runs were compared with the predictions of the mathematical model. Three sizes of calciners were used to obtain experimental data: (a) a 3-inch-diameter calciner, (b) a 12-inch-diameter calciner, and (c) a 24-inch-square calciner. This resulted in a 300-fold range in bed weights used in the experiments.

The run made in the 24-inch-square calciner was a typical run of fairly long duration in which it became necessary to add seed particles for control of the particle size of the product. Particle attrition was minimal and consideration of attrition in the model was not necessary.

Cumulative weight distribution curves generated by the computer, and the corresponding experimental curves, are shown in Figure 23. The particle size distribution predicted by the mathematical model compares favorably with the experimental distribution at each portion of the run.

Experimental and simulated particle size distribution curves for the 12-inch-diameter calciner are shown in Figure 24. As in the case of the 24-inch-square calciner, the attrition rate was low and could be neglected in the mathematical model. The agreement between the particle size distribution predicted by the model and that obtained experimentally is excellent.

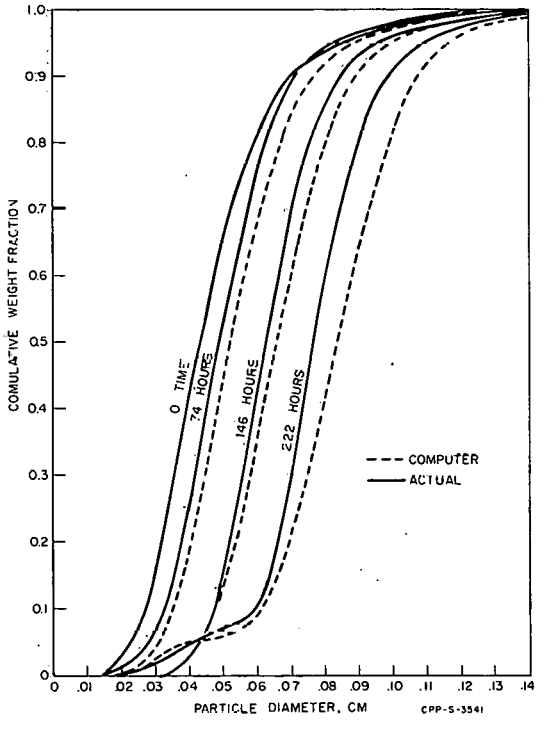

Fig. 23 Experimental and calculated particle size distributions in the 24-inch-square calciner.

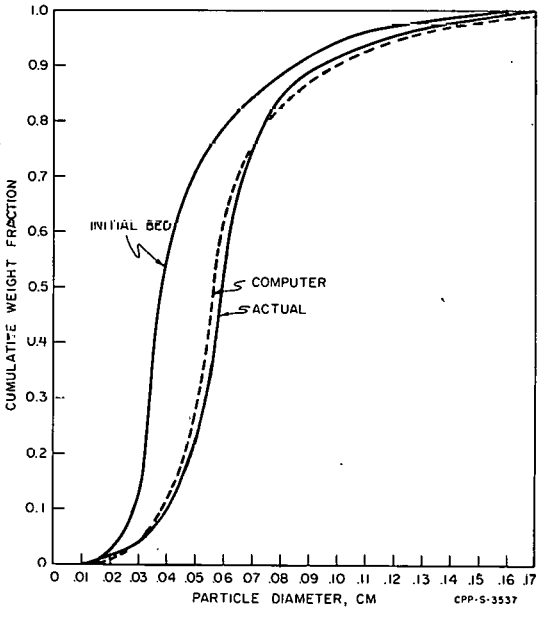

Fig. 24 Experimental and calculated particle size distributions in the 12-inch-diameter calciner.

The experimental run made in the 3-inch-diameter calciner was conducted at the Argonne National Laboratory in Lemont, Illinois [27, 28]. Comparison of these data with the computer-predicted curve (Figure 25) again gives excellent agreement.

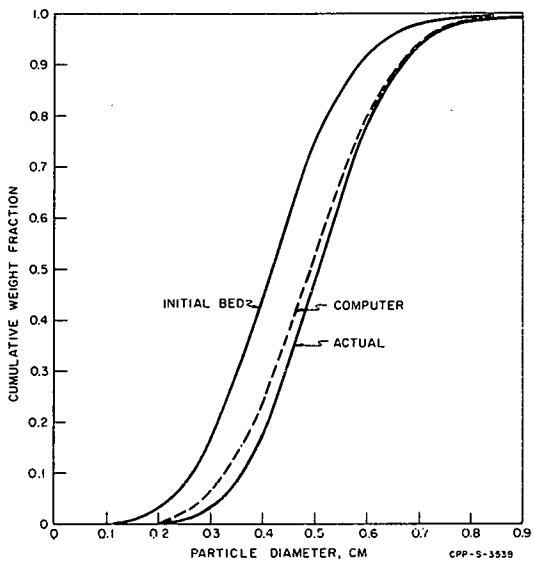

Fig. 25 Experimental and calculated particle size distributions in the 3-inch-diameter calciner.

Since there were wide variations in the sizes and operating conditions of the three calciners, the generally good agreement with the mathematical model substantiates its validity over a wide range of conditions.

The mathematical model at present has two main weaknesses: (a) elutriation rates predicted from the model have not been consistent with actual observations, (b) an expression for the rate of attrition as a function of particle size and the various operating parameters is not available. The lack of information on the process of attrition is particularly evident, and a study of the factors affecting attrition is now being planned.

2.3 Volatilization of Ruthenium from the WCF -- the Ruthenium Dioxide-Oxygen-Ruthenium Tetroxide Equilibrium
(R. R. Hammer, B. D. Penman [a];Chemistry Section)

A study of the $RuO_2(s) + O_2 = RuO_4(g)$ equilibrium was made by the transpiration technique in the temperature range 453-723°C. For the reaction above in the temperature range indicated,

$$\log Kp = -4.764 \times 10^3 T^{-1} - 0.236 .$$

Using the results of this study, a calculation was made of the amount of ruthenium which would be expected to transport from the calciner vessel as RuO_4 vapor. The amount of ruthenium calculated as RuO_4 for the off-gas stream was significantly smaller than that observed in the WCF, suggesting the presence of either other volatile species or of very small particles containing ruthenium in the WCF off-gas, or possibly the existance of non-equilibrium conditions in the system.

A complete discussion of the investigation is reported in IN-1013 [29].

[a] ARMU student from Colorado State University

3. PROPERTIES OF SOLID CALCINED WASTES

3.1 Migration of Mercury in Alumina Calcine

(D. W. Rhodes, M. W. Wilding; Chemistry Section)

After converting the highly radioactive aqueous wastes at the Idaho Chemical Processing Plant to granular solids in the Waste Calcining Facility, the solids are stored underground in large stainless steel bins. The center line temperature of the calcine may be as high as 700°C during storage due to radioactive decay of the contained fission products. The distribution of the volatile constituents of the calcine changes during the period of high heat generation, with migration occurring from the hot zone to a cooler zone.

The distribution of mercury in short-term experiments along a temperature gradient was reported earlier [1]. More recent experiments, in which the temperature profile along a column of alumina was maintained constant for six weeks, indicated that essentially all of the mercury migrated from calcine at a temperature greater than 400°C. The concentration of mercury in the calcine below 400°C gradually increased to a maximum of about 12 weight percent at approximately 125°C, forming a distinct yellow band of HgO. Below this band, the concentration of mercury was the normal 2.5 weight percent. A material balance indicated that > 95 percent of the mercury was accounted for. These results indicate that during long term storage, mercury will migrate to the outer edges of the stored calcine if the wall temperature is as high as 125°C, and will be deposited there as a layer of mercuric oxide.

3.2 Leachability of Alumina Calcine Produced in the Idaho Waste Calcining Facility

(D. W. Rhodes, B. E. Paige; Chemistry Section)

During the operation of the WCF, approximately 500,000 gallons of aqueous waste containing aluminum nitrate have been successfully converted to solid alumina calcine. The leaching rate of this calcine is of interest for two reasons: (a) to compare the relative safety of storing calcine to other forms of solid waste and (b) to determine the feasibility of recovering fission products at a future date.

Calcine is considered to be a safe form for permanent storage at the NRTS in Idaho, as it is stored in stainless steel bins in buried concrete vaults. Should any liquid enter these vaults, an alarm on the liquid-level detector in the vault sump would sound, and the liquid would then be removed by means of a steam jet. While the hydrology of the NRTS is extremely favorable for the storage of dry solid wastes, in other localities shallow ground water tables or high annual rainfall may create potential storage hazards. Therefore, from a safety standpoint, the leaching rate is of interest in case water does inadvertently contact the calcine during long term storage.

The leaching of fission products from calcine also has been considered as a means of either removing the fission products for future use or of removing long-lived fission products from the bulk of the waste solids. Previous leaching studies have involved a batch contacting technique [30] and development of a pulsed, multiple stage, counter current column [31, 32, 33]. The calcine used in this earlier work was produced in pilot plant equipment. This calcine was spiked with fission products and contained 60 to 70 percent α-alumina.

In current work, typical amorphous alumina calcine produced in the WCF during routine calcination of highly radioactive waste was used for the leaching studies. This material was leached continuously in laboratory experiments with distilled water at temperatures of 25°C and 80 to 90°C; it was also leached with dilute (0.25 to 0.5M) nitric acid at 25°C. A complete discussion of the leaching method and the results for the current work is reported in IDO-14673 [34]. A summary of the principal results is presented here.

Distilled water at 25°C leached more than 95 percent of the cesium and 33 percent of the strontium from the WCF calcine in seven weeks, with most of the leaching occurring during the first two or three days. Only 0.01 percent of the aluminum was leached in a similar period, and apparently the cerium and ruthenium were leached at the same rate as the aluminum. After 14 weeks, the cesium was essentially all removed from the calcine, and the leaching rate was decreasing rapidly; however, the leaching rate for strontium had leveled off at about 0.02 percent per day. Since other fission products and aluminum have low leaching rates, most of the cesium and some of the strontium can be recovered by circulating distilled water through the calcine at 25°C. The recovery can probably also be accomplished at higher temperatures since the leaching rate of aluminum at 80 to 90°C was not much higher than at 25°C.

During six weeks of leaching with dilute HNO_3 (0.25 to 0.5M) at 25°C, the WCF calcine disintegrated, and more than 99 percent of the alumina dissolved. The fission products were found to be uniformly distributed in the calcine. Dilute nitric acid will dissolve the amorphous alumina calcine now being produced in the WCF if the need arises, but it cannot be used to preferentially remove specific fission products from the calcine unless the calcine is first converted to α-alumina, which is insoluble in nitric acid.

3.3 Corrosion Surveillance of Calcined Solids Storage Bins
(D. W. Rhodes, T. L. Hoffman; Chemistry Section)

The Waste Calcining Facility is provided with seven new storage bins erected from Type 304 stainless steel [1] for storing calcine from aluminum and zirconium type raffinates. The best method of obtaining corrosion data in a system of this sort is to provide for surveillance of the corrosion in the vessel itself during use. Accordingly, two of these bins are provided with entry ports to allow placement and retrieval of corrosion specimens. One bin is scheduled to contain calcine from the aluminum-type raffinate, and the other calcine from zirconium-type raffinate. Welded cylinders and plates of stainless steel Types 304, 304L, and 405 and carbon steel 1025 have been installed in these bins.

If exposure time is long enough to give significant results, it is planned to withdraw a set of coupons for evaluation immediately prior to making a decision on the material of construction for a new set of bins. Other coupons will be used to monitor the long term performance of the construction materials of the bins.

4. HEAT TRANSFER STUDIES AFFECTING THE CALCINATION PROCESS AND STORAGE OF THE CALCINED PRODUCT

4.1 Heat Transfer to a Fluidized Bed by Use of Finned-Tube Heat Exchangers (W. A. Freeby; Development Engineering Section)

One limitation in the capacity of a fluidized-bed calcination process is the rate at which heat can be transferred to the material in the bed. In the ICPP waste calciner, heat is transferred from a liquid metal (NaK) inside a tube-type heat exchanger to the fluidized bed on the outside of the tubes. The controlling heat reisistance in this case is the transfer of heat from the tube wall to the bed. On the premise that increasing the area available for heat transfer on the outside of the tubes would improve the overall heat transfer rate, a study of the effect of finned surfaces on the heat exchanger tubes was undertaken. The result was a finding that the rate of heat transfer to the fluidized bed was increased by the use of finned tubes, but that the increase was not as large as the increase in heat transfer area.

The complete study and correlation of results are reported in a thesis [35] presented to the University of Idaho; actual work was performed in the Development Engineering Laboratories at the ICPP. A summary of the experimental approach and principal findings is presented here.

4.11 Experimental Approach. This study involved the steady-state heat transfer from horizontal tubes immersed in a fluidized bed to a mixture of small solid particles and air which make up the bed. Heat transfer coefficients as a function of particle size, fluidizing velocity, and fin spacing were investigated using both finned and plain tubes. The work was conducted in a twelve-inch-diameter fluidized-bed unit, shown schematically in Figure 26, with heat being transferred to the fluidized bed by steam condensing inside horizontal aluminum tubes extending into the bed. Figure 27 shows the heating system and tube configuration. The tubes were oriented to provide a triangular pitch of about 1-1/8 inch. Three separate tube bundles were used during the study: (a) transverse finnod tubes with 11 fins per inch, (b) transverse finned tubes with 5 fins per inch, and (c) plain tubes. The fluidized mixture consisted of alumina particles with mean diameters ranging from 0.41 to 0.60 mm, suspended in an upward flowing air stream at velocities of 1.5, 2, and 3 times the minimum for fluidization. The minimum fluidizing velocities were determined experimentally.

4.12 Conclusions. The results of the investigation indicate the following:

(1) Heat transfer rates from finned tubes to the fluidized bed were from 1.1 to 4.6 times those for the plain tubes, depending on the conditions used. The increased heat transfer rate ranged up to half of the proportional increase in total surface area in contact with the bed as compared to the performance of bare tubes.

(2) The heat transfer coefficients for the finned tubes ranged from 16 to 57 percent of those for plain tubes. The fact that the heat transfer areas of the finned tubes were from 4.8 to 12.1 times those of the plain tubes resulted in the greater overall heat

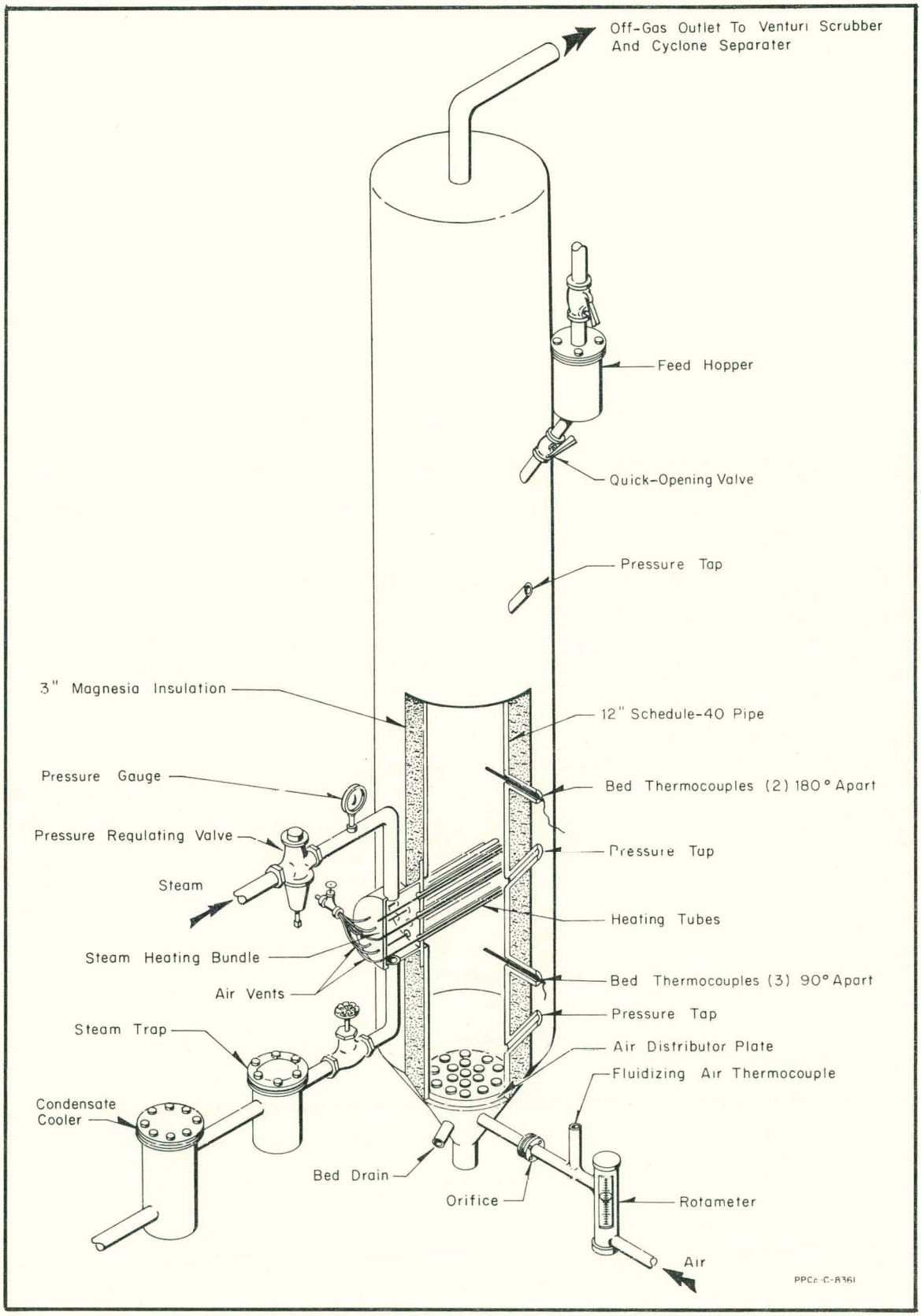

Fig. 26 Diagram of 12-inch-diameter fluidized-bed apparatus.

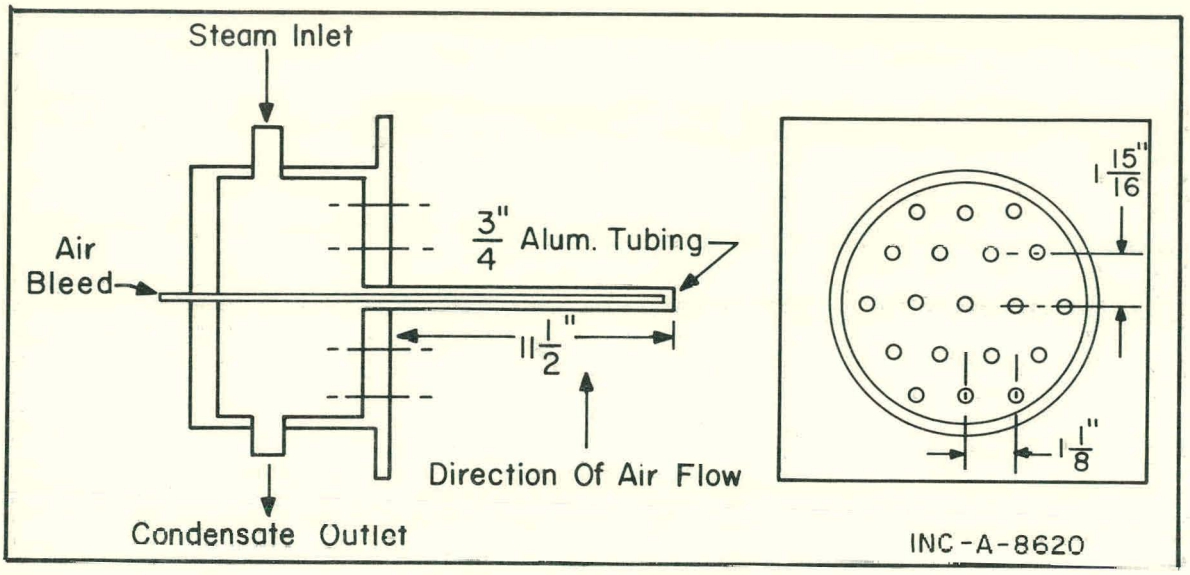

Fig. 27 Heating system and tube configuration.

transfer rates for the finned tubes in spite of the lower coefficients[a].

(3) Heat transfer coefficients increased with increased mass velocity for all tube bundles tested.

(4) Heat transfer coefficients increased with decreasing mean particle diameter at a given mass velocity.

4.2 Heat Transfer Within Calcine Storage Vaults
(J. C. Petrie; Development Engineering Section)

New solids storage bins were designed and fabricated following the successful initial campaign at the WCF which filled the original bins [1]. The new bins are now receiving radioactive solids from the second waste processing campaign at the WCF.

The pilot plant program which showed that shrouds around each of the new bins decreased the effectiveness of heat removal [1] has been expanded. The objectives of the expanded test program are to determine the effect of nearby surfaces on heat transfer from the simulated bin, and to determine the relative contribution of radiation and convection heat transfer under such conditions. Data from these tests should be helpful in designing future storage facilities. Progress to date is summarized here; however, the investigation is continuing and complete conclusions and recommendations cannot be made at this time.

4.21 Test Equipment. Details of the test equipment are shown in Figure 28. The heat source, or simulated bin, was designed to be geometrically similar to

[a] With finned tubes, it would be expected that particles would have difficulty making as intimate or as frequent contact with all parts of the finned areas as they do with the surfaces of plain tubes. Therefore, it was expected that the heat transfer coefficients for finned tubes would be less than those for plain tubes.

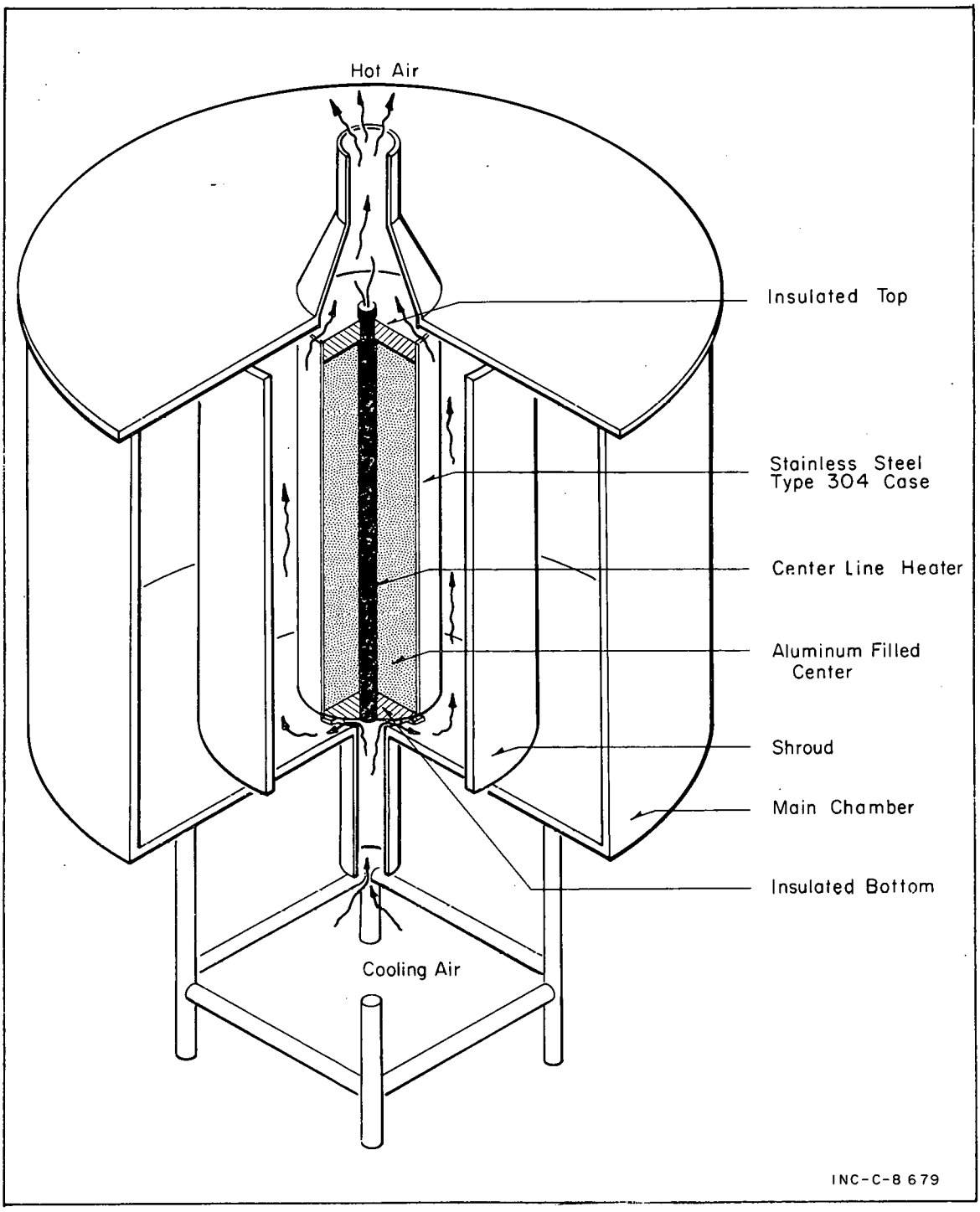

Fig. 28 Heat transfer test stand.

one of the new calcine storage bins. Heat was supplied at the center line of the apparatus by electrical resistance heaters controlled by a powerstat. From the center line heaters the heat flowed radially through the aluminum filler and the Type 304 stainless steel case. The electrical power supplied to the heaters should have been converted to a uniform heat flux through the walls of the source, end losses being minimized by the insulation at the top and bottom. Natural

air circulation through the space between the source and shroud was provided by openings at the top and bottom of the main container. Natural convection flow was induced by the temperature gradient.

The shrouds and the source were fabricated from stainless steel, Type 304, to duplicate the proposed material of construction of the new solids storage bins. Shrouds of various diameters were fabricated to test the effect on heat transfer of the separation between source and shroud. Separations tested were 0.35, 2.7, 6, and 12 inches. The 0.35-inch gap is geometrically proportional to the gap which was originally proposed for the plant installation; the 2.7-inch gap was the exact separation proposed.

Power delivered to the source, converted to equivalent heat flux through the source walls, could be varied from 50 to 750 Btu/hr-ft^2. The source was tested outside the container to provide comparative data on totally open, natural convection heat transfer.

4.22 Test Results and Conclusions. The hypothesized advantage of the proposed shrouds was to improve natural convection heat transfer and thereby decrease the surface temperature of the bin, or heat source. However, reflection of radiant heat back to the source from the shroud negated any overall improvement in heat transfer by natural convection. As the source-to-shroud separation was decreased at a given heat flux, the source wall temperature increased as shown in Figure 29.

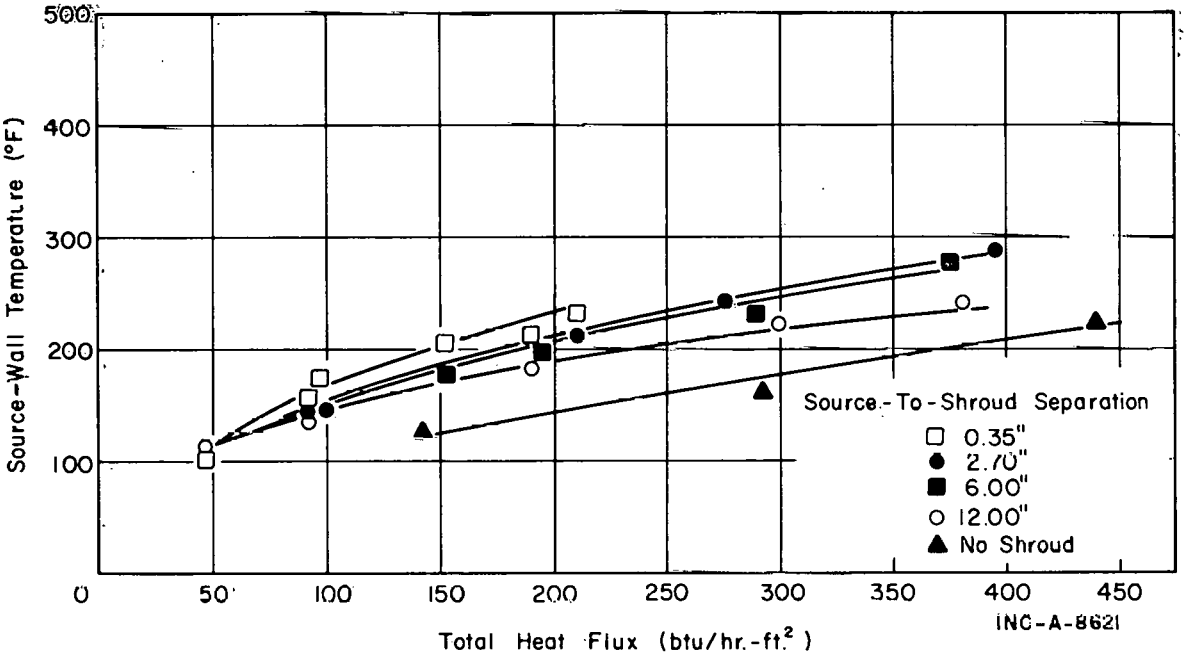

Fig. 29 Source wall temperature versus total heat flux.

The temperature profile along the height of the shroud increased linearly from botton to top. Figure 30 depicts the temperature profiles along the shroud height at various heat fluxes for the 2.7-inch source-to-shroud separation. Increasing the heat flux increased the temperatures on the shroud and also increased the temperature gradient.

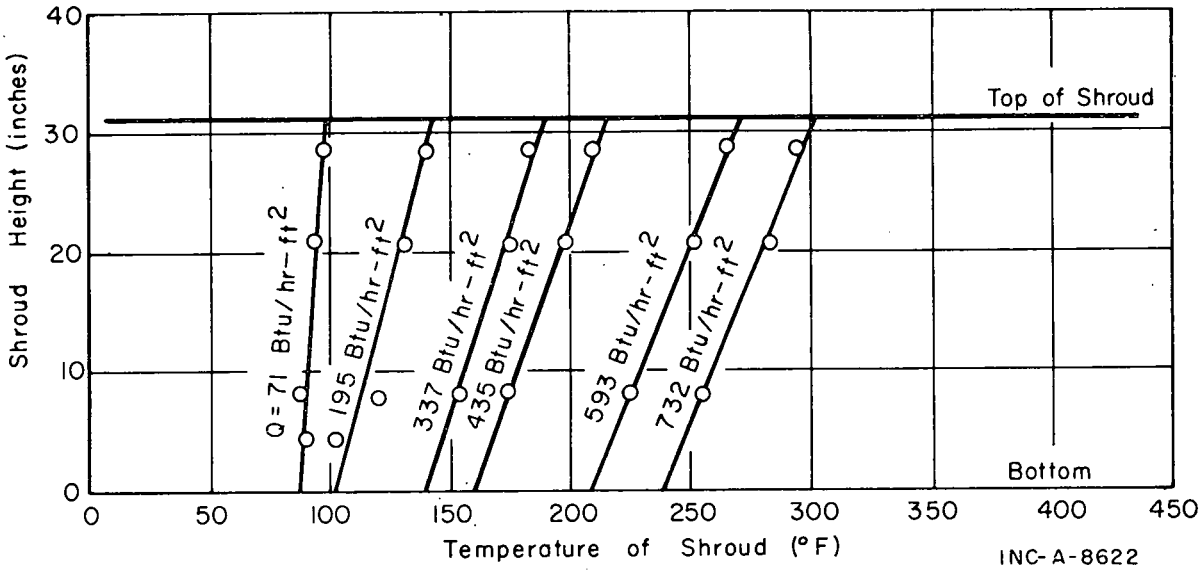

Fig. 30 Temperature profile along shroud height (2.2-in. source-to-shroud separation).

Data have been published concerning heat transfer across a totally enclosed air space where natural air circulation within the closed space could occur. The effect of circulation of the air within the gap is presented by comparing an effective thermal conductivity with the normal thermal conductivity of the air within the gap. The effective thermal conductivity is increased by convection heat transfer; heat transfer by radiation is neglected in this comparison. The comparison is shown by the lower line in Figure 31 [36].

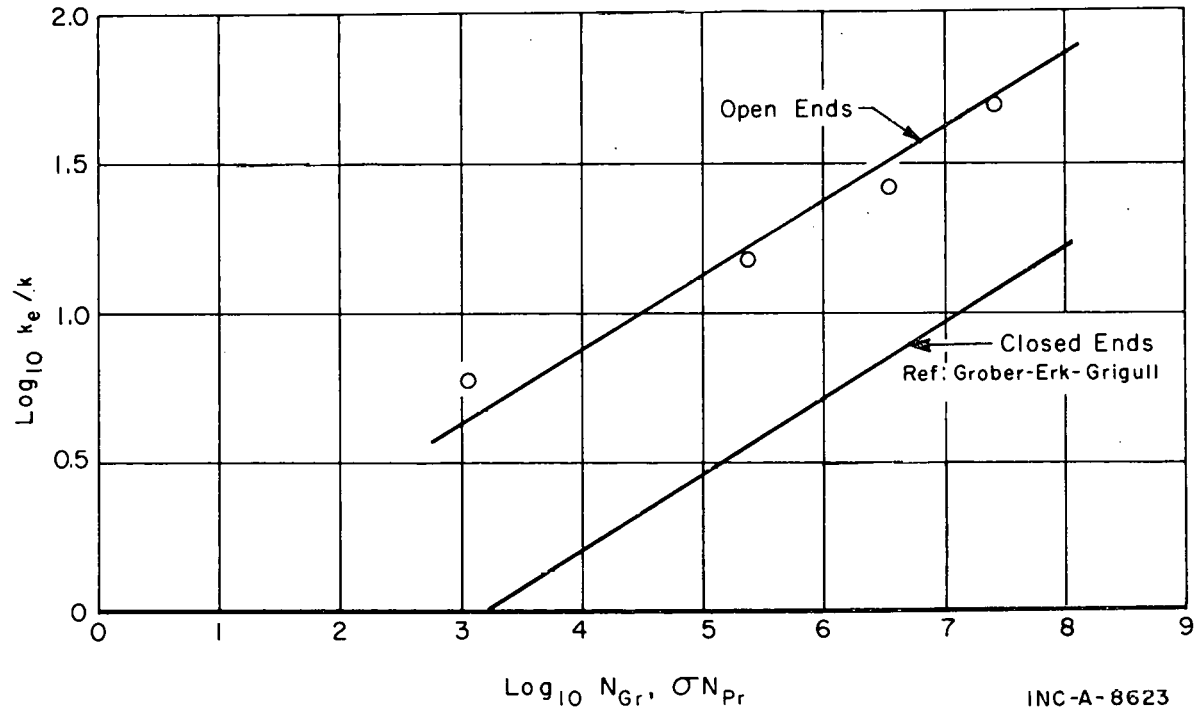

Fig. 31 Effective thermal conductivity for open-ended and totally enclosed air spaces.

Effective thermal conductivity is defined by

$$k_e = \frac{Q\ln(D_o/D_i)}{2(T_1-T_2)} \quad (1)$$

where

k_e = effective thermal conductivity, Bt/hr-ft^2-°F

Q = total heat flux, Btr/hr-ft^2

T_1 = temperature of source, °F

T_2 = average temperature of shroud, °F

D_o = diameter of shroud, inches

D_i = diameter of source, inches.

Allowing replacement of the cooling air, as in the current study, greatly increased the ratio of the effective thermal conductivity to the normal thermal conductivity of air, as shown in Figure 31.

The ratio of effective-to-normal thermal conductivities is plotted as a function of the Raleigh Number; based on the width of the gap as the characteristic length [36].

4.23 Interim Recommendation. Shrouds were shown to be unnecessary as a result of these tests. Their elimination from the storage bin design saved at least $45,000 in construction costs.

4.24 Future Studies. The effect of nearby surfaces on heat transfer will be investigated for data correlations to summarize the results of these tests.

4.3 Heat Dissipation from Buried Wastes.
(B. R. Dickey, D. E. Black; Development Engineering Section)

Current estimates indicate that both the volume and total cost of radioactive waste storage will increase sharply with the growth of the nuclear power industry. A significant reduction in the cost of future solid waste storage facilities could be achieved if the internal cooling systems and outer containment vaults could be omitted safely. If solid wastes are buried in a single container directly in the soil, the decay heat of the fission products must be dissipated by the mechanism of conduction. Since the temperature of the waste must be maintained below a specified maximum value, the factors affecting the temperature in the waste and the surrounding soil strongly influence the dimensions of the waste container.

As part of a study of lower cost methods of waste management, a program was initiated to determine the quantitative effect of significant factors on the temperature distribution in and surrounding small- and large-diameter heat sources buried in the soil. This program included: (a) formulation of mathematical models for predicting steady state and transient temperatures within the heat

source and the surrounding soil, (b) determination of the physical properties required in the mathematical models, (c) development of digital computer programs for solving the resulting equations, (d) simulation of a small-diameter buried heat source of high thermal conductivity using an electrical heater, and (e) verification of the mathematical model by comparing the calculated and experimental temperatures for both steady-state and transient conditions. The quantitative effects of the following factors on the calculated temperatures within the waste and the surrounding soil were determined:

(1) Thermal conductivity of the waste and the surrounding soil

(2) Magnitude of a time-dependent heat generation rate

(3) Dimensions of the cylindrical heat source

(4) Burial depth of the source.

A detailed description of the mathematical models, the derivation and solution of the equations based on the models, and numerical examples of calculated temperature distributions are presented in IN-1032, Mathematical and Experimental Analysis of Heat Dissipation From Cylindrical Source Buried in Soil [37]. Highlights of this study are presented in the following paragraphs.

4.31 Experimental Program. A small-diameter buried fuel element of high thermal conductivity was simulated by burying a 1500-watt electrical heater at a depth of 10 feet in the soil. The temperature and moisture content of the soil were monitored at various depths and radial distances from the heater for power levels corresponding approximately to 85-day and 135-day cooled MTR elements. The measured temperatures were compared with the calculated temperatures to determine the accuracy of the mathematical model.

Use of the mathematical model for predicting the temperature distribution within a heat source and the surrounding soil requires reasonably accurate values of the thermal conductivity and heat capacity of the waste and soil. Thermal conductivities were determined using a "thermal conductivity probe". The probe, consisting of a cylindrical rod of high conductivity material, is inserted into the medium of unknown thermal conductivity, and a constant rate of power is applied to a heating element within the probe. Temperatures obtained from sensors located at the center line of the probe are plotted versus the natural logarithm of the elapsed time. This curve asymptotically approaches a constant value of $(Q/4\pi k)$. Since Q (the power per unit length of the probe) is known, the thermal conductivity of the medium can be determined from the slope of the asymptotic line [38]. The mean specific heat of the soil was determined using a standard drop calorimeter. A summary of the physical properties of the soil and the techniques employed in their determination is shown in Table XV.

4.32 Mathematical Model. Mathematical models were formulated for predicting (a) the temperature distribution in and surrounding a small-diameter heat source of high thermal conductivity buried in soil and (b) the temperature distribution within a bin of solidified waste. Cylindrical geometry was assumed in all cases and the standard Fourier heat equation was used to describe the steady-state and transient temperatures within the source and the surrounding medium. The steady-state temperature distribution is approached only in the case of long term cooled waste.

TABLE XV

PHYSICAL PROPERTIES OF SOIL AT TEST SITE

Soil Property	Units	Value	Temperature Range (°F)	Number of Determinations	Technique Employed
Thermal Conductivity	Btu/hr-ft-°F	0.2 to 0.4	50 to 520	21	Thermal Conductivity Probe
Mean Specific Heat	Btu/lb-°F	0.18 to 0.22	90 to 250	23	Drop Calorimeter
Density	lb/ft^3	80 to 115	---	6	Gravimetric
Porosity	Percent	25 to 30	---	150	Saturation Method
Size Distribution	Wt%				
0.75 to 3 inches		70	---	24	Standard Sieve Screen
0.08 to 0.75 inch		24			
< 0.08 inch		6			
	Total	100			
Composition	Wt%		---	80	Wet Chemical Analysis
SiO_2		57			
Al_2O_3		16			
Fe_2O_3		6			
FeO		6			
MgO		2			
CaO		7			
Na_2O		2			
K_2O		3			
TiO_2		1			
	Total	100			
Moisture Content	Vol%	2 to 8	35 to 130	200	Neutron Moisture Detector

Solution of the partial differential equations satisfying the initial and boundary conditions was obtained by transform methods. An analytical solution was obtained for the steady-state temperatures, while the transient temperatures were computed by finite difference methods.

The solution for the steady-state temperatures in the medium surrounding a simulated fuel element buried in the soil is

$$T(r,z) = \left[\frac{2qL}{\pi^2 k_s} \sum_{n=1}^{\infty} \frac{K_o\left(\frac{rn\pi}{L}\right)\left[\cos\frac{n\pi d}{L} - \cos\frac{n\pi D}{L}\right]\sin\left(\frac{n\pi z}{L}\right)}{n^2 K_1\left(\frac{an\pi}{L}\right)}\right] \qquad (2)$$

where

a = radius of the simulated fuel element, ft

d, D = burial depth of the top and bottom of the heat source, respectively, ft

q = heat flux at the surface of the element, Btu/hr-ft^2

k_s = thermal conductivity of soil, Btu/hr-ft-°F

$K_o(X)$, $K_1(X)$ = modified Bessel functions of the second kind of the argument X, dimensionless

L = that depth at which an increase ΔL results in a negligible change in the calculated temperature, ft

n = finite sine transform parameter, an integer

r = radial distance from the center of the source, ft

z = depth beneath the soil surface, ft.

The steady-state temperatures within a bin containing solidified waste and in the surrounding soil are given by the following expressions:

for the waste,

$$T_1(r,z) = \frac{2L^2 q''}{\pi^3 k_c} \sum_{n=1}^{\infty} \frac{\left[\cos \frac{n\pi d}{L} - \cos \frac{n\pi D}{L}\right] U(X, X_B, k_c, k_s) \sin \left(\frac{n\pi z}{L}\right)}{n^3 \left[k_c K_o(X_B) I_1(X_B) + k_s K_1(X_B) I_o(X_B)\right]} \quad (3)$$

and for the soil,

$$T_2(r,z) = \frac{2L^2 q''}{\pi^3} \sum_{n=1}^{\infty} \frac{\left[\cos \frac{n\pi d}{L} - \cos \frac{n\pi D}{L}\right] \left[I_1(X_B) K_o(X)\right] \sin \left(\frac{n\pi z}{L}\right)}{n^3 \left[k_c K_o(X_B) I_1(X_B) + k_s K_1(X_B) I_o(X_B)\right]} \quad (4)$$

where

$I_o(X)$, $I_1(X)$ = modified Bessel functions of the first kind of the argument X, dimensionless

k_c, k_s = thermal conductivity of the waste and soil, respectively, Btu/hr-ft-°F

q'' = volumetric heat generation rate, Btu/hr-ft^3,

X = the quantity, $\frac{rn\pi}{L}$, dimensionless.

The transient temperatures in and surrounding a simulated fuel element buried in the soil are obtained by solving the following system of equations at each time step:

$$-\phi_1 \bar{u}_{1,t+\Delta t} + 2\bar{u}_{2,t+\Delta t} = -\beta_1 \bar{u}_{1,t} - Q(n)$$

$$\theta_m \bar{u}_{m-1,t+\Delta t} - \phi_m \bar{u}_{m,t+\Delta t} + \sigma_m \bar{u}_{m+1,t+\Delta t} = -\beta_m \bar{u}_{m,t} \quad (5)$$

$$\theta_{M-1} \bar{u}_{M-2,t+\Delta t} - \phi_{M-1} \bar{u}_{M-1,t+\Delta t} = -\beta_{M-1,t+\Delta t}$$

where

m = 2, 3, ... M-2 (nodal points in the radial direction)

M = last nodal point in the radial direction

$\theta_m, \phi_m, \sigma_m, \beta_m$ = known functions of the time, radial distance increment, and the thermal properties of the medium

$\bar{u}_{m,t}$ = transformed temperature at point m at time t

$Q(n)$ = function of heat flux and transform parameter, n.

Temperatures at any time $t + \Delta t$ and spatial location (r, z) can be obtained by solution of the matrix of transformed temperatures given by Equation (5). The calculational procedures required solutions of the preceding equation by a computer.

4.33 Results. The experimental steady-state temperatures and those calculated using Equation (2), for a simulated buried fuel element, are shown in Figure 32. A comparison of the experimental transient temperatures and those calculated from Equation (5) is given in Figure 33. Agreement between the experimental and the calculated temperatures indicate that the mathematical model yields reliable results.

The quantitative effects of the thermal conductivity of the waste, the heat generation rate of the waste, and the radius of the bin on the temperature distribution were calculated using Equations (3) and (4). Numerical examples using parameters of practical interest are shown in Figures 34, 35, and 36. The thermal conductivity of the solid waste, especially in the range $k_c < 0.15$, and the radius of the waste container are important factors in determining the maximum temperature within the waste and, hence, the dimensions of the waste container.

4.34 Future Applications. The results of this study will be used to determine the feasibility of burying solid radioactive wastes and spent nuclear fuel elements in containers buried directly in soil. With some modification, the mathematical models and the computer codes can be used to solve other similar heat transfer problems.

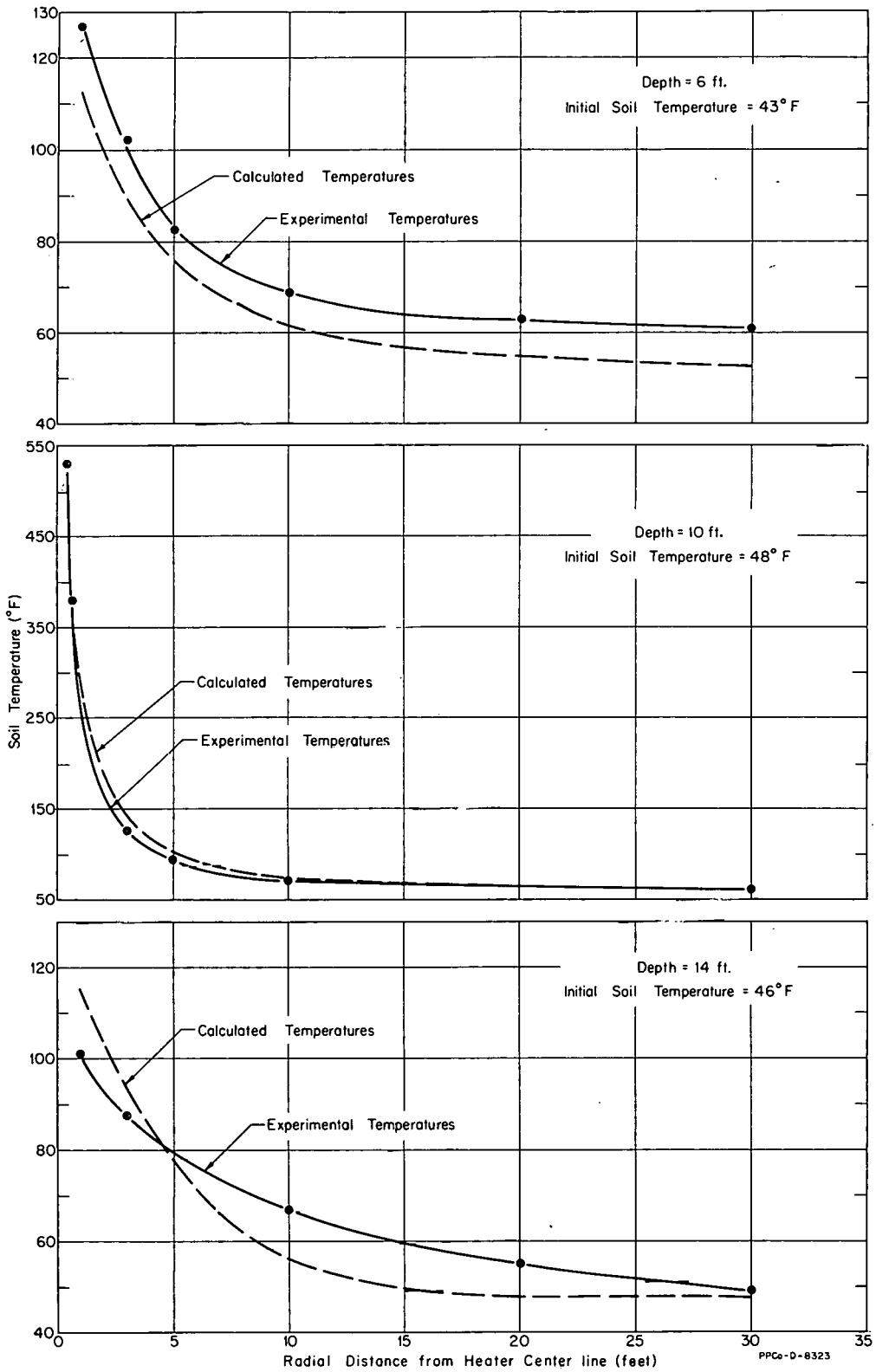

Fig. 32 Comparison of calculated and experimental steady-state temperatures for 950-watt simulated fuel element.

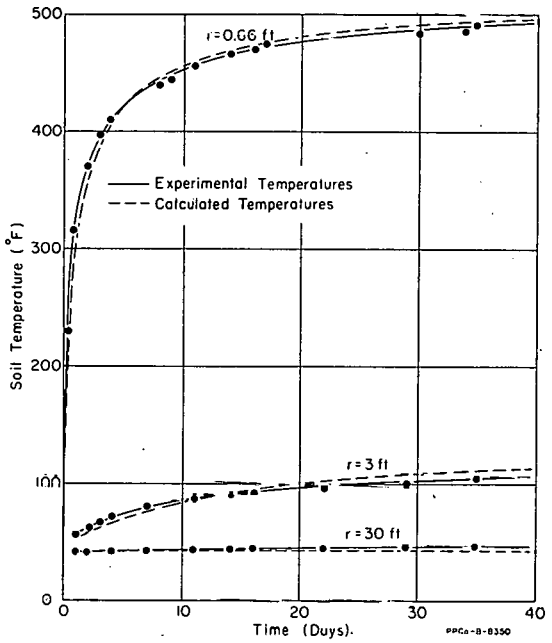

Fig. 33 Comparison of calculated and experimental transient temperatures for 950-watt simulated fuel elements ($k_{soil} = 0.5$).

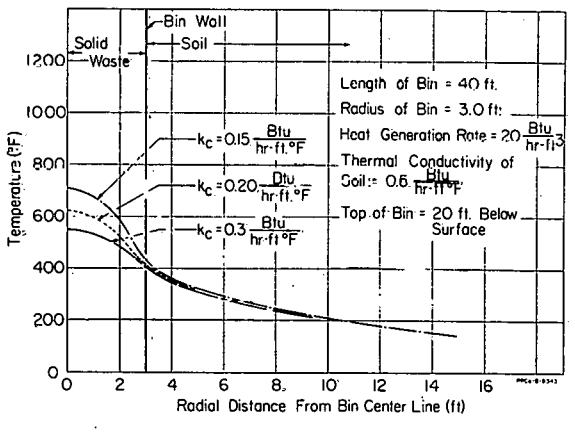

Fig. 34 Effect of source thermal conductivity on calculated steady-state temperature distributions in and surrounding a waste storage container.

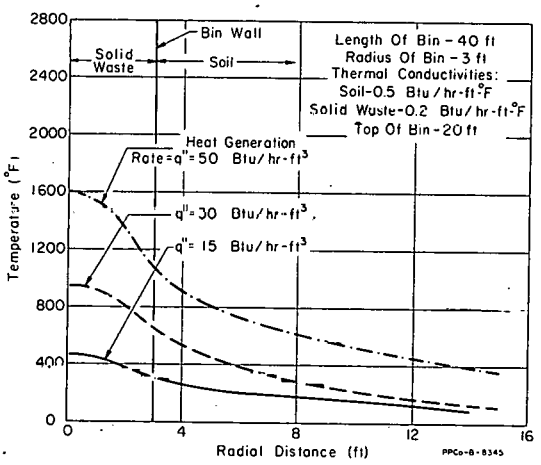

Fig. 35 Effect of heat generation rate on calculated steady-state temperature distributions in and surrounding a waste storage container.

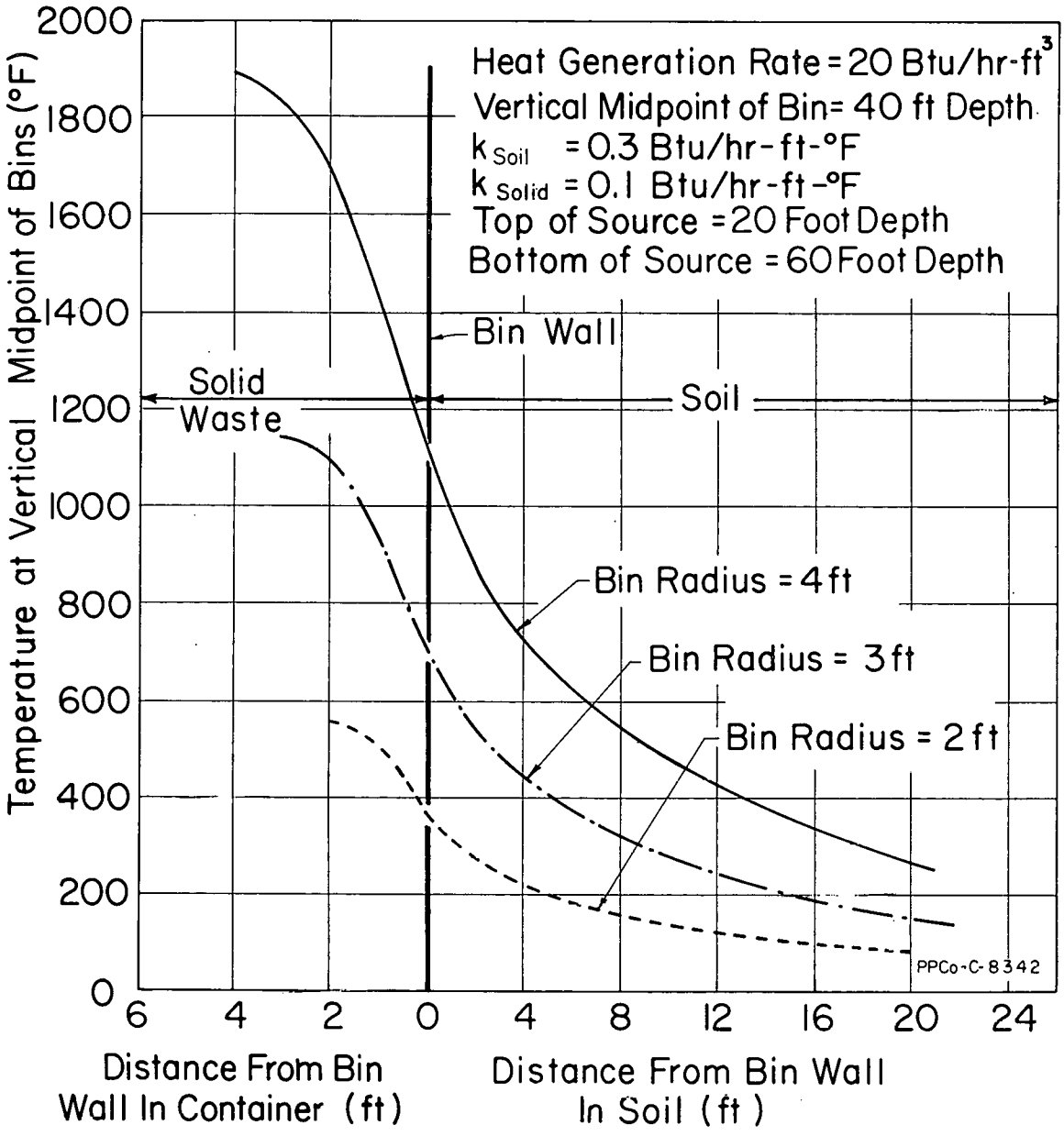

Fig. 36 Effect of source radius on calculated steady-state temperature distributions in and surrounding a waste storage container.

III. REACTOR TECHNOLOGY SUPPORT

1. LOFT ASSISTANCE PROGRAM

The Chemical and Process Development Branch has several development studies underway in support of the Loss-of-Fluid Test (LOFT) at the National Reactor Testing Station. The LOFT project is the field duplication of a loss-of-coolant or maximum credible accident for a water-cooled reactor. In this test, the coolant will be released deliberately from a 50-MW pressurized water reactor, thus permitting the fuel core to melt and release fission products into the reactor shell and containment building.

The specific development studies undertaken by this branch include: (a) the selection of surface coatings and sealants for the interior of the containment shell, (b) the development of procedures for decontamination of the facility, (c) the development of a continuous fission product sampler-monitor for the containment atmosphere, and (d) the design, construction, and operation of a fission product generation and containment unit to assist in evaluating the results of the preceding studies. Progress in each of these areas is reported although all are continuing programs and none has reached a state permitting final conclusions to be stated.

1.1 LOFT Coating and Elastomer Evaluation and Decontamination Studies (K. L. Rohde, B. J. Newby, M. E. Jacobson, C. A. Zimmerman; Chemistry Section) (R. D. Modrow; Development Engineering Section)

Studies are continuing to select a coating material for the interior of the LOFT containment building which will both duplicate the fission product plateout to be expected in a typical reactor containment building and be readily decontaminated by the remotely operated decontamination spray system in LOFT[1]. The coating should also be resistant to possible decontaminating reagents that might be used in the containment building, be resistant to pressurized steam up to 40 psig and 140°C for as long as three days, and be resistant to a radiation dose as great as 1×10^9 R in a steam atmosphere[a].

In the current studies, commerically available coatings that appeared to have promise of possessing the desired characteristics, based on previous screening studies and recommendations by manufacturers, were tested for their resistance to chemical reagents, pressurized steam, and irradiation. The coating were tested over both concrete and steel substrates and included a polyester, a urethane, and a number of epoxy coatings. These coatings, as well as a large number of other coatings and two different steel surfaces, were also tested to determine their contamination-decontamination behavior.

---

[a] The experimental work reported in this document was carried out for the specialized purpose of obtaining fission product contamination-decontamination information on materials in the specific application and environment listed in the report. Any conclusions as to the relative merits of these commercial coatings apply only to the use of the materials in the specific application and environment mentioned. The fact that some of the materials were less desirable than others for the specific application does not imply that they are generally inferior.

Iodine will represent the major contaminant for a short time after the LOFT test. If entrance to the building is to be made within a few days, it is anticipated that very high decontamination factors must be obtained for iodine. Therefore, the contamination-decontamination behavior of iodine has received the earliest and most extensive study. It is anticipated that the concentration of radionuclides of moderate and long life on the walls of the building will be great enough to require effective decontamination from many of these also. Therefore, additional effort has been devoted to studies of the behavior of fission products other than iodine when these are deposited on surfaces from a gas stream. Since it appeared likely that iodine penetration into coatings was a diffusional process, a mathematical model for unidirectional diffusion into a semi-infinite solid was selected to describe iodine penetration into coatings. Data from penetration studies in the coating evaluation program were used to test the validity of the model.

Currently it is planned to have elastomer joints in the interior concrete surfaces of the LOFT containment building to allow the concrete surfaces to expand and contract with the outer steel shell of the building. Two different elastomers were tested for their resistance to conditions that might exist in the LOFT containment building.

1.11 Physical-Chemical Testing of Coatings. The resistance of coatings to pressurized steam, irradiation, abrasion, and solutions that might be used as decontaminating reagents in the LOFT containment building was tested. Some results of these tests have been reported previously[1]; more recent results are summarized in Table XVI. Coatings were considered to have: (a) satisfactory chemical resistance to a reagent if the reagent produced little or no effect on a coating submerged at 60°C for five days; (b) questionable resistance if the coating was markedly affected between one and five days of submergence; and (c) unsatisfactory resistance if the reagent produced a marked effect in less than one day of submergence. Coatings were also considered to have: (a) satisfactory

TABLE XVI

RESISTANCE OF COATINGS TO CONDITIONS PRESENT DURING LOFT EXPERIMENT

Coating	Generic Type	Substrate	Chemical Resistance: 3M HNO_3 (60°C)	2 lb/gal Turco 4502 (60°C)	½ lb/gal Turco 4521 (60°C)	1 lb/gal Turco Alkaline Rust Remover (60°C)	Resistance to Pressurized Steam (30 to 40 psig) (3 days)	Radiation Resistance (6 (dose rate of 2×10^6 R/hr for total dose of 1×10^9 R)	Abrasion Resistance
Amercoat 66	Epoxy	Steel	U	S	S	S	S	S	S
		Concrete	U	S	S	S	S	S	-
Amercoat 66 containing glass fabric	Epoxy	Steel	U	S	S	S	S	S	-
Carboglass 1600	Polyester	Steel	S	Q	S	Q	S	S	-
Carboline B-15	Urethane	Steel	U	S	S	S	U	S	-
Devran 600	Epoxy	Steel	-	-	-	-	S	-	-
		Concrete	U	Q	U	S	U	-	-
Chemfast OX-1055	Epoxy	Steel	-	-	-	-	U	-	-
		Concrete	Q	S	S	S	S	-	-
Carboline Epoxy 150	Epoxy	Steel	-	-	-	-	Q	-	-
		Concrete	Q	Q	S	S	S	-	-

"S" = Satisfactory performance.

"Q" = Questionable performance.

"U" = Unsatisfactory performance.

resistance to pressurized steam if steam at 30 to 40 psig (133 to 140°C) for three days produced little or no effect on the coating; (b) satisfactory resistance to radiation if a beta-gamma dose rate of about 2×10^6 R/hr continued for a total dose of 10^9 R in the presence of steam had little or no effect on the coating; and (c) satisfactory resistance to abrasion if the falling sand test [a] gave a value of greater than 20 liters of sand per mil of paint. Table XVI shows that no coating passed all the tests satisfactorily; however, several of these coatings would be adequate as a covering material for the inside of the LOFT containment building if resistance to the exposure conditions were the only consideration. Decontamination behavior, however, as discussed in the following section, was disappointing for all coatings.

1.12 Contamination-Decontamination Testing of Coatings

(1) Mixed Fission Product Behavior. Coated carbon steel, uncoated carbon steel, and stainless steel coupons were contaminated with mixed fission products in the Contamination-Decontamination Experiment (CDE) Run 1. The source of fission products was molten irradiated uranium dioxide clad in Zircaloy. The temperature-pressure program for CDE Run 1 is given in Section III-1.2. Small-scale, high-pressure spraying equipment was used to decontaminate coupons. Table XVII shows the fission products found on the coupons, their relative abundance immediately after contamination, and the decontamination factors obtained by spraying. Iodine made up more than 90 percent of the activity. All fission products were poorly removed from organic protective coatings. Iodine was removed much more effectively from stainless steel than were the other fission products. It is evident from these results that effective iodine decontamination can only be obtained by removing a portion of the surface from the material being decontaminated (as evidenced by the decontamination of carbon steel with nitric acid). A comparison of the contamination behavior of mixed fission products on concrete, stainless steel, and carbon steel coupons coated with Amercoat 66 showed that the substrate had no effect on the contamination behavior of mixed fission products on coatings.

(2) Molecular Iodine Behavior. The contamination-decontamination behavior of iodine has warranted extensive study because it will represent the major contaminant on coatings for several weeks after the LOFT test. The contamination-decontamination behavior of iodine on materials contaminated in the presence of steam at atmospheric pressure has been reported[1]. Since contamination in the LOFT test will take place in the presence of steam under pressure, studies were performed to determine how iodine contamination-decontamination behavior was affected by the temperature and pressure of the steam atmosphere during contamination. Coated coupons as well as uncoated carbon and stainless steel coupons were contaminated with molecular iodine in the presence of pressurized steam held at a given pressure and temperature for 24 hours. Table XVIII illustrates how the plateout of iodine varies with steam pressure and temperature. Absolute iodine concentrations of the coupons have been normalized to those of stainless steel coupons in the same environment because it was not feasible to maintain the iodine concentration of the vapor constant with changing pressure. After normalization, the relative contamination of carbon steel remains essentially constant with increasing pressure (temperature), while the relative contamination of the protective coatings increases markedly with increasing pressure (temperature).

---

[a] ASTM Designation D968-51

TABLE XVII

CONTAMINATION-DECONTAMINATION OF MATERIALS IN CDE RUN NO. 1[a]

	Fission Product Contamination-Decontamination (decay time = 0)									
	I-131		Ru-103		Tc-99		Te-132		Mo-99	
Material	Contamination (10^9 d/m/spl)	Decontamination Factor Using Pressure Sprays	Contamination (10^5 d/m/spl)	Decontamination Factor Using Pressure Sprays	Contamination (10^7 d/m/spl)	Decontamination Factor Using Pressure Sprays	Contamination (10^8 d/m/spl)	Decontamination Factor Using Pressure Sprays	Contamination (10^7 d/m/spl)	Decontamination Factor Using Pressure Sprays
Amercoat 66	6.1	6.6	4.3	1.6	4.3	1.5	6.3	4.8	5.5	4.5
Chemfast OX-1055	3.6	9.0	4.1	4.8	4.0	2.0	3.2	4.4	1.7	1.0
Phenoline 302	6.7	5.0	6.5	8.6	1.9	1.0	3.0	3.8	---	---
Amercoat 33HB	2.1	1.5	4.7	2.8	3.5	1.6	3.7	4.5	5.5	1.0
Stainless Steel	1.1	900	3.2	20.0	7.9	6.8	3.2	9.3	1.7	7.5
Carbon Steel	4.3	9000	2.2	> 30.0	3.5	> 4000	3.1	4000	0.43	> 100
Carboline Epoxy 150	3.6	1.7	---	---	---	---	6.8	> 4.0	---	---
Devran 600	5.9	2.3	---	---	---	---	8.3	> 4.0	---	---
Devoe SX-1661	2.0	3.5	---	---	---	---	7.4	> 4.0	---	---
Contam Affix Perm	6.3	2.0	---	---	---	---	6.8	> 4.0	---	---
Plasite 7155	1.9	5.2	---	---	---	---	5.3	> 4.0	---	---

[a] Decontamination Conditions: Sprayed with 3M HNO_3 at 80°C followed by spraying with 1 lb/gal Turco Alkaline Rust Remover at 80°C.

TABLE XVIII

IODINE CONTAMINATION OF SURFACES RELATIVE TO STAINLESS STEEL AT VARIOUS STEAM TEMPERATURES AND PRESSURES

Material	5 psig (105°C)	15 psig (120°C)	40 psig (140°C)
Amercoat 66	38	65	230
Chemfast OX-1055	69	85	420
Amercoat 33HB	8	31	160
Phenoline 302	58	75	270
Carbon Steel	21	14	38

Coupons contaminated under the conditions shown in Table XVIII were decontaminated, first by spraying them with 1 lb/gal Turco Alkaline Rust Remover at 80°C, and then by autoclaving them for three days at 140°C and 40 psig. Decontamination factors obtained for the coatings by the spraying technique were all only slightly above unity and were independent of the coating and the pressure and temperature at which the coatings were contaminated. Decontamination of carbon steel by the spraying technique was poor, probably due to the thick layer of rust formed during the contamination period; decontamination of stainless steel was higher than for the other materials. Decontamination factors obtained by autoclaving were much greater than those obtained by spraying, were quite different for each material, and were larger for coatings contaminated at 5 psig than for coatings contaminated at 15 and 40 psig. Decontamination factors obtained by autoclaving for coatings contaminated at 40 psig varied from 2 to 22; for coatings contaminated at 15 psig, they varied from 2.5 to 23; and for coatings contaminated at 5 psig, they varied from 12 to 190. Contamination on stainless steel was reduced to essentially background each time; decontamination of carbon steel was probably hindered by the deep layers of rust present.

Iodine is difficult to remove from coatings because the iodine penetrates deeply into the coatings during the contamination process. This penetration varies with the coating and contamination conditions. Figure 37 shows the average penetration of four different coatings contaminated in CDE Run 1. The curve of Figure 37 represents the iodine activity found at various depths beneath the surface of the coating. To obtain an iodine decontamination factor of 100, the data in Figure 37 show that over 6 mils of coating must be removed or all the activity leached from that amount of coating. The depth of penetration appears

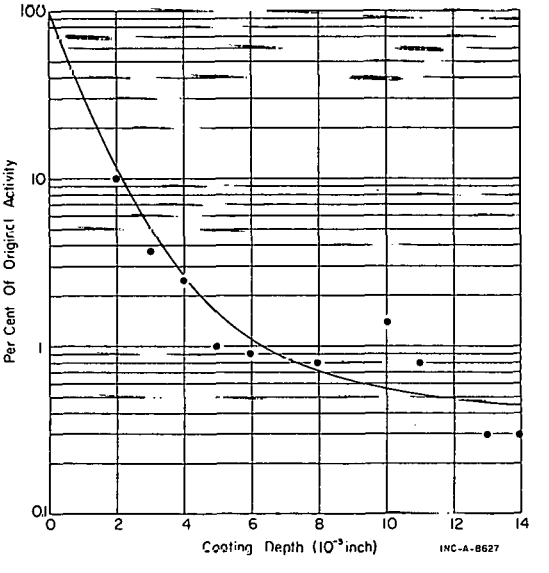

Fig. 37 Average penetration of iodine into four different protective coatings contaminated in CDE run No. 1.

to be primarily a function of the temperature of the coating and/or the total pressure of the contaminating atmosphere. As shown in Figure 38, much greater depth of penetration is experienced at 120°C and 15 psig than at 35°C and atmospheric pressure. Figure 38 also illustrates how the penetration varied with the coating. Iodine penetration could be evidence of the solubility of iodine, probably I_2, in the protective coating or of an ion exchange reaction between iodide and radicals in the coating matrix.

The age of a coating (over the range of two weeks to five months) did not have any significant effect on the iodine contamination-decontamination properties of organic protective coatings.

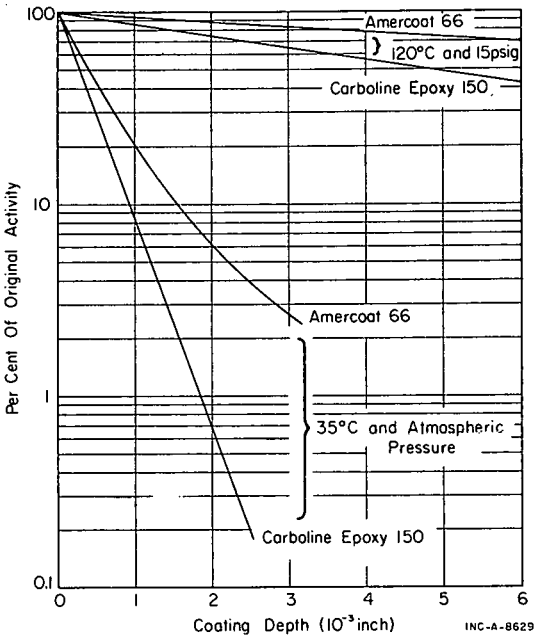

Fig. 38 Penetration of iodine into protective coatings at two steam pressures and temperatures.

(3) Optimization of the Spraying Technique of Decontamination. Several different modes of operating high-pressure sprays were evaluated with coupons contaminated in CDE Run 1. Although the decontamination factors obtained were all low, significant trends were evidenced. The results are summarized in Table XIX. Gross gamma, iodine-131, and tellurium-132 decontamination results were used for these data. Within the ranges studied it was clear that conditions which yielded the maximum impingement of reagent on the coupon surface were generally best.

Elevated temperature of the reagent at the nozzle was also favorable, and the Turco 4502 (alkaline permanganate) + Turco 4521 (oxalate-citrate solution) system was superior to the other two tested.

(4) Decontamination with Pressurized Steam. Previous work [1] has shown that pressurized steam effectively removes iodine from certain organic protective coatings (but not from steel surfaces) contaminated at 40°C and atmospheric pressure in the presence of moisture. It was shown in the section on Molecular Iodine Behavior (page 74) that iodine could be removed from organic protective coatings with pressurized steam much more effectively than with spraying techniques, even when the coatings were contaminated in the presence of pressurized steam. Apparently, iodine removal could be obtained by autoclaving certain coatings (under conditions of maximum condensation) regardless of their contaminating temperature and pressure providing the autoclaving treatment was sufficiently long. Table XX shows that increasing the autoclaving period (at 40 psig and 140°C) from one to three days markedly increased the decontamination factors obtained from coatings contaminated in the presence of steam at various temperatures and pressures.

Carbon steel, stainless steel, and coated carbon steel coupons contaminated in CDE Run 1 were autoclaved for three days at 40 psig and 140°C. The iodine-131, tellurium-132, and gross gamma decontamination factors obtained by autoclaving and chemical spraying are shown in Table XXI. Pressurized steam was

TABLE XIX

EFFECT OF SPRAY OPERATING
CONDITIONS ON DECONTAMINATION EFFECTIVENESS

Variable	Order of Effectiveness
A. Nozzle size at constant pressure	1. 3/8-in. and 1/4-in.-diameter orifice
	2. 1/8-in.-diameter orifice
B. Spraying time	1. 30 minutes
	2. 15 minutes
	3. 5 minutes
C. Spraying pressure	1. 115 psig
	2. 20 psig
D. Temperature of reagent	1. 90°C
	2. 80°C
	3. 40°C
E. Decontamination reagent	1. 2 lb/gal Turco 4502 (alkaline permangante) + 0.5 lb/gal Turco 4521 (oxalate-citrate solution)
	2. 3M HNO_3 + 1 lb/gal Turco Alkaline Rust Remover
	3. 3M HNO_3 + 0.4M oxalic acid — 0.16M ammonium citrate — 0.34M H_2O_2 adjusted to pH of 4 with NH_4OH

more effective than chemical spraying in removing iodine from coatings, but both decontamination methods were ineffective in removing tellurium. Decontamination of carbon steel with pressurized steam was probably hindered by the presence of rust formed on the steel during the contamination period; pressurized steam was probably ineffective in removing tellurium due to chemical combination of this fission product with the steel surface. Although the autoclaving was not performed under conditions of maximum condensation, which possibly resulted in reduced decontamination efficiency, it appears that partial iodine decontamination from organic protective coatings can be obtained using pressurized steam, but tellurium (and possibly other fission products) cannot be removed effectively by steam treatment.

(5) Chemically Strippable Coatings. The use of chemically strippable coatings shows promise as a means of decontaminating the interior surfaces of the LOFT containment building. Such a system consists of a permanent base coating to protect the substrate and an expendable outer coat which can be removed along with the contamination by stripping with a chemical reagent. Two such systems were contaminated in CDE Run 1. One system consisted of about

TABLE XX

EFFECT OF AUTOCLAVING TIME ON IODINE REMOVAL[a]

Coating	Length of Autoclaving Period (days)	Iodine Decontamination Factors: From Coupons Contaminated at 5 psig and 105°C	From Coupons Contaminated at 15 psig and 120°C	From Coupons Contaminated at 40 psig and 140°C
Amercoat 66	1	1.9	3.0	1.1
	3	190.0	23.0	22.0
Chemfast OX-1055	1	1.2	1.2	1.3
	3	67.0	11.0	19.0

[a] Conditions: Coatings contaminated in the presence of pressurized steam; autoclaving conditions were 40 psig and 140°C.

TABLE XXI

DECONTAMINATION OF MATERIALS CONTAMINATED IN CDE RUN NO. 1

Material	Decontamination Factors By: Chemical Spraying[a] Gross Gamma	Chemical Spraying[a] Iodine-131	Chemical Spraying[a] Tellurium-132	Autoclaving[b] Gross Gamma	Autoclaving[b] Iodine-131	Autoclaving[b] Tellurium-132
Amercoat 66	3.1	2.8	4.2	11.0	11	3.0
Chemfast OX-1055	4.4	3.5	4.5	15.0	40	1.6
Carboline Epoxy 150	2.2	1.7	> 4.0	12.0	32	1.7
Devran 600	2.5	2.3	> 4.0	17.0	180	1.9
Carbon Steel	> 200.0	> 600.0	> 30.0	9.0	13	2.1
Stainless Steel	3.0	> 60.0	> 20.0	1.4	---	1.8

[a] Sprayed with 3M HNO_3 at 80°C for 10 minutes, rinsed with water, sprayed with 1 lb/gal Turco Alkaline Rust Remover at 80°C for 10 minutes, and rinsed with water.

[b] Autoclaved at 40 psig and 140°C for three days.

5 mils of Turco Contam Affix Rem over Amercoat 66; the other system consisted of about 5 mils of Turco Guard 200 over Amercoat 66. The outer coat of the former system can be stripped with alkaline reagents; the outer coat of the latter system can be stripped with organic solvents. An average iodine-131 decontamination factor of 130 and a gross gamma decontamination factor of 220 were obtained by stripping the Turco Contam Affix Rem with 0.2M sodium hydroxide at 80°C without damaging the base coat; an average iodine-131 decontamination factor of 210 and a gross gamma decontamination factor of

340 were obtained by stripping the Turco Guard 200 with perchlorethylene at 80°C without damaging the base coat.

1.13 A Model for the Penetration of Iodine into Protective Coatings. The penetration of iodine into protective coatings on the walls of the containment building is one of the major problems in achieving decontamination from short-lived isotopes. To obtain a better understanding of this penetration, a mathematical analysis was undertaken. Since it appeared likely that the penetration of iodine into protective coatings was a diffusional process, a mathematical model for unidirectional diffusion into a semi-infinite solid was selected. Data from penetration studies in the coating evaluation program were used to test the validity of the model. The model [39] used in this preliminary study was:

$$\frac{C}{C_o} = 1 - \phi \left[\frac{x}{2\sqrt{Dt}} \right] \tag{6}$$

where

C = the concentration of the diffusing substance at depth x

C_o = the concentration in the solid at the surface

t = the time of diffusion

D = the diffusion constant for the process.

The right hand side of Equation (6) is known as the complementary error function. Tabulated values for this relationship are readily available [39].

Inasmuch as the experimental program to date has been an empirical one, the penetration experiments have been poorly designed to yield fundamental information. However, the results of several experiments have been analyzed with very encouraging results.

(1) Method of Analysis. A number of penetration experiments yielded data which fit the equation

$$\ln \frac{A}{A_o} = -\lambda x \tag{7}$$

where

A = the activity per unit area observed at depth x

A_o = the activity per unit area at x = 0.

Since the activity per unit volume is the derivative of the activity per unit area with respect to depth, the required concentration ratio could be obtained using the value of λ obtained in Equation (7) by the following relationship:

$$\frac{C}{C_o} = e^{-\lambda x} \tag{8}$$

where

C = the concentration of activity per unit volume at depth x

C_o = the concentration at the surface, x = 0.

For a known diffusion time, the diffusion constant for the process can be obtained by application of Equation (6).

(2) Boundary Conditions. The simple form of diffusion theory applied here requires that a constant concentration of the diffusing substance be maintained in the surface of the solid and that the depth of the solid be large (semi-infinite) compared to the increments of depth examined. Neither of these conditions is fulfilled perfectly in the present experiment. There is considerable uncertainty that the iodine generator used maintains a constant iodine concentration in the atmosphere for the duration of the test. The plateout velocity is largely unknown. The increments of depth examined are large compared to the total thickness of the coating, and in some cases the inner boundary, where the coating joins the substrate (carbon steel), is approached. Under these conditions the applicability of the model must be explored carefully to determine if it can be used to represent the system.

The variation in the diffusion coefficient, D, for the data of Table XXII was in the form of a trend toward larger values of D as x increased, suggesting some lack of applicability of the chosen model.

TABLE XXII

DIFFUSION COEFFICIENTS FOR IODINE IN PROTECTIVE COATINGS

		Contamination Conditions			cm^2-sec^{-1} (X 10^{-9})	
Experiment	Coating	Temperature (°C)	Time (hours)	Other Conditions	D	σ for Mean D
1	Amercoat 66	35	1.0	Examined immediately	0.66	0.1
2	Amercoat 66	35	1.0	Examined after 13 days	0.68	0.2
3	Amercoat 66	35	2.5	-----	0.65	0.1
4	Amercoat 66	60	1.0	-----	0.79	0.2
5	Carboline Epoxy 150	35	1.0	Examined immediately	0.45	0.1
6	Carboline Epoxy 150	35	1.0	Examined after 13 days	0.41	0.09
7	Carboline Epoxy 150	35	1.0	Nitropropane added to solvent	0.27	0.07
8	Carboline Epoxy 150	35	2.5	-----	0.68	0.07
9	Carboline Epoxy 150	60	1.0	-----	13.0	0.90

(3) Interpretation of Diffusion Data.

(a) The Diffusion Period. Comparison of the results of Experiments 1 and 3 and Experiments 5 and 8 in Table XXII, wherein the diffusion periods were 1.0 and 2.5 hours, shows excellent adherence to the model for Amercoat 66 and only a general agreement for Carboline Epoxy 150.

(b) Temperature. Comparison of the results of Experiments 1 and 2 and Experiments 5 and 6 of Table XXII indicates that the diffusion process occurring over a period of one hour at 35°C in the contaminated atmosphere essentially stops when the coupons are removed from the contaminated atmosphere and stored at 20°C. This suggests that the diffusion process is either highly sensitive to temperature or dependent entirely on a fresh supply of iodine vapor or a carrier such as water vapor. The diffusion coefficient for Carboline Epoxy 150 was much higher when the contamination experiment was conducted at 60°C (Experiment 9) than it was when the contamination took place at 35°C (Experiment 5). When Carboline Epoxy 150 is heated from 35 to 60°C it becomes soft and sticky, which apparently permits this increased iodine penetration. The diffusion coefficients for Amercoat 66 were similar at 35 and 60°C.

(c) Alteration of the Coating Matrix. Nitropropane was added to the Carboline Epoxy 150 used in Experiment 7. This alteration of the coating matrix reduced the penetration of iodine (compare Experiment 5 with Experiment 7).

(4) Concentration-Depth Relationship After Decontamination. In another series of experiments, the diffusion coefficients were calculated for the activity-depth profile found after contamination and decontamination. Samples of Amercoat 66 and Carboline Epoxy 150 were contaminated with iodine at 120°C and 1.9 atm for 24 hours. Under these conditions the iodine activity is found at high concentration deep within the coating, and decontamination by spraying and by autoclaving is relatively ineffective. In Experiments 10 through 13 of Table XXIII, such contaminated coupons were sprayed and autoclaved and then the

TABLE XXIII

USE OF THE DIFFUSION MODEL TO DESCRIBE THE CONCENTRATION-DEPTH RELATIONSHIPS FOR IODINE AFTER CONTAMINATION AND DECONTAMINATION

		$cm^2 \cdot sec^{-1}$ ($\times 10^{-9}$)	
Experiment	Coating	D (24 hours)	σ for Mean D
10	Amercoat 66	3.8	0.4
11	Amercoat 66	5.2	0.4
12	Carboline Epoxy 150	3.8	0.4
13	Carboline Epoxy 150	2.1	0.3

penetration determined. The diffusion coefficients based on a 24-hour period are shown. The model gives a good representation of the concentration over depths of 10 mils as evidenced by the low standard deviations for D. Considering the

opportunity for further movement during the autoclaving period, the selection of a 24-hour period for the calculation of D is purely arbitrary.

(5) Implications of the Diffusion Data. Even the limited data presented in the preceding paragraphs are of considerable importance to the nuclear safety program. For example, the tremendous increase in diffusion of iodine in Carboline Epoxy 150 between 35 and 60°C suggests that it or a similar coating could be used as an effective iodine trap. The fact that this change is associated with the softening of the coating is certainly a clue to the desired formulation and properties of a coating designed for trapping at a given temperature.

The observation that the iodine concentration-depth profile remains constant between the period immediately after exposure to 13 days after exposure is also interesting, since this suggests a considerable stability of the sorbed iodine and and absence of back diffusion.

It may be possible to determine the activation energy of the diffusion process by measurements at various temperatures, although this approach might be limited by the thermal stability of the coating and the iodine species. Such data, if obtained, might give an insight into the diffusion mechanism.

The ability to measure penetration and to estimate diffusion coefficients, both in a relatively simple manner, is being refined in connection with the coating evaluation program.

1.14 Physical Testing of Elastomers. Currently it is planned to have elastomer joints in the interior concrete surfaces of the LOFT containment building to allow the concrete surfaces to expand and contract with the outer steel shell of the building. Coated elastomers must be resistant to conditions that might exist in the building. A polyurethane base sealant and a silicone rubber sealant (both coated with epoxy organic protective coatings and uncoated) were tested for their resistance to pressurized steam, dry heat, γ-radiation, and to solutions that might be used as decontaminating reagents. The bond between both elastomers and concrete failed in a short time when subjected to alkaline reagents at 60°C and pressurized steam (30 psig), but this situation was markedly improved when the elastomers were covered with epoxy coatings. The epoxy coatings over both elastomers cracked badly and peeled from the elastomer within a few hours, however, when exposed to pressurized steam (30 psig) and dry heat (100°C). The epoxy-coated silicone rubber elastomer was unaffected by a beta-gamma radiation dose of 1×10^9 R in the presence of steam; under the same conditions, the epoxy coating over the urethane elastomer failed due to excessive swelling in the elastomer and loss of bond between elastomer and concrete. Although the silicone rubber elastomer is preferred over the urethane elastomer, neither elastomer seems to be suitable for use in the LOFT containment building at the present time.

1.2 Contamination-Decontamination Experiment

(L. T. Lakey, D. E. Black, R. D. Modrow; Development Engineering Section)

The Contamination-Decontamination Experiment (CDE) was installed to augment the LOFT support studies being conducted at the ICPP. The CDE is used to produce high-level fission product mixtures under conditions simulating those anticipated in the LOFT. In the CDE, the fission product mixture is generated by melting a small, highly irradiated and short-cooled fuel capsule in the presence of steam using a radio-frequency induction furnace.

The fission products released are transported by the steam to a simulated containment shell. These fission product mixtures are used in studies of contamination and decontamination of various protective coatings and equipment, in testing of various LOFT sampling devices, and for the development of analytical methods.

Installation of CDE in Cell 2 of the ICPP Hot Pilot Plant was completed in December 1965. The first of two successful tests in the CDE was conducted in December 1965, and the second in May 1966. A description of the CDE and a summary of the data available from the runs are summarized in the following sections.

1.21 Description and Operation of Equipment. The CDE, as shown in Figures 39 and 40, contains two major elements -- an induction furnace for

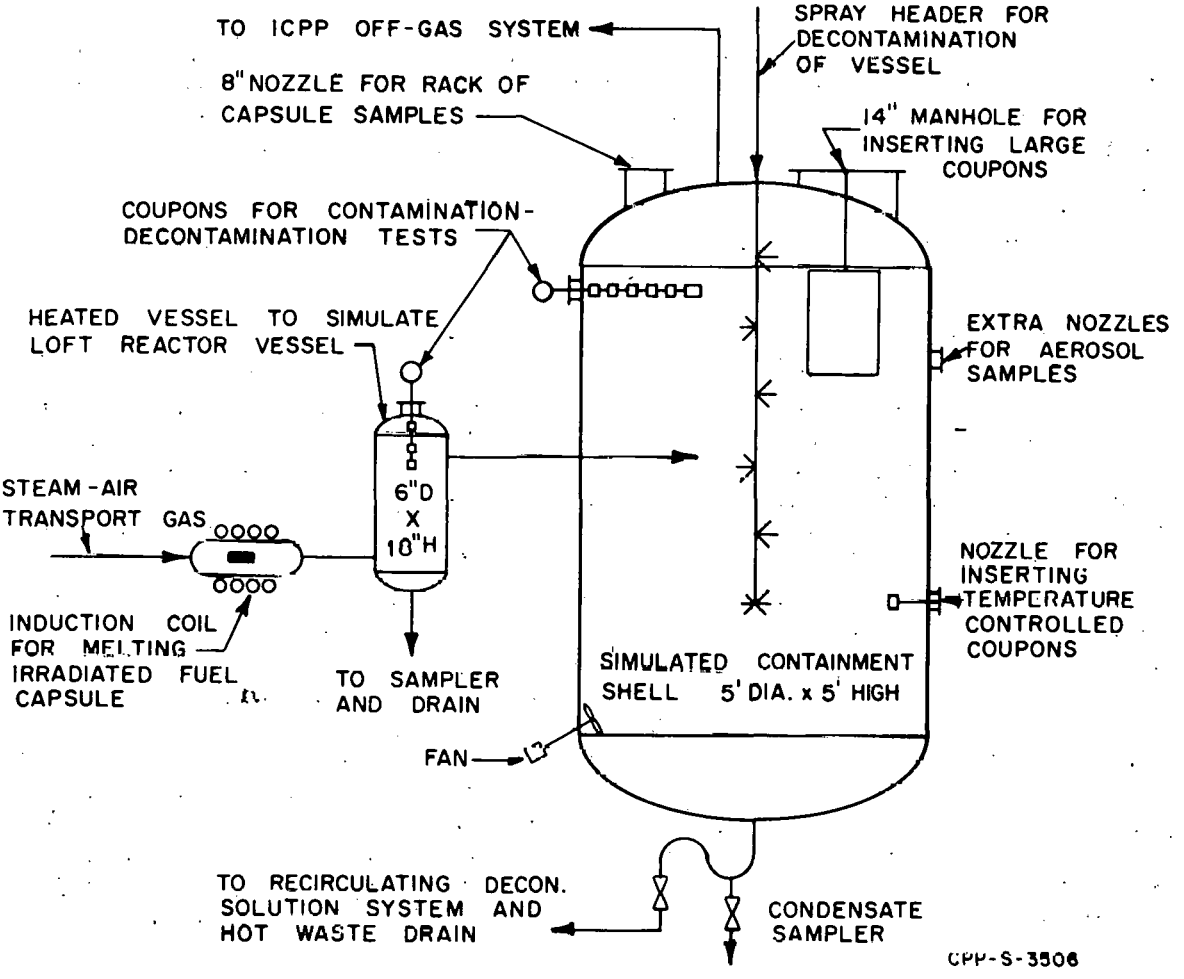

Fig. 39 Schematic diagram of the Contamination-Decontamination Experiment (CDE).

melting the fuel pin, and a simulated containment vessel. The induction furnace, a 1-7/8-inch-diameter by 12-inch-long quartz tube, is heated by a 50 kW, 2 to 7 megacycle induction generator. Heated glycol is circulated through a glass jacket around the quartz tube to prevent condensation of the steam normally used as the carrier gas inside the furnace. A choice of air, nitrogen, or steam can be passed over the fuel during the meltdown.

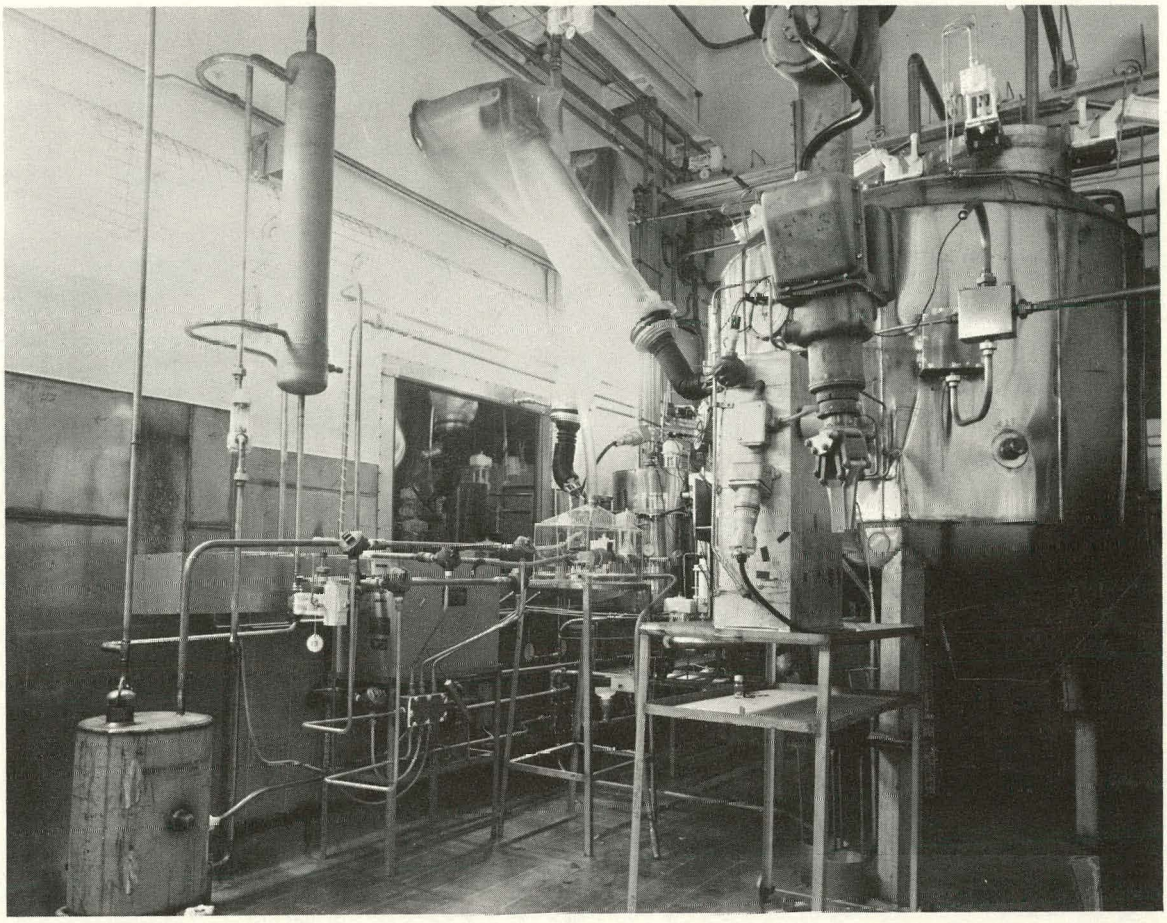

Fig. 40 Photograph of the Contamination-Decontamination Experiment.

The simulated containment vessel, a 5-foot-diameter by 5-foot-high tank, is fabricated of stainless steel to reduce the decontamination effort required between test runs. The containment vessel can be heated to 135°C. The quartz furnace tube, which limits the maximum operating pressure of the system, has been tested and found to be capable of withstanding 30 psig [a]. Nozzles, sampling devices, and other test equipment are provided in the containment vessel for inserting coupons to be contaminated. A liquid sampler and collection pot are used to sample and to determine the volume of condensate collected. Decontamination solutions for the CDE are prepared in a service area adjacent to the test cell and are pumped to spray nozzles located in the cell and inside the vessels. The decontamination solutions are recirculated and sampled remotely using a pump and collection tank located in the cell.

The test equipment is vented to an ICPP off-gas cleanup system containing charcoal beds (for iodine removal) and filters. After cleanup, the equipment off-gas is discharged to the 250-foot-high ICPP stack. Charcoal filters have been

---

[a] A simulated reaction vessel capable of being heated to 800°C was located between the furnace and the containment vessel for CDE Run 1, but was removed prior to CDE Run 2 to increase the quantity of fission products transported from the furnace to the containment vessel.

installed over the outlets for ventilation air from the cell to remove any iodine released in the cell. The cell ventilation air is also discharged to the 250-foot-high stack. Operations within the cell are viewed through three shielding windows and are performed remotely using three sets of minipulators and a three-ton crane provided in the cell. The waste solutions from the CDE are collected and sampled in the Hot Pilot Plant waste tanks prior to transfer to the ICPP waste disposal system.

Fission product mixtures are generated by melting Zircaloy-clad fuel pins (9/16-inch diameter by 3-1/2 inches long) containing enriched UO_2 pellets. The fuel pins are encased in aluminum jackets to reduce the temperature of the pin during irradiation. Following irradiation in the Materials Testing Reactor, a fuel pin is transported to the ICPP Hot Pilot Plant where the aluminum jacket is dissolved in caustic. The fuel pin is then inserted into the quartz furnace tube and melted by induction heating. During the meltdown, steam is passed over the fuel pin to carry the fission products into the simulated containment vessel where the environmental conditions and atmospheric composition are adjusted to match the anticipated LOFT containment building conditions. After melting of the fuel pin is complete, the containment vessel is isolated and the temperature of the containment atmosphere is decreased to ambient temperature over a 24-hour period to match the expected decay of the LOFT containment temperature. During this period, samples of the containment atmosphere and condensate are collected intermittently. At the end of this period, the containment vessel is vented and the plateout coupons and other sample devices are removed. The test equipment and cell are then decontaminated in preparation for the following run.

The principal operating conditions for the first two tests are compared in Table XXIV.

1.22 Results of Tests. The successful completion of two tests with high-level fission products has demonstrated the operability of the CDE. Operation of the test equipment and facilities was generally satisfactory and only minor problems were encountered in containing the fission products and in decontaminating the test equipment following each test. The first test was performed at ambient pressure after it was found that the ground-glass joints of the furnace tube would not seal above 5 psig pressure. The furnace joints were redesigned for the second test and will now withstand pressures up to 30 psig. In the second test, a sampling pump used to circulate containment atmosphere through the gas-particulate samplers failed. The circulation system is being redesigned to eliminate the pump for the third CDE run.

Numerous coupons were contaminated in Runs 1 and 2 for the LOFT coating selection and decontamination studies described in Section III-1.1. The hanger used to support the coupons in the containment vessel is shown in Figure 41.

Containment atmosphere was drawn through two gas-particulate sampling cartridges in Run 1; four were installed for Run 2. Also, two of the LOFT gas-particulate capsule samplers were installed for Run 2. The evaluation effort on the LOFT gas-particulate samplers is being performed under the direction of the ICPP Analytical Branch and is reviewed in the CPP Analytical Annual Report [40], along with the development effort on analytical methods.

Other results are described in the following paragraphs.

TABLE XXIV

COMPARISON OF OPERATING CONDITIONS
FOR THE FIRST TWO CDE RUNS

Condition	Run 1	Run 2
Fuel Element:		
Diameter (inches)	9/16	9/16
Length (inches)	3-1/2	3-1/2
Cladding	Zircaloy-2	Zircaloy-2
Meat	UO_2 pellets	UO_2 pellets
Total uranium (grams)	80	80
Enrichment (percent)	1-1/2	8
Fuel Element Burnup (MWd/Tonne)	1400	1930
Irradiation Flux Level (n/cm^2-sec)	8×10^{13}	9×10^{13}
Total Activity in Fuel Element at Reactor Shutdown (curies)	12,600	33,600
Iodine-131 Activity in Fuel Element at Reactor Shutdown (curies)	75	201
Cooling Time until Fuel Element Meltdown (hours)	32	10
Time after Start of Heating until Initial Melting Occurred (minutes)	23	5
Time Fuel Pin was Molten (minutes)	44	30
Composition of Transport Gas over Fuel Element	Steam and 3% air	Steam and 3% argon
Velocity of Transport Gas over Fuel Element (ft/sec)	3.45	2
Furnance and Containment Vessel Pressure During Meltdown (psig)	0	22
Containment Atmosphere Temperature During Meltdown (°C)	100	125
Composition of Containment Atmosphere During Meltdown	100% steam (air and steam added after meltdown to achieve 36% air and 64% steam at 22 psig)	36% air and 64% steam
Number of Sampling Systems Installed:		
Raw gas sample bombs	1	1
Gas-particulate cartridges	2	4
Gas-particulate capsules	0	2
Plateout capsules	0	2
Plateout coupons (ambient temperature)	168	114
Plateout coupons (heated)	12	16
Plateout coupons (cooled)	12	16

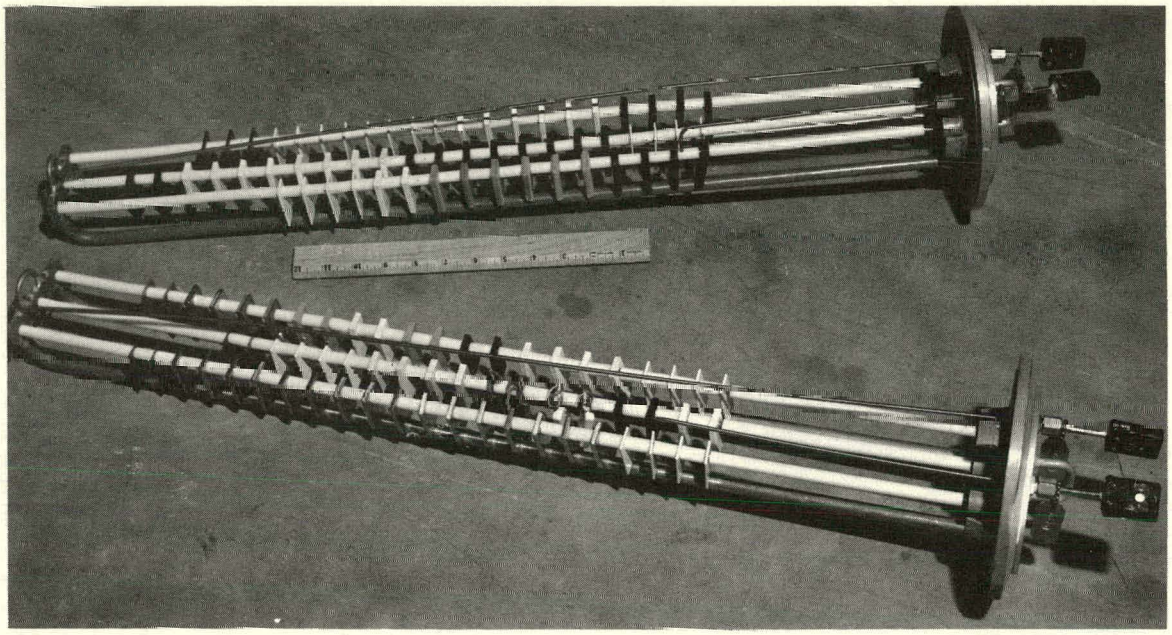

Fig. 41 Coupon support assembly.

(1) Fission Product Behavior. The fission products, other than the noble gasses, that were detected outside the furnace following Run 1 are listed in Table XXV. As expected, the predominant fission products were the iodines, tellurium-132, ruthenium-103, and molybdenium-technitium-99. Comparisons shown in Table XXVI of the quantities of these fission products found after Run 1 with those expected to be present from the burnup estimates show that a large portion (31 to 90 percent) were not accounted for. The trend toward higher losses with increasing volatility indicates that the fission products unaccounted for may

TABLE XXV

FISSION PRODUCTS DETECTED[a]
OUTSIDE FURNACE -- CDE RUN NO. 1

	I-131[b]	Te-132	Ru-103	Mo/Tc-99	Zr/Nb-95	Ba/La-140	Cs-137	Sr-89
Containment Condensate	X	X	X	X			X	X
Containment Wash Water	X	X	X	X	X		X	X
Containment Decontamination Solution	X	X	X	X	X		X	X
Containment Atmosphere	X	X	X	X		X	X	
Deposition Coupons -- Ambient	X	X	X	X				
Deposition Coupons -- Heated	X	X	X	X		X		
Deposition Coupons -- Cooled	X	X	X	X		X		
Reactor Wash Water	X	X	X	X	X		X	X
Reactor Decontamination Solution	X	X	X	X	X		X	X

[a] Other than noble gases.

[b] Includes I-132, I-133, and I-135.

TABLE XXVI

FISSION PRODUCT BALANCE -- CDE RUN NO. 1

Fission Product	Released[a] (percent)	Accounted For[b] (percent)
I-131	94	33
Mo-99	92	10
Ru-103	84	18
Zr-95	77	24
Sr-89	76	28
Ba-140	69	38
Cs-137	53	69
Ce-141	40	61

[a] Determined by comparing fission products found in fuel residue with those estimated to be in fuel from burnup calculations.

[b] Includes fission products found in the furnace tube, in the containment vessel, condensate, atmosphere, rinse and decontamination solutions, and on the plateout coupons.

have been in gases vented from the containment vessel. Analytical results from Run 2 are not yet available for comparison with Run 1 results.

(2) Effect of Condensation on Fission Product Plateout. Provisions were made in the first two CDE runs to control the temperatures of two groups of plateout coupons to determine the effect of condensation upon the extent and type of fission product plateout. A coupon support assembly used for this purpose is shown in Figure 42. Steam was passed through one support assembly to heat the coupons while water was passed through the other to cool the coupons. In Run 1, one group of coupons was held approximately 50°C above the containment vessel temperature and the other group was maintained approximately 30°C below the containment temperature. In Run 2, these differences were 15 and 20°C, respectively.

As evident in Figure 43, the major constituent of the fission product activity on the heated (noncondensing) coupons was iodine. On the cooled (condensing) coupons, the major constituents were the particulate forms (Tc-99, Te-132) of fission product activity. Examination of early scans of coupons contaminated in Run 2 indicates that the same general behavior occurred in Run 2.

(3) Contamination of Paint Applied Over Various Base Materials. A comparison was made of the types of fission product activity found on a four-coat epoxy paint that had been applied over concrete, carbon steel, and stainless steel bases. These coupons were contaminated in Run 1 and the results are shown in Figure 44. Though the data are scattered, they indicate that the base material under this coating has little effect on the fission product plateout.

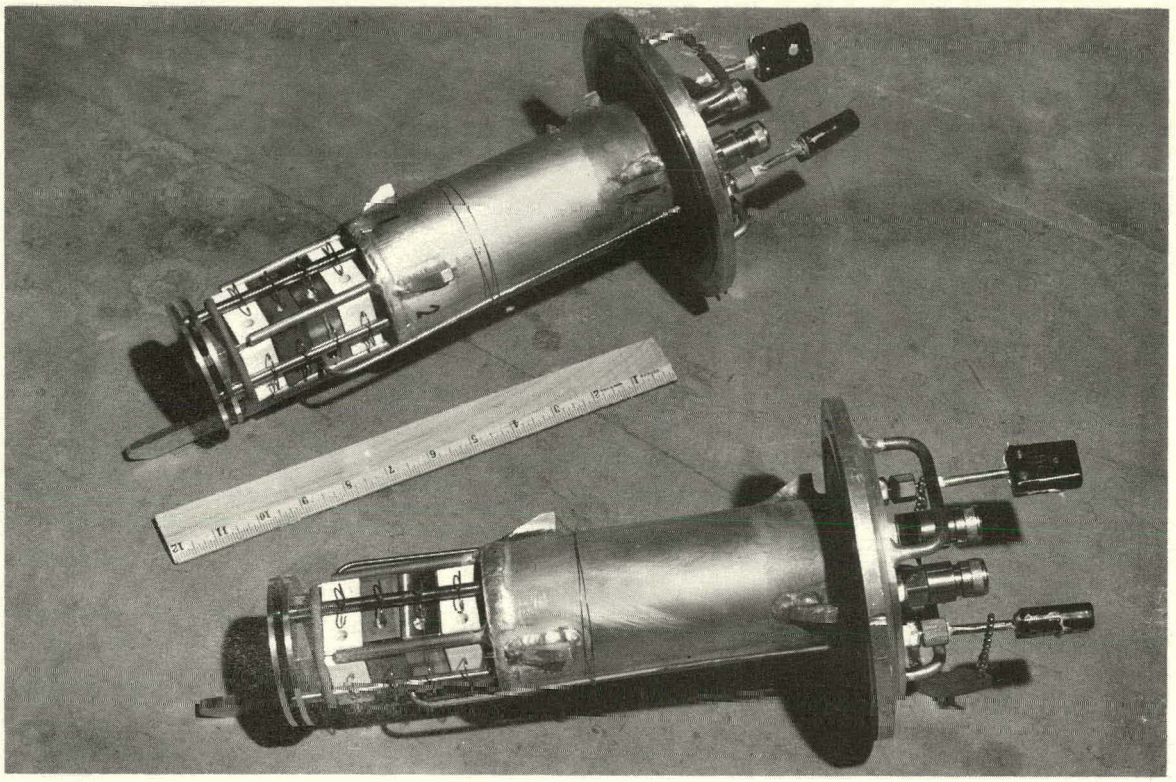

Fig. 42 Coupon support assembly adapted for temperature control.

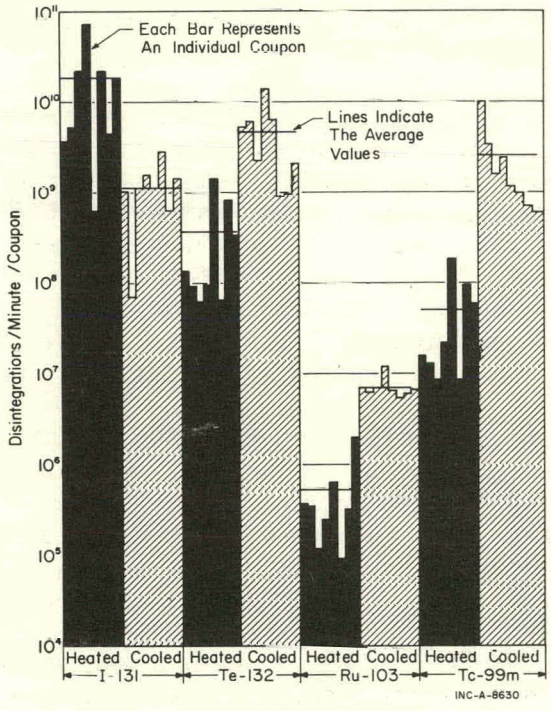

Fig. 43 Contamination of hot and cold carbon steel surfaces coated with Amercoat-66 (CDE run No. 1).

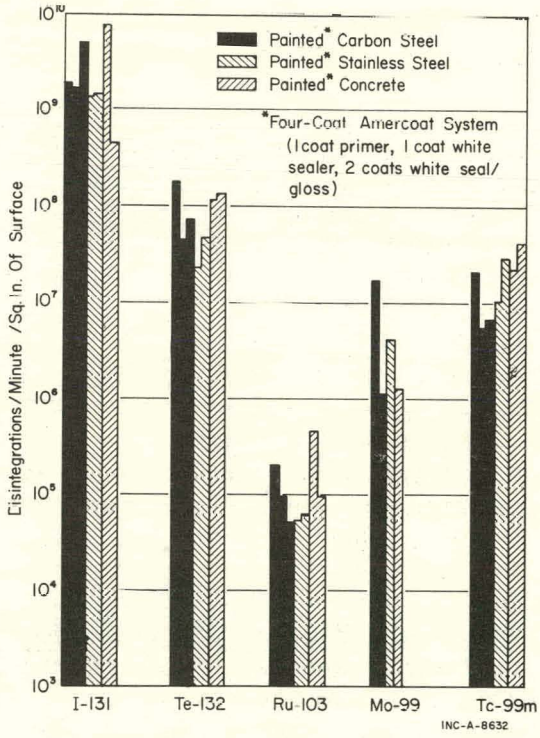

Fig. 44 Contamination of Amercoat-66 over various bases.

1.3 Continuous Sampler-Monitor for the Containment Building Atmosphere (R. E. Schindler; Development Engineering Section)

A Continuous Sampler-Monitor (CSM) is being developed for use in sampling the containment building atmosphere to determine the fission product concentrations during the Loss-of-Fluid Test (LOFT). The CSM, for which a schematic flow sheet is shown in Figure 45, uses a scrubber to sample the atmosphere continuously and to separate the fission products into two streams (gas and liquid) which flow separately through the containment wall to radiation monitors and samplers located outside the building. The scrubber, located in the containment atmosphere to avoid problems with fission product plateout on long sampling lines, washes nearly all of the condensable fission products out of the atmosphere sample into a liquid stream, leaving essentially only rare gas fission products in the gas stream. Gross gamma radiation monitors, located outside the containment building, where the background radiation is moderate and the equipment is accessible, will provide a continuous record of the gross fission product activities in both streams. Samples taken from each stream will be analyzed for the major isotopes using spectrum stripping techniques.

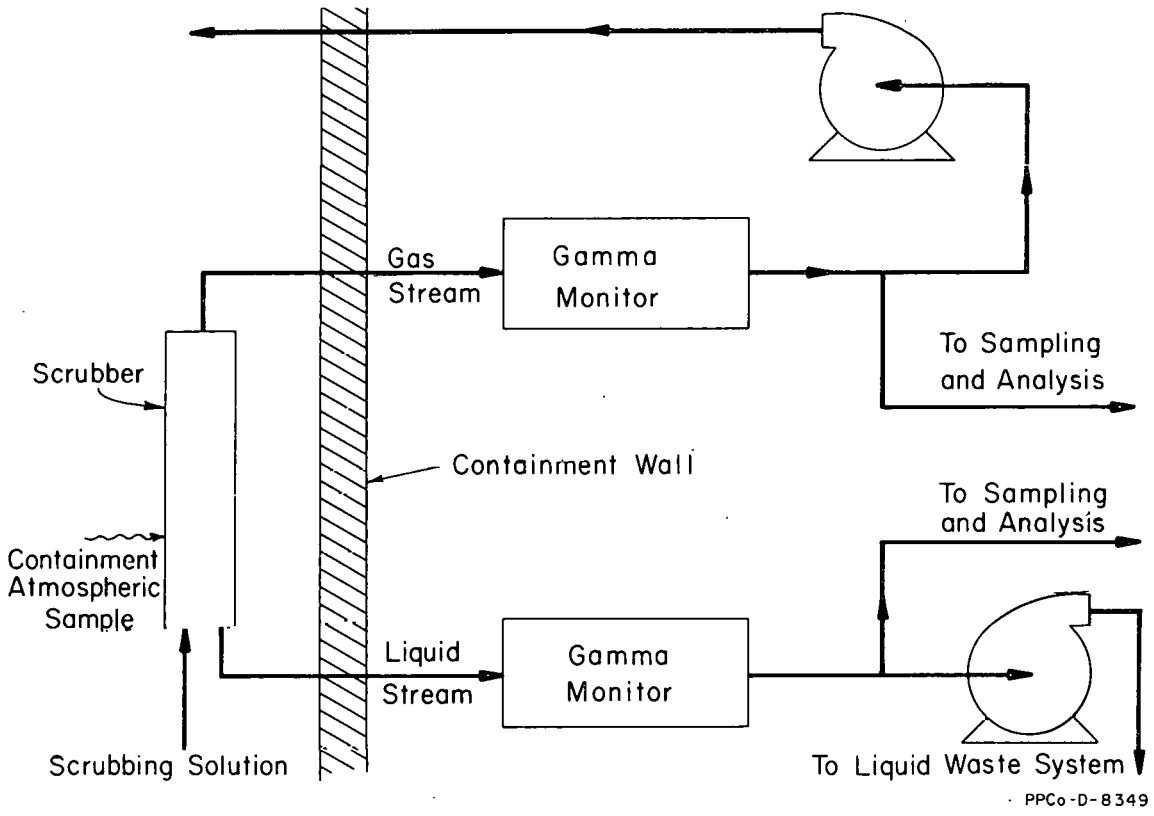

Fig. 45 Schematic of continuous sampler-monitor.

Since I-131, a biologically hazardous isotope, may be adsorbed on airborne particles as well as present in the gaseous state, scrubber designs selected use a high-pressure spray which is relatively effective in removing particles. Two scrubber designs using small high-pressure nozzles operated at 500 psi are shown in Figures 46 and 47. The atmosphere sample passes through the hollow-cone spray sheet, where it is scrubbed, and then goes to the demisting section consisting of either a set of horizontal settling plates or a porous plastic filter.

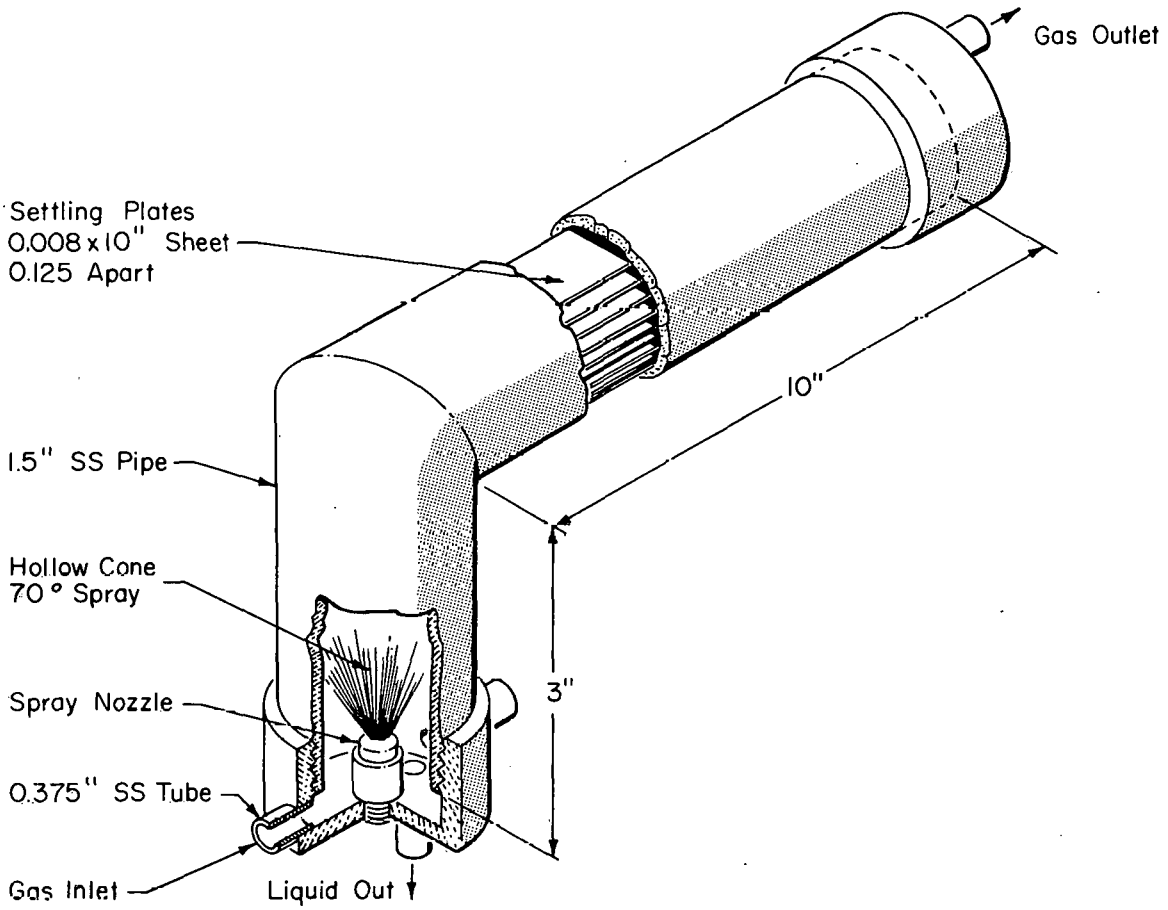

Fig. 46 Spray scrubber with settling plates.

Table XXVII shows the measured penetrations of elemental iodine vapor through the scrubber shown in Figure 46 when using different scrubbing solutions. Owing to the short contact time between the gas sample and the spray, solutions such as NaOH, with rapid reaction rates, were the most effective for removing iodine vapor. Test results were complicated by adsorption of about one-third of the iodine within the scrubber -- probably on the stainless steel surfaces of the scrubber. The scrubber design was changed to that shown in Figure 47, with the hope of reducing surface adsorption by reducing surface area and using inert construction materials. An overall scrubbing efficiency of 90 percent is a goal which appears to be both attainable and adequate for scrubber performance.

A series of tests to evaluate the ability of a scrubber to remove fine particles has been started using fluorescein as a test dust. Initial results showed removal of 97 to 98 percent of fluorescein dust with a mean diameter of 0.55 microns. Several solutions are being evaluated for their ability to sorb methyl iodide. This work is reported in the next section (III-1.4).

The scrubber shown in Figure 47 is being installed in the Contamination-Decontamination Experiment vessel for testing in the next meltdown; meanwhile, laboratory tests on particle removal and methyl iodide removal are continuing.

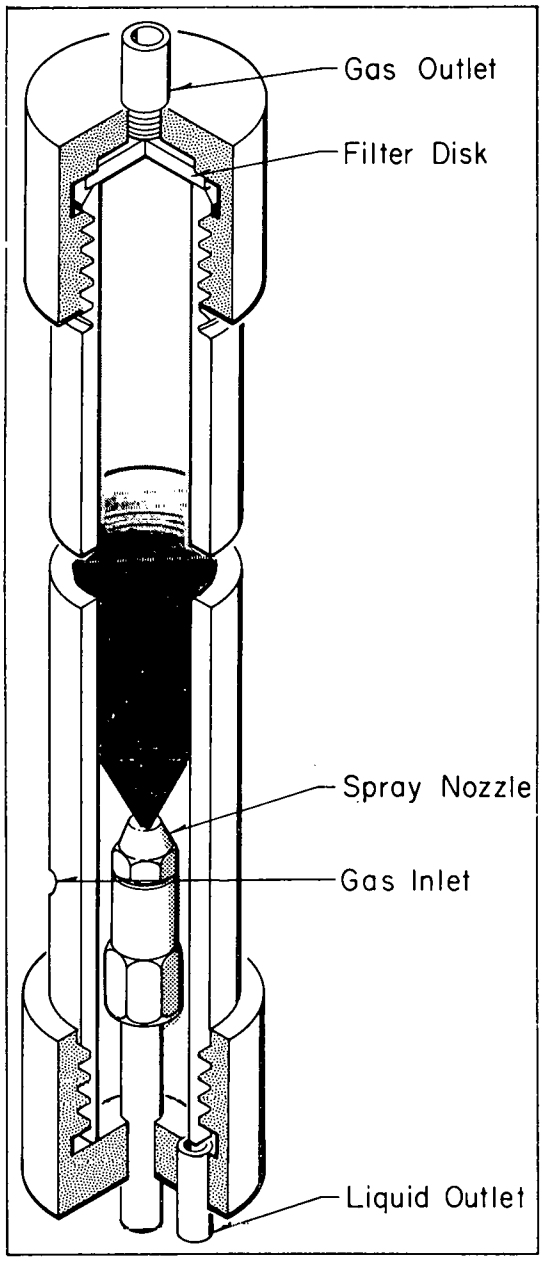

Fig. 47 Spray scrubber with filter.

TABLE XXVII

PENETRATION OF IODINE VAPOR THROUGH SCRUBBER

Scrubbing Solution	Penetration (percent)
Water	7
5 percent HNO_3, 0.001N Hg^{++}, 0.001N Hg^{+}	1
0.1N NaOH	< 0.3

1.4 Evaluation of Scrub Solutions for Removal of Methyl Iodide from Gas Streams

(R. R. Hammer; Chemistry Section)

The Continuous Sampler-Monitor (CSM) discussed in Section 1.3, immediately preceding, is intended to remove some 90 percent of the gaseous fission products, other than rare gases, from the LOFT containment gas sampler. The fission product iodine, probably occurring as elemental iodine, hydrogen iodide, and methyl iodide, will constitute a major problem.

The purpose of the current work is to find solutions which will effectively remove methyl iodide from gas streams. These solutions will then be tested in the continuous sampler for removal of all three iodine species that are expected to be present in the LOFT containment building.

1.41 Experimental Procedure. The test apparatus consisted of a flowmeter and three glass traps in series. Water-pumped nitrogen at a flow rate of 50 ($\pm$ 10) cc/min was passed through the first trap containing methyl iodide (CH_3I) labeled with I-125. The partial pressure of CH_3I was controlled by maintaining the trap at a constant temperature with a slush bath; a carbon tetrachloride slush bath was used to obtain CH_3I pressures of about 10 mm, and either carbon disulfide or methyl alcohol slush baths were used to obtain CH_3I pressures of about 10^{-4} mm. The gas stream was then passed into the second trap through a course glass cylindrical frit to disperse the gas in the scrub solution contained in the trap. A constant temperature bath was used to maintain the scrub solution at a constant temperature, within 1/4°C of the desired temperature, during the run. The gas stream was then passed into the final trap cooled with liquid nitrogen to remove the residual CH_3I in the gas stream. At the end of a run an isopropyl alcohol solution of untagged CH_3I was added to the final trap. Aliquot portions of the

isopropyl solution and the scrub solutions were counted with a well-type scintillation counter. From the relative activity of the scrub solutions and the isopropyl alcohol solutions, the scrubbing efficiencies of the various solutions were determined.

1.42 Results. In Table XXVIII, Part 1, are listed the scrubbing efficiencies of solutions at CH_3I pressures of approximately 10 mm, and in Part 2 are the

TABLE XXVIII

EFFICIENCY OF SCRUBBER SOLUTIONS FOR REMOVING CH_3I

Part 1 -- Conditions: 50°C, 50 cc/min flow rate. Partial pressure CH_3I: 3 to 17 mm in N_2 atmosphere.

Solution	Scrubber Efficiency (percent CH_3I removed)
0.1M $KBrO_3$, 0.3M H_2SO_4	91.4 ± 7.6
0.1M $Hg(NO_3)_2$, 1M KI	58.0 ± 28
0.1M $KBrO_3$, 0.3M H_2SO_4	97.5 ± 1.0[a]
$Hg_2(NO_3)_2$ saturated	99.2 ± 1.9[b]
1M HNO_3, 0.0009M $Hg(NO_3)_2$ 0.0009M $Hg_2(NO_3)_2$	75.8 ± 7.6[c,d]
$Hg(NO_3)_2$ saturated	62.9 ± 16[d]
1.5M NaClO	2.1 ± 0.5
0.1M KIO_3, 0.3M H_2SO_4	2.3 ± 1.7
1M $AgNO_3$	97.9 ± 2.1[d]
0.1M I_2, 1.0M KI	44.3 ± 3.2
1.0M $Na_2S_2O_3$	96.8 ± 0.7
1.0M $KClO_3$, 0.3M H_2SO_4	0 ± 0.5
0.1M $KMnO_4$, 0.3M H_2SO_4	99.1 ± 1.0
1.0M HNO_3	2.2 ± 1.5
1.0M NaOH	63.5 ± 4.2
0.1M $KBrO_3$, 0.6M HNO_3, 5.4×10^{-4}M $Hg(NO_3)_2$ 5.4×10^{-4}M $Hg_2(NO_3)_2$	95.6 ± 7.4

TABLE XXVIII (Contd.)

EFFICIENCY OF SCRUBBER SOLUTIONS FOR REMOVING CH_3I

Part 2 -- Conditions: 50°C, 50 cc/min flow rate. Partial pressure CH_3I: approximately 10^{-4} mm.

Solution	Scrubber Efficiency (percent CH_3I removed)
0.1N Na_2SO_3, 0.5N NaOH	95.9 ± 24
0.1N $Na_2S_2O_3$	87.4 ± 10
10% by volume $N_2H_4H_2O$	94.3 ± 2.3
0.05M $KBrO_3$ 0.5N HNO_3 0.0005M $Hg_2(NO_3)_2$ 0.0005M $Hg(NO_3)_2$	89.2 ± 6.5
1M $Na_2S_2O_3$	98.3 ± 7.3
0.1M $KbrO_3$, 0.3M H_2SO_4	91.8 ± 8.8
Distilled water	0 ± 11
0.1M $KMnO_4$, 1.0N NaOH	70.3 ± 6.7[d]

[a] CH_3I concentration approximately threefold greater in Experiment 3 than in Experiment 1.

[b] Precipitate formed.

[c] The scrubber efficiency was probably higher than this figure indicates, since all of the mercury salts were precipitated before the run was concluded.

[d] At 60°C.

scrubbing efficiencies for various solutions at CH_3I pressures of approximately 10^{-4} mm. The scrubbing efficiencies for solutions tested at both high and low CH_3I pressures, within experimental error, were independent of the partial pressure of CH_3I. It is, therefore, very probable that the three to four orders of magnitude lower CH_3I pressures, which are expected in the LOFT experiment, will have little effect on the scrubbing efficiency of the solution used in the continuous sampler.

Of the several scrubbing solutions tested, sodium thiosulfate was one of the more effective for removal of CH_3I; moreover, it is an effective reagent for

removal of elemental iodine. The temperature dependence of the scrubbing efficiency of solutions of sodium thiosulfate is shown in Figure 48. Apparently there is a maximum in the scrubbing efficiency at about 50°C. In Figure 49 the scrubbing efficiency of basic thiosulfate solution is given as a function of temperature. Also shown are the scrubbing efficiencies of a solution of 1M NaOH, and a solution of 1M NaOH with 0.1M $KMnO_4$. It can be readily seen from this figure that sodium thiosulfate definitely enhances the scrubbing efficiency of sodium hydroxide solutions, while potassium permanganate does not significantly affect the scrubbing efficiency of sodium hydroxide solutions. Results from experiments with basic thiosulfate solutions suggest that both OH^- and thiosulfate are involved in the reaction; however, further work would be necessary to determine the mechanism of reaction.

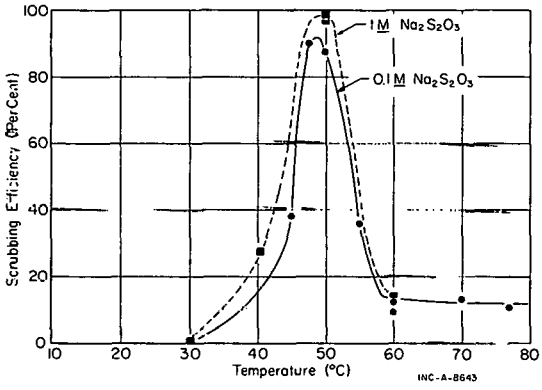

Fig. 48 The scrubbing efficiency of thiosulfate solutions for methyl iodide as a function of temperature.

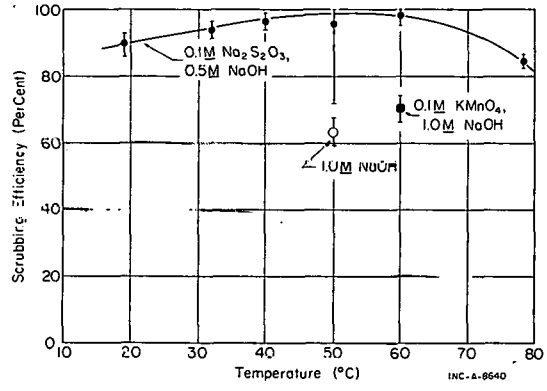

Fig. 49 The scrubbing efficiency of basic solutions for methyl iodide.

Much higher scrubbing efficiencies were observed for a number of solutions than were observed by British workers [41]. The higher scrubbing efficiencies observed in this work were probably the result of the greater contact obtained between the gas stream and the scrub solutions with the course glass frit than with the bubblers in series used by the British workers.

The solutions which seem to have the greatest promise as scrub solutions for removal of CH_3I from gas streams are:

(1) 0.1M $KBrO_3$, 0.3M H_2SO_4

(2) $Hg_2(NO_3)_2$ (saturated)

(3) 1M $AgNO_3$

(4) 0.1M $KMnO_4$, 0.3M H_2SO_4

(5) 0.1M $KBrO_3$, 0.3M HNO_3, 5.4×10^{-4}M $Hg(NO_3)_2$, 5.4×10^{-4}M $Hg_2(NO_3)_2$

(6) >0.1M $Na_2S_2O_3$ at 50°C

(7) 0.5M NaOH, 0.1M $Na_2S_2O_3$

(8) 10 percent by volume $N_2H_4 \cdot H_2O$.

2. FISSION GAS RETENTION OF TEST REACTOR FUELS

(M. R. Fox, M. E. Jacobson; Chemistry Section)

Preliminary fuel degassing studies of two types of fuel plates have been completed in a joint effort by the Analytical and Chemical and Process Development Branches. This study was undertaken to determine the relative fission gas retention properties of fuel plates consisting of (a) UAl_4 particles in an aluminum matrix and (b) U_3O_8 particles in an aluminum matrix. Both fuel plates were completely clad in Type 6061 aluminum.

Before the fission gases were collected, each plate was pre-heated for 48 to 72 hours at 300°C to assure dryness. Each plate was then heated to 600°C and held for about 40 minutes, then heated to 630°C and held for about 40 minutes, and finally heated to 670°C and held for about 30 minutes. The fission gases which were released at each of these temperatures were collected in reservoirs of known volume, and were measured by an increase in pressure in each reservoir.

As may be seen from the results presented in Figures 50 and 51, there is a difference in rates of release of fission gases from the two types of plates. Figure 51 shows the percent of the fission gases released at each temperature studied, and Figure 50 shows the time dependence of fission gases released at each of these temperatures. At all three temperatures the U_3O_8-type fuel plate released its fission gases at a lower rate than the aluminide fuel plate. This may imply a difference in mechanism of fission gas release. Whatever the differences in rates are caused by, they must be related to differences in properties of the fuel particles themselves, because both fuel plates have identical matrices and claddings. Another conclusion which may be drawn from Figure 50 is that there is no significant effect of burnup on the fission gas release of the two aluminide fuel plates. These plates had burnup values of 24 and 18 percent. The oxide-type fuel plate had a burnup value of 26 percent.

There appears to be a sharp threshold at which the fission gases begin to evolve from the plates. This occurs in the temperature range of 575 to 600°C and occurs at about the same temperature for both types of fuel. The early part of the time-temperature curve of a fuel plate is shown in Figure 52 and is typical of the behavior encountered in the degassing of both types of fuel.

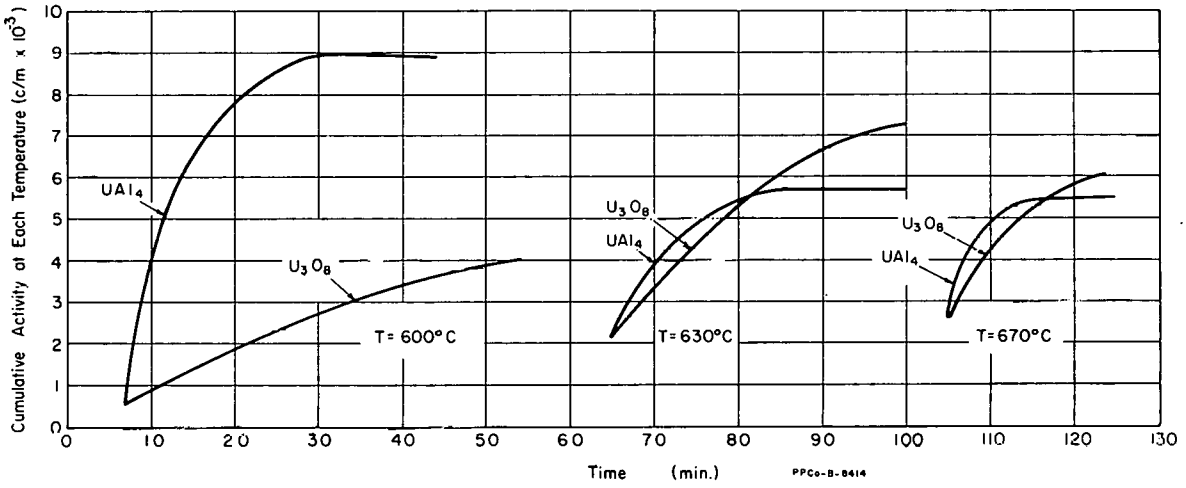

Fig. 50 Time dependence of fission gas release.

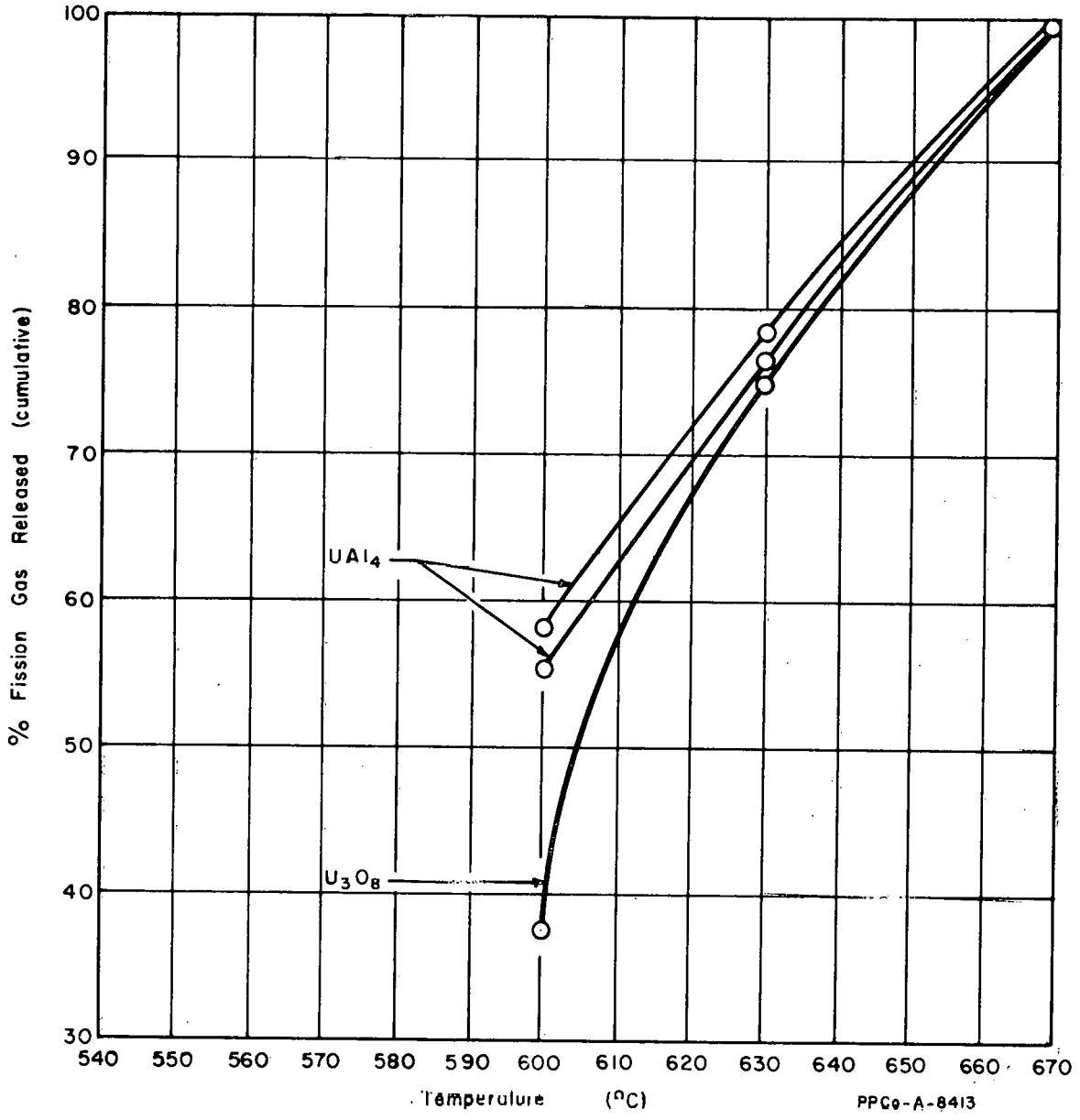

Fig. 51 Percent fission gas released (cumulative).

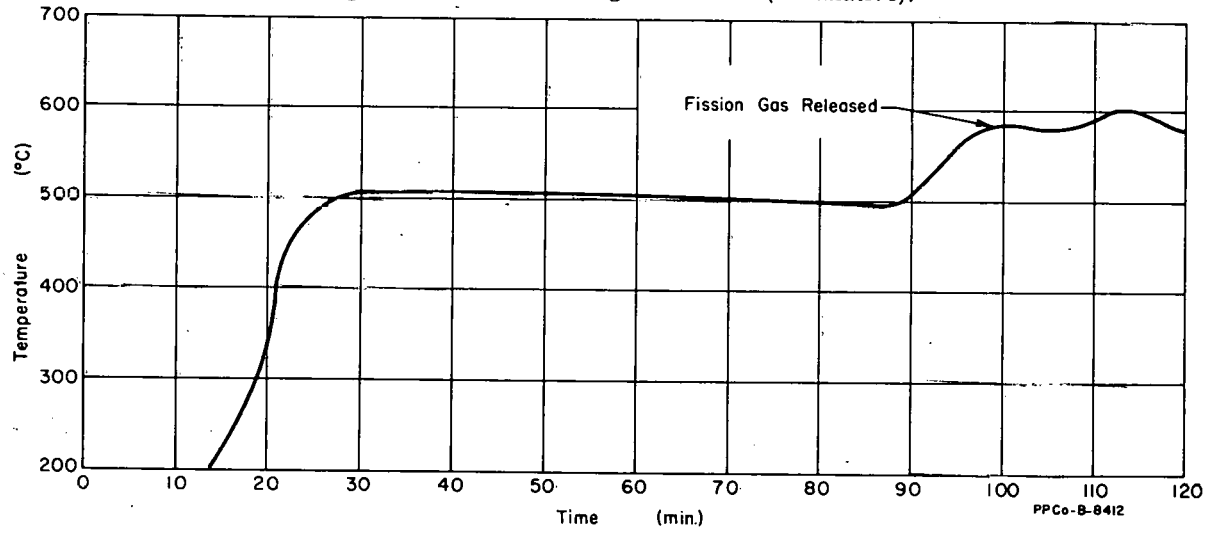

Fig. 52 Segment of heating curve for a typical fuel plate.

IV. REFERENCES

1. J. R. Bower (ed.), Chemical and Process Development Branch Annual Report Fiscal Year 1965, IDO-14661 (February 1966).

2. B. R. Wheeler et al, Uranium Recovery from Aluminum Alloyed Fuel ICPP Run No. 21, IDO-14669 (January 1966).

3. G. F. Offutt et al, First Zirconium Alloyed Fuel Reprocessing Campaign Using Soluble Nuclear Poison, IDO-14675 (to be published).

4. W. P. Palica et al, Uranium Recovery from Aluminum Alloyed Fuel at ICPP, December 1965 and January 1966 (to be published).

5. D. A. Orth and T. W. Olcott, "Purex Process Performance Versus Solvent Exposure and Treatment", Nucl. Sci. and Eng., 17 (December 1963) pp 593-612.

6. J. R. Bower, Zirconium Processing Capability of the Idaho Chemical Processing Plant, IDO-14645 (October 1964).

7. J. R. Bower (ed.), Chemical Processing Technology Quarterly Progress Report, January - March 1964, IDO-14638 (June 1964).

8. M. J. Graber et al, Results of ATR Sample Fuel Plate Irradiation Experiment, IDO-16958 (March 1964).

9. O. W. Parrett, The Determination of Excessive Emulsification by Coalescence Behavior Measurements, IDO-14486 (November 1959).

10. J. R. Bower (ed.), Chemical Processing Technology Quarterly Progress Report, April - June 1962, IDO-14593 (September 1962).

11. J. R. Bower (ed.), Chemical Processing Technology Quarterly Progress Report, January - March 1964, IDO-14638 (June 1964).

12. L. A. Decker and R. R. Hammer, A Study of Three Methods for Reprocessing Graphite Fuels: Mixed Acid Oxidation, Grind Leach, and Electrolytic Disintegration, IN-1018 (to be published).

13. J. R. Bower (ed.), Chemical Processing Technology Quarterly Progress Report, October - December 1960, IDO-14553 (May 1961).

14. M. E. Weech et al, Interim Report on the Development of an Air Pulser for Pulse Column Application, IDO-14559 (September 1961).

15. J. R. Bower (ed.), Chemical Processing Technology Quarterly Progress Report, October - December 1961, IDO-14583 (March 1962).

16. M. E. Whatley et al, Chemical Technology Division, Unit Operations Section Monthly Progress Report, August 1963, ORNL-TM-776 (June 1964) pp 6-23.

17. J. R. Bower (ed.), Chemical Processing Technology Quarterly Progress Report, July - September 1963, IDO-14625 (February 1964).

18. F. E. Romie, "Heat Transfer to Fluids Flowing With Velocity Pulsations in a Pipe", Ph. D. Thesis, University of California, 1956.

19. Catholic University of America, Simulated Nuclear Reactor Vibrational Heat Transfer Quarterly Progress Report, February 1, 1963 - April 30, 1963, CUA-NE-28 (1963).

20. R. Lemlick, "Vibration and Pulsations Boost Heat Transfer", Chem. Eng., 68 (May 15, 1961) pp 171-174, 176.

21. M. Leva, Fluidization, New York: McGraw-Hill Book Company, Inc., 1959.

22. E. S. Grimmett and B. P. Brown, Physical and Operational Features of a Pulsed Continuous Countercurrent Liquid-Solids Contactor, IDO-14541 (April 1961).

23. E. S. Grimmet and G. W. Hogg, "Effects of Pulsation on Heat Transfer in a Liquid-Fluidized Bed Process", Paper presented at 58th National Meeting of the American Institute of Chemical Engineers, Dallas, Texas (February 1966).

24. L. T. Lakey and J. R. Bower (eds.), ICPP Waste Calcining Facility Safety Analysis Report, IDO-14620 (December 1963).

25. J. W. Loeding et al, The Fluid-Bed Calculation of Radioactive Waste, ANL-6322 (May 1961).

26. E. S. Grimmett, Particle Growth and Size Distribution in Fluidized Bed Processes -- A Mathematical Model with Computer Solutions, IDO-14650 (April 1966).

27. A. A. Jonke et al, Fluidized-Bed Process for the Production of Uranium Tetrafluoride (Green Salt) from Uranyl Nitrate, ANL-5363 (December 1954).

28. Argonne National Laboratory, Chemical Engineering Division Summary Report for January, February, and March 1955, ANL-5422 (May 1955).

29. R. R. Hammer and B. D. Penman, The Ruthenium Dioxide - Oxygen - Ruthenium Tetroxide Equilibrium, IN-1013 (to be published).

30. M. E. McLain and D. W. Rhodes, Leaching of Fission Products from Calcined Process Waste, IDO-14440 (April 1958).

31. C. E. Stevenson, Idaho Chemical Processing Plant Technical Progress Report for April Through June 1959, IDO-14494 (March 1960) p 64.

32. J. I. Stevens (ed.), Idaho Chemical Processing Plant, Radioactive Waste Disposal Projects Technical Progress Report for January - March 1960, IDO-14530 (August 1960) p 20.

33. J. R. Bower (ed.), Chemical Processing Technology Quarterly Progress Report , April - June 1960, IDO-14534 (November 1960) p 44.

34. B. E. Paige, Leachability of Alumina Calcine Produced in the Waste Calcining Facility of the Idaho Chemical Processing Plant, IDO-14673 (to be published).

35. W. A. Freeby, Heat Transfer Coefficients for Finned Tubes Inside a Fluidized Bed, M. S. Thesis, University of Idaho, Moscow, Idaho (April 1966).

36. H. Grober et al, Fundamentals of Heat Transfer, 3rd ed. New York: McGraw-Hill Book Company, Inc., 1961.

37. D. E. Black and B. R. Dickey, Mathematical and Experimental Analysis of Heat Dissipation from a Source Buried in Soil, IN-1032 (to be published).

38. J. H. Blackwell, "A Transient-Flow Method for Determination of Thermal Constants of Insulating Materials in Bulk. I. Theory", J. Appl. Phys., 25 (February 1954) pp 137-144.

39. L. S. Darken and R. W. Gurry, Physical Chemistry of Metals, New York: McGraw-Hill Book Company Inc., 1963, pp 347-444.

40. R. C. Shank et al, Annual Report of Division Analytical Branch for 1965, IDO-14679 (to be published).

41. D. A. Collins, R. Taylor, and L. R. Taylor, "The Removal of Methyl Iodide From Reactor Effluent Gasses", in International Symposium on Fission Product Release and Transport Under Accident Conditions, April 5-7, 1965, Oak Ridge, Tennessee, CONF-650407 (1965) pp 853-868.

V. REPORTS AND PUBLICATIONS ISSUED DURING FISCAL YEAR 1966

1. IDO REPORTS

1. W. B. Kerr, L. T. Lakey, and R. G. Denney, Development of a Continuous Electrolytic Process for Recovery of Uranium from High-Enriched Stainless Steel and Nichrome Fuel, IDO-14643 (October 1965).

2. E. S. Grimmett, Particle Growth and Size Distribution in Fluidized Bed Processes -- A Mathematical Model with Computer Solutions, IDO-14650 (April 1966).

3. J. C. Petrie et al, Fluidized Bed Calcination of Simulated Zirconium Fluoride Waste in Exploratory Pilot Plant Tests, IDO-14653 (July 1965).

4. D. W. Rhodes and M. M. Wilding, Decontamination of Radioactive Effluent with Clinoptilolite, IDO-14657 (July 1965).

5. R. W. Legan et al, ICPP Processing of VBWR Stainless Steel Fuel (April 14 to June 2, 1965), IDO-14658 (December 1965).

6. L. A. Decker, ICPP Laboratory Studies on Combustion - Nitric Acid Leach Process for Power Fuel, IDO-14659 (Confidential) (August 1965).

7. G. E. Lohse et al, Operation of the Waste Calcining Facility with Radioactive Aqueous Waste Report on the First Processing Campaign, IDO-14662 (September 1965).

8. D. W. Rhodes and M. E. Jacobson, Measurement of Heat Generation Rate of Highly Radioactive Calcined Alumina, IDO-14665 (October 1965).

9. J. C. Petrie and E. D. Cooper, A Flow Diverter-Valve for Granular Solids, IDO-14666 (March 1966).

10. B. R. Wheeler et al, Uranium Recovery from Aluminum Alloyed Fuel ICPP Run No. 21, IDO-14669 (January 1966).

11. M. M. Wilding and D. W. Rhodes, Stability Studies of Highly Radioactive Alumina Calcine During High Temperature Storage, IDO-14670 (February 1966).

12. B. E. Paige, Leachabilities of Glass Prepared From Highly Radioactive Calcined Alumina Waste, IDO-14672 (February 1966).

13. B. J. Newby and K. L. Rohde (eds.), An improved Aqueous Process for Zirconium Alloy Nuclear Reactor Fuels. Part III. Continuous Dissolution in Hydrofluoric Acid with Soluble Poison, IDO-14674 (June 1966).

2. PAPERS PRESENTED AT TECHNICAL SOCIETY MEETINGS

1. B. E. Paige, "Leachability of Glass Prepared From Highly Radioactive Calcined Waste", Paper presented at the 150th National Meeting of the American Chemical Society, Atlantic City, New Jersey (September 1965).

2. L. T. Lakey and W. B. Kerr, "Pilot Plant Development of an Electrolytic Dissolver for Stainless Steel Alloy Fuels", Paper presented at the 150th National Meeting of the American Chemical Society, Atlantic City, New Jersey (September 1965).

3. G. E. Lohse, E. J. Bailey, and D. W. Rhodes, "Status of the Fluidized Bed Calcination Process for Conversion of Radioactive Wastes to Solids", Paper presented at the 150th National Meeting of the American Chemical Society, Atlantic City, New Jersey (September 1965).

4. E. S. Grimmett, "Particle Growth and Size Distribution in Fluidized Bed Processes - A Mathematical Model with Computer Solutions", Paper presented at the 58th Annual Meeting of the American Institute of Chemical Engineers, Philadelphia, Pennsylvania (December 1965).

5. C. B. Amberson and D. W. Rhodes, "Treatment of Intermediate and Low-Level Radioactive Wastes at the NRTS", Paper presented at the Joint IAEA - ENEA Symposium on Practices in the Treatment of Low and Intermediate Level Radioactive Wastes, Vienna, Austria (December 1965).

6. E. S. Grimmett and G. W. Hogg, "Effects of Pulsation on Heat Transfer in a Liquid-Fluidized Bed Process", Paper presented at 58th National Meeting of the American Institute of Chemical Engineers, Dallas, Texas (February 1966).

7. J. C. Petrie and D. E. Black, "Development of Air Distributor Caps for a Fluidized Bed Process", Paper presented at 58th National Meeting of Chemical Engineers, Dallas, Texas (February 1966).

8. B. M. Legler, E. J. Bailey, and J. C. Petrie, "Fluidized Bed Calcination of New Types of High-Level Wastes", Paper presented at Symposium on Solidification and Long-Term Storage of Highly Radioactive Wastes, Richland, Washington (February 1966).

9. G. E. Lohse and R. E. Commander, "Initial Operation of the Idaho Waste Calcining Facility with Radioactive Feed", Paper presented at Symposium on Solidification and Long-Term Storage of Highly Radioactive Wastes, Richland, Washington (February 1966).

10. D. W. Rhodes, "Storage and Further Treatment of Product from Fluidized Bed Calcination of Radioactive Wastes", Paper presented at Symposium on Solidification and Long-Term Storage of Highly Radioactive Wastes, Richland, Washington (February 1966).

11. J. L. Lockhard, G. E. Lohse, and J. W. Garner, "Economics of Waste Management Involving Fluidized Bed Calcination", Paper presented at Symposium on Solidification and Long-Term Storage of Highly Radioactive Wastes, Richland, Washington (February 1966).

12. B. J. Newby and K. L. Rohde, "Decontamination of Protective Coatings Following a Loss of Coolant Accident", Paper presented at International Symposium on the Decontamination of Nuclear Installations, Harwell, United Kingdom (May 1966).

13. W. G. Morrison, J. A. Buckham and A. L. Ayers, "Soluble Poison for Nuclear Safety Control During Fuel Processing", Paper presented at National American Nuclear Annual Meeting, Denver, Colorado (June 1966).

PHILLIPS
PETROLEUM
COMPANY

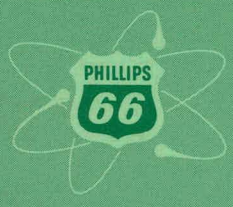

ATOMIC ENERGY DIVISION